THE UNIVERSITY OF CHICAGO

THE IMPACT OF ADAPTIVE IMMUNITY ON THE DEVELOPMENT AND PROGRESSION OF ORAL SQUAMOUS CELL CARCINOMA

A DISSERTATION SUBMITTED TO

THE FACULTY OF THE DIVISION OF THE BIOLOGICAL SCIENCES

AND THE PRITZKER SCHOOL OF MEDICINE

IN CANDIDACY FOR THE DEGREE OF

DOCTOR OF PHILOSOPHY

COMMITTEE ON IMMUNOLOGY

BY

JAIME LINDSEY CHAO

CHICAGO, ILLINOIS

JUNE 2021

To my parents and grandparents.

TABLE OF CONTENTS

LIST OF FIGURES

LIST OF TABLES

Supplementary Tables

Supplementary tables may be found online.

ACKNOWLEDGEMENTS

There are truly too many people to thank, without whom this thesis would not be possible. I am forever grateful to everyone who supported, guided, and mentored me before and during my Ph.D. I can honestly say I would not be where I am today without each and every one of you.

First and foremost, I owe a great deal of gratitude to Pete. Pete's guidance and endless support throughout my thesis work was invaluable to bring this project to life, and make it the best work possible. Establishing a new project and mouse model in the lab is no easy feat, but with Pete's support and encouragement I was able to succeed and thrive in the project. Throughout, Pete ensured I was connected with key collaborators with important expertise, including Mark Lingen, Tanguy Seiwert, and Evgeny Izumchencko. Beyond guiding my project, Pete is always pushing me to think critically and creativity. I am incredibly grateful for this. Not only was this instrumental in allowing me to think deeply about the important implications of our findings, but it made me the scientist I am today and has given me the confidence to pursue big goals. Pete always encourages lively scientific discussions, both in one-on-one meetings and as a lab group, which leads to a really great environment to be around. I could not have imagined a better mentor for my Ph.D., thank you Pete.

To the Savage lab, it has been incredible to be surrounded by exceptionally smart and collaborative people. Being a part of the Savage lab has been such a positive experience and I have truly enjoyed coming to work every day. To past members Saki, Sven, Dan, Dana, Victoria, Mary, and Sharon. You are the reason I decided to join the Savage lab and were all central to the start of my thesis work, providing key insight and great discussion of immunology concepts. A special thank you to Dana. Since I first interviewed at COI, you have been my go-to person, so helpful

throughout our time as graduate students, especially during the stressful times, and continue to be a huge source of support as a colleague and friend. To current members Christine, Dave, and Donald. I cannot put into words how grateful I am to have shared space, ideas, and much needed happy hours over the years. I feel fortunate that I was able to overlap in lab the most with you all. Christine, thank you for teaching me the retrogenic protocol and for all the great discussions regarding our projects. Dave, thank you for always being around for a great scientific discussion. We may not agree on much but it's so fun to have discussions and different perspectives. To the newer members, Matt and Riley. It's so great to have fresh faces in lab! Your energy and willingness to help out this past year has been super helpful, especially during a pandemic. Finally, thank you Divya for organizing our lab space and helping with logistics and equipment. Your presence has been an invaluable addition for our team.

To the Kline lab, great neighbors and friends. It has been fantastic having joint lab meetings and sharing space. You are always available for engaging conversations, technical help, and bailing us out when we run out of reagents. A special thank you to the incredibly kind and helpful Xiufen, and fellow graduate students Brendan and Sravya.

I would not have made it to the Immunology program at the University of Chicago without my former mentors Michelle, Uttiya, and Angelo. To Michelle, thank you for providing me a great first-time lab research experience. My experience in your lab as an undergrad was the true beginning of my interest and love for bench research, especially in immunology. To Uttiya and Angelo, thank you for guidance and support while I was in the lab and beyond. Your confidence in me as a scientist has meant so much to me.

To my committee members Marisa, Anne, and Kay. Thank you for your helpful suggestions and comments during my committee meetings. I always looked forward to my

committee meetings and they were vital in guiding my project, particularly in the early days. It has been incredibly inspiring to have exceptionally intelligent scientists who are women as mentors.

All of the work presented in this thesis would not be possible without the cores at the University of Chicago. To the CAT facility, thank you for your help and expertise for flow and cell sorting. To the ARC, thank you for maintaining our mouse colony. A big thank you to the HTRC for all of the tissue pathology. Mark, thank you for training me in analyzing H&E sections, and for being a great mentor and source of support from the start. Terri, thank you for all of your help and guidance for IHC stains.

To all of the labs, students, faculty, and everyone else who make up the COI community. I am in debt to you all for providing a challenging and enriching academic environment, and pushing me to become the best immunologist I can be. The collaborative and supportive community that is on display during seminars, work in progress, journal clubs, and beyond has been my favorite parts of graduate school. Not only is everyone open to sharing ideas and conversations, but also reagents and resources when needed.

To all of the incredible friends I have made. I would not have able to get through this without you all. To Chris, Ryan, Steven, Andrew, Chanie, and Matt. I could not have asked for a better cohort to start this journey with. To Chris, Ryan, Steven, Jess, Hailey, and Matt. I cannot express enough how much your friendship and countless lunches have made this experience the most enjoyable. Thank you for your endless support and encouragement. I cannot wait to see the wonderful things you all will accomplish in the future.

To my friends, both near and far. First, thank you to the Wallace family for welcoming me to Chicago and providing me a place to call home while in Chicago. To Melissa, Regan, Christina, Sam, Staci, Adam, Athenas, Charlie, Jurgis, Mel, and Sean. I am incredibly grateful for your

friendships over the years. You are a source of joy in my life, and a place to escape to for a much-needed vacation.

Finally, to my family. Nothing in my life would be possible without your unconditional love and support. My accomplishments are your accomplishments. To my parents. Your continuous love and support have given me the confidence to believe in myself, allowing me to accomplish whatever it is I set my mind to. To my brothers Justin, Nick, and Eric. I am grateful to have such a wonderful built-in support system – we are each other's biggest cheerleaders. To my extended family, all of my aunts and cousins. Thank you for your love, support, and genuine interest in my research. And to my grandparents. I quite literally would not be here and able to take advantage of the incredible opportunities I've had if it weren't for you. This is for you.

ABSTRACT

Immune suppression by $CD4^+FOXP3^+$ regulatory T (Treg) cells and tumor infiltration by $CD8^+$ effector T cells represent two major factors impacting response to cancer immunotherapy. Using deconvolution-based transcriptional profiling of human HPV-negative oral squamous cell carcinomas (OSCCs) and other solid cancers, we demonstrated that the density of Treg cells does not correlate with that of $CD8^+$ T cells in many tumors, revealing polarized clusters enriched for either $CD8^+$ T cells or $CD4^+$ Treg and conventional T cells. In a mouse model of carcinogen-induced OSCC characterized by $CD4^+$ T cell enrichment, late-stage Treg cell ablation triggered increased densities of both $CD4^+$ and $CD8^+$ effector T cells within oral lesions. Notably, this intervention did not induce tumor regression, but instead induced rapid emergence of invasive OSCCs via an effector T cell-dependent process. Thus, induction of a T cell-inflamed phenotype via therapeutic manipulation of Treg cells may trigger unexpected tumor-promoting effects in OSCC.

ABBREVIATIONS

4-NQO	4-nitroquinoline N-oxide
APC	Antigen presenting cell
CFA	Complete Freund's Adjuvant
DT	Diphtheria toxin
HNC	Head and neck cancer
HNSCC	Head and neck squamous cell carcinoma
HPV	Human Papillomavirus
IFN-γ	Interferon gamma
mAb	Monoclonal antibody
MHC	Major histocompatibility complex
OSCC	Oral squamous cell carcinoma
SLO	Secondary lymphoid organ
Tconv cell	Conventional T cell
TCR	T cell receptor
TCRrg	TCR retrogenic
Treg cell	Regulatory T cell

INTRODUCTION[a]

Overview of adaptive immunity

Our immune system consists of two interconnected branches that have evolved to work in concert to protect ourselves from harmful pathogens: the innate immune system and the adaptive immune system. While the innate immune response operates on the order of hours to days and responds to conserved triggers associated with perturbations to immune homeostasis, the adaptive immune response requires days to weeks to culminate but has the capacity to specifically target a given pathogen through the diverse antigen receptors expressed on the cell surface of B and T lymphocytes, the cells that make up the adaptive immune system.

The immune system has the daunting task of coordinating a robust response to dangerous, invading pathogens while maintaining homeostasis and avoiding tissue destruction and pathology to healthy tissues. Immune cells have to distinguish between healthy host tissues and harmful foreign material. Innate immune cells accomplish this goal through expression of germline encoded pattern recognition receptors (PRRs), which signal when engaged with ligands that contain molecular motifs or patterns common to pathogens but exogenous to the host (e.g. lipopolysaccharide or cytosolic dsDNA)[2,3]. Adaptive immune cells, on the other hand, undergo a process called V(D)J recombination during their development, in which DNA segments within the B cell receptor (BCR) or T cell receptor (TCR) loci are rearranged and random nucleotides are inserted to produce a unique BCR or TCR expressed on the cell surface[4]. Each B cell expresses a unique BCR with the potential to recognize distinct antigens, whereas each T cell expresses a unique TCR with the potential to recognize short protein-derived peptides presented on host-

[a] Parts of this section are reproduced, with modifications, from Chao, J.L. and Savage, P.A. (2018) Unlocking the Complexities of Tumor-Associated Regulatory T cells. *Journal of Immunology* 200:415-421.[1]

derived MHC molecules displayed on the cell surface by antigen presenting cells (APCs). While B cells are well-known for their capacity to produce antibodies, T cell function is divided based on T cell lineage: $CD8^+$ T cells exhibit cytotoxic function and recognize peptides presented on MHC class I (MHCI), $CD4^+$ $Foxp3^{neg}$ T conventional (Tconv) cells provide helper functions to both $CD8^+$ T cells and B cells and recognize peptides presented on MHC class II (MHCII), and $CD4^+$ $Foxp3^+$ regulatory T (Treg) cells, which also recognize peptides presented on MHCII, are critical for the prevention of autoimmunity and maintenance of homeostasis.

$CD8^+$ T cells and $CD4^+$ Tconv cells are required for clearance of many pathogens and establish memory populations to quickly and efficiently eliminate subsequent infections of the same pathogen. A major principle of the T cell response is to direct the immune response against the invading pathogen while avoiding collateral damage to self-tissues, a principle known as self-tolerance. $CD8^+$ T cells and $CD4^+$ T cells achieve this goal through a variety of coordinated mechanisms that occur both in the thymus during T cell development and in the peripheral secondary lymphoid organs[5,6]. During thymic development, developing thymocytes undergo V(D)J recombination, resulting in the expression of a unique TCR on the cell surface that are tested for two major features, both affected by the coreceptor CD8 or CD4: 1) sufficient interaction with self MHC molecules, endogenous proteins that complex with small, protein-derived peptides expressed on the cell surface, and 2) low reactivity to self-peptide:MHC complexes. These features ensure that the TCR of interest has specificity to endogenous MHC molecules yet does not exhibit strong reactivity to self-peptide:MHC complexes. If these features are not met, the thymocyte expressing the TCR of interest, or T cell clone, can undergo distinct fates, including death by neglect, negative selection via apoptosis, or divergence into alternative cell lineages[7]. One of these alternative cell lineages is $CD4^+$ $Foxp3^+$ Treg cells[8]. Upon exiting the thymus and seeding into

peripheral secondary lymphoid organs, Foxp3$^+$ Treg cells act in trans to suppress self-reactive CD8$^+$ T cells and CD4$^+$ Tconv cells populating the peripheral repertoire, a key mechanism to maintaining homeostasis and resolving inflammatory responses after pathogen clearance. Differentiation into the Foxp3$^+$ Treg cell lineage can also occur in the periphery, particularly for T cell clones reactive to non-harmful microbes[9]. In this setting, upon engagement with cognate peptide:MHCII, CD4$^+$ Tconv cell clones reactive to antigens derived from certain non-harmful microbes are instructed to upregulate Foxp3 and differentiate into Treg cells based on environmental cues, such as TGF-β and APC type[10,11]. It is hypothesized that peripheral Treg differentiation ensures beneficial commensal species are maintained and not expelled, and serves as a mechanism to divert CD4$^+$ Tconv cells away from alternate effector T helper states, both key in maintaining host physiology and immune homeostasis[8]. Other mechanisms of self-tolerance in the periphery include ignorance, where self-peptides are not presented or sequestered from recognition, and anergy, a cell intrinsic state of hypoactivation induced by repeated or continuous TCR signaling[6]. Maintaining self-tolerance is critical, as a break in any of the mechanisms described above can contribute to autoimmune disease.

Defining the relationship between adaptive immune cells and tumorigenesis

While T cell responses directed against self-tissues are not desired in many contexts and are the underlying cause for many autoimmune diseases, since the late 1800s it has been suggested that an inflammatory response, induced by bacterial infection or mimicked through administration of a mixture of heat-killed bacteria known as "Coley's toxins", can promote tumor regression in some subjects[12]. More recent data from clinical samples and mechanistic studies in mouse models have demonstrated a vital role for T cells in an effective anti-tumor immune response, resulting in

immune-mediated tumor destruction under distinct settings. In early days, this idea was conceptualized in the immunosurveillance hypothesis proposed by Burnet, which postulates that T cells evolved partly to prevent cancers by constantly surveying and eliminating emerging tumor cells[13]. More recently, the model has been revised to reflect emerging data demonstrating a role for T cells in shaping a developing tumor, known as the immunoediting hypothesis.

The immunoediting hypothesis states that a developing tumor can be shaped by the T cell-mediated anti-tumor response, which acts to eliminate tumor clones that display highly antigenic peptides via MHC, rendering the tumor less immunogenic over time[14]. Neo-antigens arise through mutations in the cancer cell DNA, leading to expression of an altered self-peptide that is novel to the endogenous T cell repertoire and therefore recognized as a foreign peptide. Early research in mouse models addressing the immunoediting hypothesis include studies which demonstrated that carcinogen-induced tumors derived from immunocompromised mice are more immunogenic than those derived from immune-competent mice[15]. In these studies, *Rag2*$^{-/-}$ mice lacking B cells and T cells were more susceptible to sarcomas induced by the chemical carcinogen methylcholanthrene (MCA) compared to wild-type mice with an intact immune system. Additionally, MCA-induced sarcomas derived from *Rag2*$^{-/-}$ were rejected when injected in immunocompetent wild-type hosts. In contrast, tumors derived from wild-type mice continued to grow when transplanted into secondary wild-type hosts, suggesting that MCA-induced tumors that grew initially in the absence of adaptive immunity were more immunogenic than those derived from immune-competent mice. While evidence of immunoediting in human tumors is limited, some recent studies report supportive observations. First, analysis of genomic datasets of solid tumor biopsies found downregulation of HLA expression or loss-of-function mutations in HLA and β2m[16]. Furthermore, loss of HLA heterozygosity, and therefore reduced potential of neo-antigen presentation, was

observed in a subset of non-small cell lung cancers and lung adenocarcinomas[17]. Interestingly, lung adenocarcinomas with HLA loss of heterozygosity had higher T cell infiltration than those that did not, suggesting that loss of HLA heterozygosity was in response to the presence of a strong T cell response. Together, these data suggest that cancers that develop in patients are under selective pressures to be less immunogenic to avoid detection by the immune system. Finally, the predicted heterogeneity of tumor-derived neo-antigens was suggested to influence prognosis and response to checkpoint blockade therapy for patients with non-small cell lung cancer[18]. These studies suggest tumor heterogeneity can be a major factor in influencing the impact of immunoediting.

To provide a mechanistic framework for the immunoediting hypothesis, the cancer-immunity cycle has emerged over the past decade as a model to conceptualize key findings and ideas, from expression of tumor-associated proteins to priming and activation of tumor-specific T cells[19]. The genomic alterations associated with and contributing to tumorigenesis can lead to tumor cell expression of mutated or aberrantly expressed proteins. These altered proteins serve as a source of tumor-associated antigens that are acquired, processed, and presented by APCs for recognition by $CD8^+$ or $CD4^+$ T cells in the draining lymph node. Upon successful T cell priming, T cells specific for tumor-associated antigens are activated, proliferate, differentiate, and exit the lymph node to traffic to the tumor site. There, effector T cells have the capacity to induce tumor control via release of cytolytic molecules or production of anti-tumor modulatory factors. Each step of the proposed cancer-immunity cycle can be modulated by distinct stimulatory or inhibitory factors, and therefore has the potential to be manipulated therapeutically[19]. For example, once resident within tumors, the release of cytolytic molecules or other factors by activated T cells can be modulated by the cell surface expression of numerous co-stimulatory and co-inhibitory

receptors. Interrupting co-inhibitory receptor-ligand axes is the target of many emerging therapies known as checkpoint blockade, which aims to promote tumor destruction by blocking the co-inhibitory signal to direct a robust T cell-mediated inflammatory response (discussed below)[20]. Many checkpoint blockade therapies, including anti-PD-1 and anti-CTLA-4, have been approved for multiple cancer types, demonstrating that T cells can be successfully targeted and mobilized for therapeutic benefit in human subjects.

Immunotherapy: Harnessing the endogenous immune response for clinical benefit

The concept that T cell responses can promote an anti-tumor response is the foundation for the emerging set of treatments known as immunotherapy. The goal for many immunotherapy treatments is to induce and mobilize a robust immune response to promote tumor regression. A variety of immune-based treatment strategies are FDA-approved or in clinical trials, including adoptive cell therapy (ACT) using autologous or TCR-transduced tumor-infiltrating lymphocytes[21,22], vaccination approaches that target tumor-associated antigens[23,24], and checkpoint blockade[20]. Checkpoint blockade utilizes monoclonal antibodies specific for negative regulators or their ligands to block the negative feedback signaling pathways on activated T cells. Since the 1990s, various immune molecules such as CTLA-4 and PD-1 have been identified and verified as important negative regulators of an ongoing T cell response, and often referred to as T cell "checkpoints"[25–27]. CTLA-4 expression is inducible on activated T cells and binds B7 molecules with higher affinity and avidity than CD28, the co-stimulatory receptor, thus outcompeting CD28 for ligands and sequestering B7 molecules. PD-1 is also expressed on activated T cells and its ligands are PD-L1 and PD-L2 expressed on hematopoietic and non-hematopoietic cells. Upon ligation, PD-1 provides inhibitory signals to activated T cells. Based on these roles in inhibiting

activated T cells, proof-of-concept studies in mouse models have highlighted the potential of checkpoint blockade therapy where monoclonal antibodies specific for CTLA-4, PD-1, and/or PD-L1 are used to promote an inflammatory response in tumor-associated T cells and induce tumor regression[28,29]. The past 20 years of translational research has been a triumph, as clinical trials have successfully treated cancer patients with checkpoint therapies, leading to FDA-approval of anti-CTLA-4, anti-PD-1, and anti-PD-L1 for use across a variety of tumor types[20]. For many tumor types, up to 20% or more of patients who are treated with checkpoint blockade experience clinical benefit, with a subset of patients maintaining long-term progression-free survival. Furthermore, the panel of emerging antibody therapeutics has expanded to include other inhibitory and activating receptors, such as OX40, 4-1BB, TIM-3, Lag3, and GITR.

Limitations of immunotherapy and potential adverse consequences

Although checkpoint blockade therapy has successfully been implemented in the clinic[20,30,31], a large fraction of patients do not respond to therapy or do not maintain a durable response. Clinical studies demonstrate that a large fraction of non-responders have tumors with minimal T cell infiltrate at baseline, as objective responses are largely restricted to “T cell-inflamed" tumors with a high density of T cell infiltrate at baseline[32–35]. The lack of a substantial T cell infiltrate could be due to inefficient T cell priming in the draining lymph node, defects in T cell trafficking to the tumor, or limited survival of effector T cells within the tumor. Therefore, there has been substantial efforts in recent years to understand the mechanisms restricting or promoting T cell density within tumors, and devising therapeutic strategies to induce a T cell-inflamed phenotype in “cold” tumors. Strategies to promote a T cell-inflamed phenotype include inducing innate cell activation to improve T cell priming, such as through STING agonists,

promoting tumor-associated APCs to secrete chemokines to improve T cell trafficking to the tumor site, and metabolic or epigenetic modulation of the tumor environment to promote T cell survival within the tumor[36]. Emerging strategies also include the specific targeting of immune suppressive cell populations, in the hopes of releasing the cellular restrain on the effector T cell response. In this regard, understanding the functions and biology of tumor-associated regulatory T (Treg) cells are of interest.

While the precise cellular and molecular mechanisms of checkpoint blockade efficacy, and the factors limiting clinical response, are the subject of active investigation, pre-clinical observations utilizing mouse models have demonstrated that an inflammatory immune response may have distinct outcomes, implying that checkpoint blockade may have a detrimental effect depending on the tumor and patient setting. For example, IFN-γ is a canonical cytolytic molecule often associated with a robust effector $CD8^+$ T cell response. Traditionally, IFN-γ is thought to play an anti-tumor role by having a direct effect on tumor cells by inhibiting tumor cell growth, promoting the upregulation of MHCI and neo-antigen presentation for tumor cell killing by tumor-reactive $CD8^+$ T cells, or imparting a transcriptional program that renders tumor cells less fit while promoting T cell infiltration[15,37,38]. However, IFN-γ has also been shown to have a tumor-promoting effect in some contexts, depending on the dose, tumor stage, or treatment setting[39–42]. Beyond IFN-γ, other aspects of T cell-mediated inflammation and T cell-derived factors can contribute to tumor development and progression. In an autochthonous mouse model of breast cancer, IL-4 derived from $CD4^+$ T cells were shown to promote tumor metastasis[43]. Similarly, another study utilizing breast cancer cell lines demonstrated the role of $Foxp3^+$ Treg cells in promoting tumor metastasis via RANKL-RANK signaling to carcinoma cells[44]. Observations of tumor-promoting inflammation is not restricted to animal models. It is well appreciated that

patients with Inflammatory Bowel Disease (IBD), a disease characterized by chronic inflammation of the gastrointestinal tract, are at an increased risk for developing colorectal cancer[45,46]. To mechanistically determine the interaction between inflammation and colorectal cancer, studies in mouse models of intestinal adenomas and carcinomas have demonstrated a role for Foxp3$^+$ Treg cells in promoting tumor development and progression[47,48]. While Treg cells are known for their immunoregulation function, it was demonstrated that Foxp3$^+$ Treg cells can acquire an inflammatory phenotype, particularly upregulation of IL-17A, to promote tumor progression[47,48]. In these studies, transfer of Treg cells from non-tumor-bearing mice provided an anti-tumor effect for host protection, suggesting that the tumor environment fosters a Treg cell population which exhibit a phenotype that is tumor-promoting. These studies and observations highlight the dual role of the immune response in both inhibiting and promoting tumorigenesis (Figure 1). Furthermore, it has been observed that some patients can experience "hyper-progression," a phenomenon characterized by accelerated tumor growth kinetics following immunotherapy[49–53], suggesting that checkpoint blockade has the potential to exacerbate disease in a fraction of patients. Therefore, understanding the impact of promoting or inhibiting a patient's T cell response, whether through checkpoint blockade or other therapeutic modalities augmenting other steps along the cancer-immunity cycle, is critical to improving treatment options and treatment outcomes.

Regulatory T cells: a key regulatory population enriched in the tumor environment

Regulatory T (Treg) cells express the lineage-defining transcription factor Foxp3 and are often found at elevated densities in tumor lesions relative to lymphoid and non-lymphoid sites. Treg cells throughout the body are essential for the prevention of autoimmunity and the maintenance of immune homeostasis, and function by suppressing the activation and

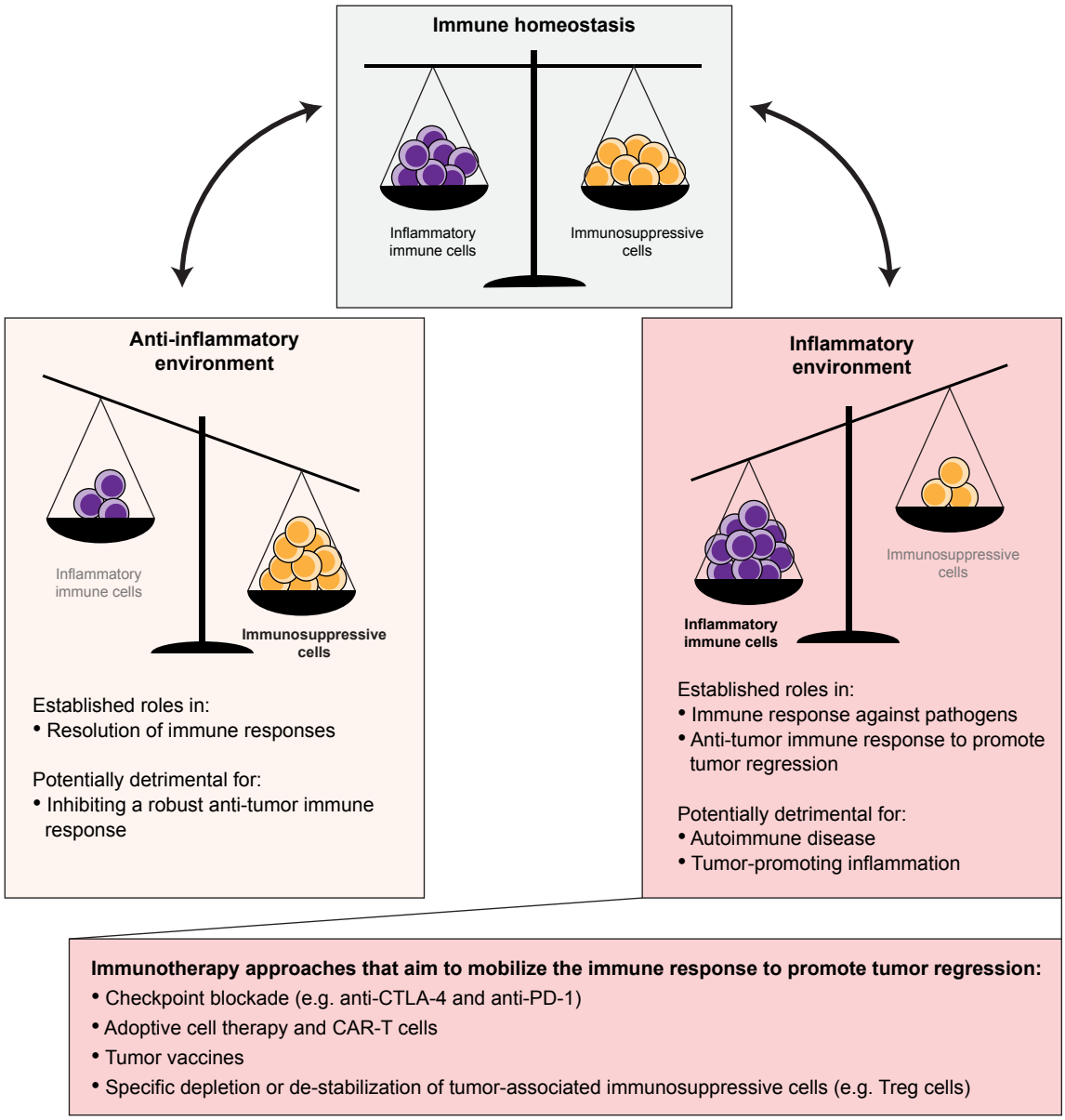

Figure 1. Immune homeostasis in health and disease

In health, inflammatory cells, including effector T cells, and immunosuppressive cells, including Foxp3^{+} regulatory T cells, exist in balance to one another to maintain immune homeostasis (top panel). The immune system must oscillate between an inflammatory environment (right panel) and an anti-inflammatory environment (left panel) at the appropriate time and place to maintain health and prevent disease. For example, an inflammatory response is necessary upon infection with an invading pathogen, while an anti-inflammatory response is critical to resolve inflammatory immune responses to return to homeostasis. Promoting an inflammatory immune environment within a tumor can promote tumor progression, but immune cells can contribute to tumor-promoting inflammation in distinct contexts. These concepts highlight the dual role immune cells can have in both inhibiting and promoting tumorigenesis, and the potential unwanted consequences of therapeutic strategies that aim to promote inflammation in the tumor environment (bottom panel).

differentiation of $CD4^+$ helper T cells and $CD8^+$ cytotoxic T cells reactive to autologous, environmental, or tumor-expressed antigens. Numerous correlative studies have revealed that for some cancers, the density of tumor-infiltrating Treg cells has prognostic significance[54–57], suggesting that Treg cells may have a functional impact on tumor development and progression. Interestingly, in some cancers such as hepatocellular carcinoma, a high Treg cell density is predictive of poor clinical outcome, consistent with the paradigm that Treg cells promote tumor progression by suppressing tumor-specific T cell responses. In contrast, a high Treg cell density is predictive of improved clinical outcome in other cancers such as colorectal carcinoma. While the precise mechanisms driving this association are undefined, these disparate findings suggest that the role of Treg cells in shaping tumorigenesis may be highly context-dependent, varying considerably at different organ sites.

Given the pivotal role of Treg cells in immune suppression and the prevalence of these cells in many human cancers, it is thought that Treg cells constitute a major barrier to therapeutic efforts to mobilize the immune system to induce tumor regression. This idea has spurred concerted efforts to develop modalities to enhance cancer immunotherapies by inducing the selective depletion or modulation of intratumoral Treg cells, while simultaneously leaving Treg cells elsewhere in the body unaffected. However, the functions and mechanisms of tumor-associated Treg cells remains incompletely defined. In recent years there has been a growing appreciation that Treg cells exhibit substantial phenotypic and functional diversity[58–60], highlighting the potential diverse functions and impact of tumor-associated Treg cells. First, Treg cells may promote tumor progression by restricting anti-tumor immunity or by acquiring a pro-inflammatory phenotype. Alternatively, Treg cells may also play a role in inhibiting tumor progression, for example by suppressing tumor-promoting inflammation. Finally, Treg cells may serve non-

immune related functions and module the tumor environment by regulating tissue remodeling, repair, or metabolism. Understanding the function and biology of tumor-associated Treg cells in specific contexts is key as many available and emerging therapies aim to specifically manipulate tumor-associated Treg cells, or the molecular targets are highly expressed on tumor-associated Treg cells, such as PD-1, CTLA-4, OX40, 4-1BB, TIM-3, Lag3, and GITR.

Targeting intratumoral Treg cells to promote tumor regression

The prevailing model in the field dictates that Treg cells support a pro-tumor environment, either by inhibiting the anti-tumor immune response or acquiring a pro-inflammatory phenotype that supports tumor growth, suggesting that depletion or de-stabilization of tumor-associated Treg cells would result in tumor control or tumor regression. Indeed, early studies using mouse models of orthotopic tumors found that systemic Treg cell depletion delayed tumor growth and enhanced tumor control[61,62]. In these studies, transient Treg cell depletion was associated with an increase in tumor-infiltrating effector T cells, and the pro-inflammatory cytokine IFN-γ was shown to be important in promoting tumor control upon Treg cell depletion. However, because depletion of Treg cells was systemic in these models, it is difficult to ascertain the specific functions of Treg cells resident within tumors versus those circulating in the periphery or within lymph nodes. Furthermore, systemic Treg cell depletion cannot be sustained because of autoimmune consequences[63]. Therefore there is great interest in targeting tumor-associated Treg cells for specific depletion or de-stabilization, while leaving Treg cells elsewhere in the body unperturbed to maintain immune homeostasis.

To this end, monoclonal antibodies targeting molecules highly expressed on intratumoral Treg cells have gained attraction as an approach to specifically target tumor-associated Treg cells.

Early studies in mice demonstrated that administration of distinct anti-CTLA-4 antibody clones induced the depletion of intratumoral Treg cells without impacting intratumoral conventional T cells or Treg cells outside of the tumor, resulting in slowed outgrowth of transplantable melanomas[64]. Interestingly, the efficacy of these antibodies was dependent on the presence of tumor-infiltrating myeloid cells expressing activating Fc receptors, implying a role for Fc receptor-dependent, ADCC-mediated Treg cell depletion. In addition, the authors suggested that the selectivity of anti-CTLA-4 antibody in driving the preferential depletion of Treg cells was largely due to the elevated cell-surface expression of CTLA-4 by intratumoral Treg cells relative to conventional T cells within the tumor, a concept that may be broadly relevant for therapeutic antibodies targeting other T cell-expressed receptors. Working in parallel, Selby and colleagues performed similar studies in mice using an anti-CTLA-4 antibody clone of fixed antigen-binding specificity in which the constant region of the antibody was changed to different isotypes known to engage activating Fc receptors with varying affinities[65]. It was found that the therapeutic efficacy of anti-CTLA-4 antibody treatment correlated with the ability of the Fc region to bind activating Fc receptors, again suggesting a role for ADCC in determining *in vivo* antibody activity. These two studies highlight the importance of both the Fab and Fc regions of an antibody in determining the therapeutic efficacy of an antibody of interest. Consistent with these findings, additional studies in mice have demonstrated similar requirements for therapeutic antibodies targeting other T cell-expressed co-receptors such as GITR[66,67] and OX40[68], for which specific antibodies are currently under clinical development for the treatment of human cancer[69].

In addition to ADCC-mediated Treg cell depletion, anti-CTLA-4 blockade was recently demonstrated to promote an altered metabolic and functional state of intratumoral Treg cells in a transplantable mouse model, particularly for Treg cells isolated from a glucose-rich tumor

environment[70]. Compared to a glucose-deplete tumor environment, intratumoral Treg cells isolated from a glucose-rich tumor environment had the capacity to consume more glucose *ex vivo*. Furthermore, anti-CTLA-4 treatment improved survival in mice harboring tumors with a glucose-rich environment, which was associated with an increased percentage of intratumoral Treg cells expressing TNF-α and IFN-γ[70]. Importantly, Treg cells isolated from draining lymph nodes did not exhibit aberrant TNF-α or IFN-γ expression. This study highlights the notion that Treg cells may have unique requirements to function and thrive in the unique milieus associated with cancer, including altered metabolic states as well as tissue remodeling, angiogenesis, and hypoxia[70,71].

While the precise mechanism of anti-CTLA-mediated Treg instability is undefined, Zappasodi et al. provide evidence that the unique requirements of intratumoral Treg cells could be targeted to specifically modulate tumor-infiltrating Treg cells without impacting Treg cells elsewhere in the body. Some of the first work demonstrating this concept came from studies examining the role of neuropilin-1 (Nrp1) expression by Treg cells. Nrp1 is a type I transmembrane protein that is highly expressed by Treg cells and has been suggested to play a key role in Treg cell function[72,73]. Nrp1 functions as a receptor for both vascular endothelial growth factor (VEGF), a critical regulator of blood vessel formation, and semaphorin-4a (Sema4a), a cell-surface protein that has well-defined roles in axonal guidance but is also expressed by dendritic cells, B cells, and T cells. Work from Hansen and colleagues demonstrated that Nrp1-expressing Treg cells migrate in response to tumor-derived VEGF *in vitro*, and showed that Treg-specific deletion of Nrp1 slowed the outgrowth of transplantable and autochthonous tumors without inducing systemic autoimmunity, suggesting a role for Nrp1 expression on tumor-associated Treg cells[74]. Although a direct connection between VEGF production and Treg-specific Nrp1 function has yet to be demonstrated *in vivo*, these findings raise the intriguing possibility that Nrp1 may play a key role

in coordinating Treg cell responsiveness to VEGF-dependent angiogenic signals in the tumor environment. In parallel studies, work from Vignali and colleagues demonstrated that Nrp1 functions as a receptor for Sema4a on Treg cells, and revealed a key role for Nrp1 ligand engagement in maintaining Treg cell functionality within tumors[75,76]. Using mutant mice in which Nrp1 is conditionally deleted on Treg cells, they showed that Nrp1 expression was dispensable for Treg-mediated maintenance of systemic tolerance and immune homeostasis[75]. However, challenge of Nrp1 mutant mice with transplantable B16 melanomas revealed slower tumor outgrowth and enhanced anti-tumor T cell responses, consistent with the findings of Hansen et al. Blockade of the Sema4a-Nrp1 axis using monoclonal antibodies significantly slowed tumor growth, indicating that transient Nrp1 blockade can have measurable effects. Mechanistic analysis showed that tumor-infiltrating Treg cells in Nrp1 mutant mice maintained normal levels of Foxp3 expression, but exhibited a dysregulated transcriptional program and aberrant production of cytokines such as IFN-γ[76], reminiscent of anti-CTLA-4 blockade in mice bearing glycolysis-deficient tumors[70]. Interestingly, loss of Nrp1 was dominant, in that conditional deletion of Nrp1 on 50% of Treg cells induced T cell-intrinsic defects but also led to the dysregulation of the remaining Nrp1-expressing intratumoral Treg cells[76]. Together, these studies in mice demonstrate that disruption of Nrp1 expression by Treg cells specifically affects Treg cell activity in the tumor environment without impacting Treg cell function elsewhere in the body, revealing the existence of a distinct pathway that can be specifically targeted to modulate intratumoral Treg cell activity. Further work will be needed to determine whether Nrp1 signaling plays a key role in Treg cell function in human cancers, and to assess the relative contributions of VEGF and Sema4a-signals in coordinating the activity of Nrp1-expressing Treg cells in the tumor environment.

In other areas of inquiry, Luo et al. demonstrated that the transcription factor Foxo1 antagonizes Treg maturation and tumor infiltration[77]. Using mutant mice in which Foxo1 expression in Treg cells is resistant to downregulation, the authors observed that the homozygous mutant mice exhibited defects in effector Treg cell (eTreg) differentiation associated with decreased Treg cell trafficking to non-lymphoid organs, resulting in autoimmune reactions mediated by $CD8^+$ T cells. Moreover, the outgrowth of transplantable and genetically driven tumors was slowed in homozygous mutant mice, indicative of impaired Treg cell activity and enhanced anti-tumor immunity. Interestingly, the investigators also identified a "sweet spot" in which heterozygosity of the constitutively-activate Foxo1 mutant allele led to enhanced anti-tumor immunity without inducing widespread autoimmunity. Thus, this study identified Foxo1 activity as a key determinant of the differentiation of eTregs, and demonstrated that this axis can be modulated genetically to restrict the trafficking and fitness of intratumoral Treg cells without altering Treg-mediated immune regulation in the secondary lymphoid organs. Given that Foxo1 is an intracellular transcription factor that is widely expressed by many cell types and functions downstream of the PI3K-Akt pathway, it is unclear whether the “tuning” of Foxo1 activity in genetic mouse models can be recapitulated using small-molecule drugs targeting this pathway. Regardless, these data reveal that subtle perturbations in Treg cell signaling can induce major functional changes that dissociate Treg cell function in the tumor environment from Treg cell activity elsewhere in the body.

Collectively, these studies demonstrate that in mice, intratumoral Treg cells exhibit unique requirements for proper function and fitness in the tumor context, and show that these requirements are divergent from the functional requirements of Treg cells tasked with preventing autoimmunity and maintaining immune homeostasis in secondary lymphoid organs. In agreement with this

concept, recent observations from high-resolution surveys have revealed a core set of genes specifically upregulated by Treg cells isolated from a range of human tumors, suggesting a tumor-specific signature that may be common to Treg cells from many cancer types (discussed below). Future studies probing the functional role of these pathways in coordinating intratumoral Treg cell activity, and determining the feasibility of targeting these pathways using antibodies or small-molecule agents will be key to further our understanding of the unique requirements and impact of tumor-associated Treg cells.

Analysis of tumor-infiltrating Treg cells in human cancers

Beyond CTLA-4, CD25, and other well-defined immunomodulatory receptors, an improved understanding of the unique features of tumor-infiltrating Treg cells may provide key insight into the function of these cells in the tumor context, and reveal novel targets for the selective modulation of Treg cells for therapeutic benefit. In this light, recent studies from the last few years report high-resolution surveys of Treg cells infiltrating human cancers. In one study, Plitas et al. performed transcriptional and phenotypic analysis of Treg cells isolated from breast cancer lesions, and compared these to Treg cells isolated from normal breast parenchyma or peripheral blood[78]. The authors found that breast tumors contained elevated percentages of Treg cells relative to normal breast tissue, and that intratumoral Treg cells were highly proliferative and expressed high amounts of CD25, CTLA-4, and PD-1 proteins. RNA sequencing of purified cell populations revealed that the transcriptional profiles of intratumoral Treg cells and Treg cells from normal breast tissue were very similar, suggesting that much of the transcriptional program of breast cancer-infiltrating Treg cells may be associated with residency in mammary tissue. The analysis also revealed that CCR8, a receptor for chemokines such as CCL1 and CCL18, was selectively

expressed by both intratumoral Treg cells and Treg cells in normal breast parenchyma, suggesting that CCR8-dependent signals may be important for Treg cell recruitment, positioning, or function at these sites. Notably, the authors demonstrated that CCR8 protein was also expressed by intratumoral Treg cells from human colorectal carcinoma (CRC), melanoma, and lung adenocarcinoma samples, suggesting that CCR8 may be relevant in multiple cancer types. A recent proof-of-concept study demonstrated that treatment with an anti-CCR8 antibody was capable of promoting intratumoral Treg cell depletion and tumor regression in a small panel of transplantable tumor mouse models, providing pre-clinical evidence that CCR8 can be targeted therapeutically to promote tumor regression[79].

In parallel studies, De Simone and colleagues analyzed bulk Treg cells and $CD4^+$ T helper cell subsets isolated from CRCs and non-small-cell lung cancers (NSCLC), enabling a direct comparison of the transcriptomes of Treg cells from cancers originating at different organ sites[80]. Interestingly, this revealed a set of transcripts that were preferentially upregulated by Treg cells in both CRC and NSCLC compared to Treg cells and conventional T cells from normal non-lymphoid tissues and blood. Single-cell analysis of intratumoral Treg cells using quantitative PCR confirmed that many of these signature genes were also upregulated in Treg cells isolated from other cancer types, including breast cancer, gastric cancer, and metastases of NSCLC and CRC. In addition, Zheng and colleagues performed single-cell RNA sequencing of T cells isolated from the blood, tumor, and normal tissue of patients with hepatocellular carcinoma[81]. Transcriptional analysis of single FOXP3-expressing Treg cells identified ~400 genes that were preferentially upregulated by intratumoral Treg cells relative to Treg cells isolated from normal adjacent tissue. Importantly, Zheng et al. performed a meta-analysis and noted that 31 genes in the intratumoral Treg cell signature were identified in the three human studies highlighted here, as well as a fourth

study of cells isolated from human melanomas[82], indicating that intratumoral Treg cells isolated from different cancer types may express a conserved "tumor specific" Treg cell signature. This signature includes many genes encoding well characterized immunomodulatory cell-surface receptors, including CTLA-4, GITR, 4-1BB, TIGIT, OX40, ICOS, and CD27. Given that these markers are also expressed by a fraction of Treg cells throughout the body, these proteins may represent the "usual suspects" that appear in the conserved tumor-specific Treg cell signature based on upregulation in the tumor environment. Importantly, the conserved 31-gene signature also includes genes encoding proteins not previously implicated in tumor-infiltrating Treg cell biology, such as *MAGEH1* (encoding a type II MAGE family protein of unknown function), *IL1R2* (encoding a decoy receptor for IL-1), *TFRC* (encoding a transferrin receptor), *FCRL3* (encoding an Fc receptor-like protein), and *CCR8*. It remains unknown whether these proteins are important for Treg cell function in the tumor environment, or reflect adaptation required to survive and thrive within neoplastic lesions.

Beyond the characterization of transcriptional profiles, the single-cell RNA sequencing studies of Zheng et al. provided a unique glimpse into Treg cell clonality within human tumors. The investigators were able to determine αβTCR sequences for the majority of single Treg cells, which revealed that a substantial fraction of intratumoral Treg cells expressed αβTCRs that were found recurrently in a given tumor. In contrast, Treg cells isolated from peripheral blood and intratumoral conventional T cells exhibited diverse αβTCR sequences with few recurrent clones. In accordance with this, Plitas et al. utilized βTCR sequencing of bulk T cell populations to demonstrate that breast cancer-infiltrating Treg cells exhibited reduced clonal diversity relative to naive-phenotype peripheral Treg cells[78]. These findings provide direct evidence of expansion or enrichment of distinct Treg cell clones in human tumors, a finding that is consistent with previous

work in mice suggesting that developing tumors drive the enrichment of oligoclonal Treg cell populations[83]. While the specificity of tumor-infiltrating Treg cells in patients remain largely unknown, studies in mice suggest that at least some clonally expanded Treg cell clones are reactive to organ-specific self-peptides that are expressed and presented by APCs at steady-state and upregulated in the tumor setting[83]. These findings suggest that the enrichment of some oligoclonal Treg cells in the tumor environment may be partly due to reactively to self-antigens, rather than antigens unique to the tumor environment.

Taken together, these studies demonstrate that in the human cancers analyzed thus far, the transcriptional program of tumor-infiltrating Treg cells may represent a composite signature blending a tissue-specific signature associated with the organ of cancer origin with an additional tumor-specific signature that may be common to Treg cells from many cancer types (Figure 2). These findings pave the way for future mechanistic studies probing the functional role of these pathways in coordinating intratumoral Treg cell activity, and determining the feasibility of targeting these pathways using antibodies or small-molecule agents. Furthermore, it will be key to determine the impact of modulating various aspects of tumor-associated Treg cell biology in either promoting tumor regression or enhancing tumor development and progression. Understanding the cellular and molecular mechanisms of tumor-associated Treg cell biology, whether immune-related or immune-independent functions, is critical to determine best strategies of modulating them therapeutically and to identify optimal contexts for particular therapeutic strategies.

Beyond immune suppression: newly defined functions of Treg cells in non-lymphoid tissues

In recent years, a growing number of studies have revealed unique functions of Foxp3$^+$ Treg cells in non-lymphoid sites that appear to be independent of their well-defined roles in

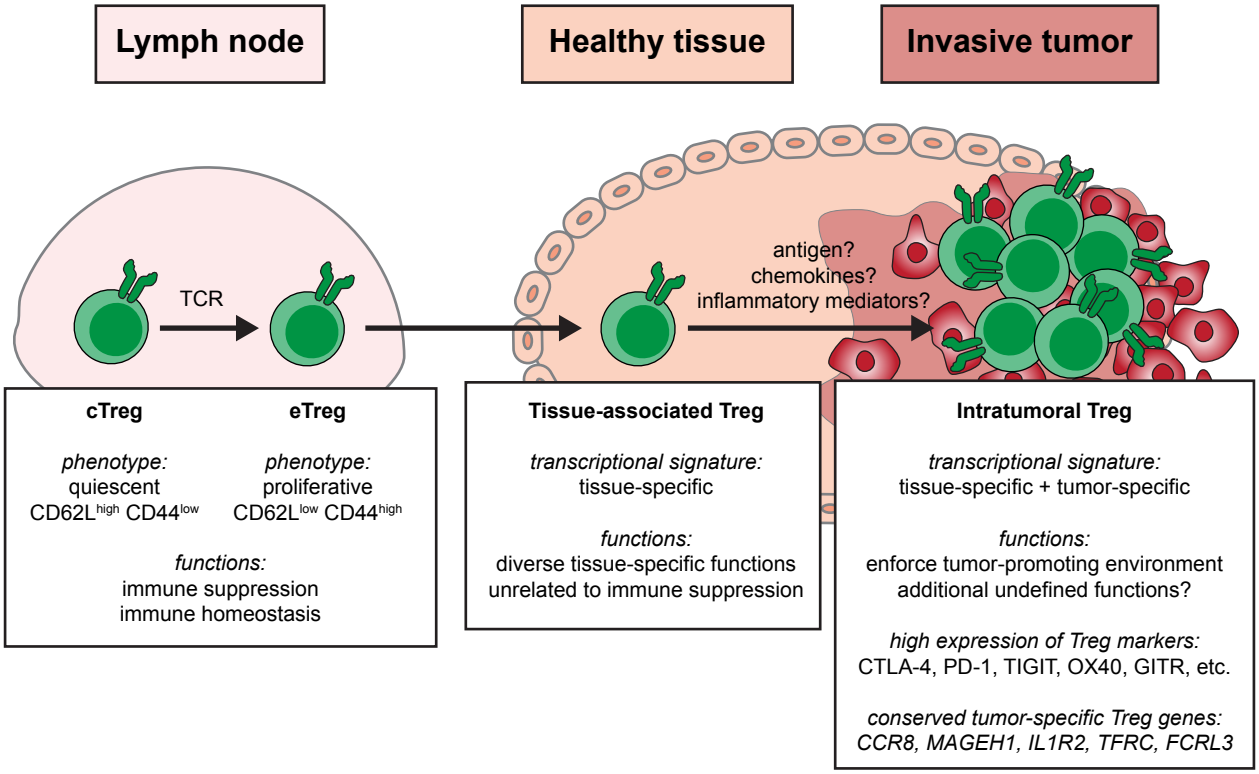

Figure 2. Hallmarks of tumor-infiltrating Treg cells

A conceptual model highlighting the phenotypic and functional diversity of Treg cells in lymphoid organs, nonlymphoid tissue sites, and tumor lesions is shown. cTreg cells and eTreg cells in the lymph nodes and spleen are thought to mediate the suppression of autoimmune reactions and the maintenance of immune homeostasis. cTreg cells are characterized by a quiescent "naive" phenotype and can differentiate into activated-phenotype eTreg cells in a TCR-dependent process. Tissue-associated Treg cells present in different nonlymphoid sites exhibit tissue-specific transcriptional programs unique to the tissue of residence, and they can mediate diverse context-dependent functions that are independent of immune suppression. The mechanisms driving Treg cell enrichment and expansion within tumors are unknown but may involve responsiveness to antigen, chemokines, and inflammatory mediators. Intratumoral Treg cells are characterized by the following hallmarks: 1) evidence of oligoclonal expansion; 2) a composite transcriptional signature that blends a tissue-specific Treg cell signature associated with the tissue of cancer origin with a conserved tumor-specific signature that is common to Treg cells from different cancer types; 3) high expression of common Treg markers known to function as immunomodulatory receptors, including CTLA-4, PD-1, TIGIT, OX40, and GITR; and 4) expression of transcripts encoding proteins with undefined roles in intratumoral Treg cell biology, including CCR8, MAGEH1, IL1R2, TFRC, and FCRL3. Beyond suppression of antitumor T cell responses, additional functions of intratumoral Treg cells have yet to be clearly defined. The arrow suggests a precursor–product relationship, which has been defined for the cTreg-to-eTreg cell transition, but remains hypothetical for tissue-associated and intratumoral Treg cell populations.

suppressing adaptive immunity and maintaining immune homeostasis. While the relevance of these functions to tumor-associated Treg cells is highly speculative at this time, these findings expand our view of Treg cell functional diversity, suggest that the functions of intratumoral Treg cells may be manifold and context-dependent, and force a re-visitation of the paradigm that the primary function of tumor-infiltrating Treg cells is to suppress anti-tumor immunity.

In seminal work, Mathis and Benoist demonstrated that Treg cells play a key role in regulating obesity-related inflammation of the visceral adipose tissue (VAT)[84–86]. The investigators showed that the densities of Treg cells in the VAT are greatly diminished in insulin-resistant mouse models of obesity, and that sustained expansion of Treg cells induced normalization of blood glucose levels in mice fed a high fat diet, indicating that Treg cells can affect adipose-associated inflammation and metabolic function. The investigators used transcriptional profiling to reveal that VAT Treg cells preferentially express an array of transcripts not typically expressed by Treg cells at other sites, and showed that at least two of these factors are critical for the optimal accumulation of Treg cells in VAT. First, it was shown that PPAR-γ, a receptor that is important for adipocyte differentiation, is highly expressed by VAT Treg cells and is required for Treg cell enrichment in adipose tissue. Second, it was shown that the majority of VAT Treg cells express the IL-33 receptor ST2, and that Treg cell density in the VAT was diminished in ST2-deficient mice. Notably, IL-33 has been shown to function as an "alarmin" that triggers inflammatory responses when released from stressed or dying cells[87], suggesting a role for the IL-33/ST2 axis in driving the homing and/or expansion of Treg cells at sites of tissue damage. Together, these studies laid the groundwork for a paradigm suggesting that Treg cells at non-lymphoid sites mediate functions that are independent of immune suppression, express unique

gene expression profiles that are required for optimal function and fitness in the local environment, and are responsive to antigen-independent inflammatory mediators[58].

In other areas, additional work has defined a unique role for Treg cells in promoting tissue repair in non-lymphoid organs[88,89], and identified Amphiregulin (Areg) as a key factor produced by Treg cells at sites of tissue damage. In one study, Burzyn and colleagues demonstrated that clonally expanded Treg populations accumulate in acutely injured muscle tissue and in the damaged muscle of *Dmd* mutant mice, a mouse model of muscular dystrophy[89]. Transient depletion of Treg cells impaired muscle repair, and was associated with increased cellular infiltrates, increased fibrosis, and a failure of myeloid cells to switch to a pro-regenerative phenotype. As with VAT-associated Treg cells, muscle-infiltrating Treg cells exhibited a unique transcriptional program that was distinct from splenic Treg cells. One of the genes preferentially expressed by muscle-infiltrating Treg cells was the gene encoding Areg, an epidermal growth factor (EGF) family ligand that signals through the EGF receptor system. Treg cells were found in close proximity to regenerating muscle myofibers *in situ*, and promoted the differentiation of muscle satellite cells *in vitro*, suggesting that Treg cells may function to promote muscle regeneration in part by direct communication with muscle progenitor cells. In a separate study, Arpaia and colleagues generated mice with Treg-specific deletion of Areg and examined the impact of this deficiency on immune regulation and tissue repair in the lung in the context of an ongoing viral infection[88]. Notably, the authors found that Areg expression by Treg cells was dispensable for the maintenance of immune homeostasis and the regulation of virus-specific T cell responses. In contrast, Areg mutant mice exhibited increased tissue damage and a rapid decline in lung function following influenza virus infection, demonstrating that Treg cells restrict tissue damage via Areg production in this setting. Additional mechanistic data revealed that Areg

production by Treg cells *in vitro* was triggered by exposure to IL-18 and IL-33, but not by TCR stimulation, suggesting that TCR-independent cues in the microenvironment may be the primary drivers of Areg production by Treg cells. In follow-up studies, Green et al. demonstrated that T cells, including Treg cells, isolated from the lungs of mice inoculated with a lung cancer cell line express Areg[90]. T cell specific loss of Areg led to slowed tumor growth, suggesting that Treg-derived Areg can contribute to tumor growth. Taken together, these findings raise the intriguing possibility that a key function of intratumoral Treg cells in lung cancers and other solid cancers may lie in regulating tissue remodeling and repair through the production of Areg and other factors. Notably, the studies of Plitas et al. revealed that Areg is significantly upregulated by a subset of intratumoral Treg cells in breast cancer lesions isolated from patients[78], lending credence to this idea.

Finally, a recent study by Ali et al. further expanded the newly defined roles of tissue-associated Treg cells, demonstrating a pivotal role for skin-resident Treg cells in promoting the differentiation of hair follicle stem cells (HFSCs)[91]. The authors demonstrated that Treg cells are localized in close proximity to the HFSC niche within hair follicles, and that inducible ablation of Treg cells suppressed hair growth. Interestingly, it was also shown that Treg cell expression of Jagged1 (Jag1), a Notch ligand that is highly expressed by Treg cells at this site, was required for optimal HFSC proliferation and induction of the active growth stage of hair follicle formation. Thus, these findings suggest a model in which skin-associated Treg cells function at steady state to promote hair follicle development via engagement of Notch receptors on HFSCs. Interestingly, Notch pathway activation or inhibition has been implicated as a driver of tumorigenesis in some human malignancies, including melanoma[92–94]. These concepts raise the possibility that Treg cells

may shape cancer development by direct cell-cell crosstalk with cancer cells or cancer stem cells via Jag1-Notch interactions.

Collectively, the studies discussed above highlight our expanding view of the functional diversity and specialization of Treg cells in distinct tissue environments throughout the body, and reveal broad principles regarding Treg cell biology in non-lymphoid tissues. Specifically, tissue-associated Treg cells can respond to antigen-independent inflammatory mediators, and express unique gene expression profiles that are required for optimal function and survival in the local environment. From a functional standpoint, tissue-associated Treg cells exhibit diverse functions that are independent of immune suppression; these functions may include conserved mechanisms such as the augmentation of tissue repair via Areg production, or specialized tissue-specific functions such as metabolic regulation or stimulation of stem cell differentiation. The finding that the transcriptional programs of intratumoral Treg cells from various human cancer types are similar to the programs of their Treg cell counterparts in normal adjacent tissue suggests that the principles defined for tissue-associated Treg cells may be directly relevant for Treg cell activity in the tumor context. This suggests that the functions of intratumoral Treg cells may be diverse and highly context-dependent, and highlights a key need to examine additional functions of tumor-infiltrating Treg cells beyond their defined roles in the suppression of anti-tumor immunity.

Carcinogen-induced head and neck cancer: an archetypal cancer for understanding anti-tumor immunity

Head and neck cancers (HNCs), which are cancers that arise in the head and neck region, including but not limited to the nasal cavity, the pharynx, and the oral cavity, are the seventh most common cancer worldwide and accounts for 3-4% of all cancers in the United States[95]. While a

fraction of HNCs are associated with human papillomavirus (HPV) infection, a large proportion of HNCs are HPV-negative and associated with heavy smoking, suggesting these cancers are carcinogen-induced. Indeed, genomic analysis of HPV^+ and HPV-negative HNCs reveal distinct gene expression profiles and mutational profiles[96–98], suggesting HPV^+ and HPV-negative HNCs have distinct etiologies. Current strategies to treat HNCs include surgery, radiation therapy, chemotherapy, and/or targeted therapy such as immunotherapy[95], but even with a variety of treatment options, prognosis has not improved. Therefore, there is a critical need to improve and expand the available treatment options for patients. A key gap in knowledge in this quest is the understanding of immune cells and the immune response in HNC. Although the role of the immune response in HNC is largely unknown, several lines of observation suggest carcinogen-associated HNC represents an intriguing cancer type to understanding the immunological factors impacting tumor progression and response to therapy. First, HPV-negative HNCs harbor a high mutational load[99–101], leading to a higher likelihood for the generation and expression of neo-antigens for recognition as foreign by effector T cells[14]. Second, gene expression analysis of patient samples reveal the upregulation of immune response and immune related genes, as well as detection of infiltrating T cells in a subset of HPV-negative HNCs by immunohistochemistry (IHC)[97,101,102], suggesting an ongoing T cell response in a subset of HPV-negative HNC. Third, clinical trials report that a proportion of patients respond to anti-PD-1 treatment[103,104], indicating that the immune response can be mobilized for an anti-tumor immune response.

While it is clear immune cells, and in particular T cells, are associated with carcinogen-induced HNCs in some circumstances, the role of the immune system is largely unknown in this context. At steady state, it is not known if the immune system promotes the progression of carcinogen-associated HNC, slows progression, or has little impact. Moreover, recent studies

suggest that HNC may have a unique immune cell infiltrate, warranting a closer examination of the cellular players that impact tumor progression. First, early data suggest that while T cell-inflamed cancers are more responsive to anti-PD-1 therapy overall, some smoking-associated HNC patients have T cell-inflamed tumors at baseline but do not respond to immunotherapy[104], suggesting that a T cell-inflamed tumor at baseline is necessary but not sufficient for effective response to immunotherapy. Second, a study of HNC patients treated with anti-PD-1 or anti-PD-L1 therapy reported that over 25% of patients experienced "hyper-progression" characterized by accelerated tumor growth kinetics following therapy[53], suggesting that checkpoint blockade may accelerate disease in a fraction of patients. Third, prognostic studies have revealed that high intratumoral Treg cell density is associated with a favorable prognosis for a fraction of HNC patients[56,101,105,106], a finding inconsistent with the notion that intratumoral Treg cells promote HNC and negatively impact clinical outcome by suppressing tumor-reactive effector T cells. These reports demonstrate that the processes governing endogenous anti-tumor immunity and the response to therapy are likely to vary based on a variety of factors such as host genetics, cancer genetics, the microbiota, as well as the local tissue environment, and highlight a critical need for mechanistic insight in tractable animal models that accurately mimic carcinogen-induced HNSCC development and progression.

Approach to understanding the impact of the endogenous immune response to HNC

As discussed above, there is a critical need to understand the adaptive immune response to HNC and the functional cell types involved to continue to improve therapies for HNC that target the relevant molecular and cellular players. Traditionally, pre-clinical studies in mice have relied on the use of transplantable tumor cell lines or genetically engineered cancer models[107]. However,

these models do not recapitulate some aspects of human cancer. For example, many transplantable tumor models involve injection of tumor cells at an ectopic site and the resulting tumors are clonal, fast growing, and do not contain the high mutational loads of many carcinogen-induced cancers such as HPV-negative HNC. Furthermore, although tumors from genetically engineered mouse models develop in situ, the genome of each cancer cell is altered in a similar manner and engineered alterations typically occur in both transformed cells and non-transformed neighboring cells. Therefore, there are potential limitations in the physiological accuracy of these model systems when it comes to mimicking human tumor development and heterogeneity. To overcome these obstacles, the approach utilized in this project is an autochthonous mouse model of carcinogen-induced oral squamous cell carcinoma (OSCC), a major subtype of HNC. In this model, C57Bl/6 mice are exposed to the chemical carcinogen 4-nitroquinoline N-oxide (4-NQO) for 20 weeks to induce oral lesions in the tongue epithelium[108–112]. Importantly, previous studies have reported that the progression and histopathology induced in the tongue epithelium by 4-NQO exposure closely resembles that of human HPV-negative OSCC, including characteristic progression from pre-neoplastic dysplasia to invasive OSCC[108,111,113–115]. Therefore, the 4-NQO mouse model provides a physiologically accurate and tractable system to understand the relationship between the endogenous immune response and carcinogen-induced OSCC by allowing for mechanistic studies not possible in humans.

MATERIALS AND MATHODS[b]

Patient samples

Two OSCC transcriptomic data cohorts of patients with locoregionally advanced disease were utilized, The Cancer Genome Atlas–Head-and-Neck Squamous Cell Carcinoma (TCGA-HNSC) data set[96] restricted to HPV-negative OSCC data (n = 259) and the Chicago HNC (head and neck cancer) Genomics Cohort (CHGC)[97] restricted to HPV-negative OSCC data (n = 78). Only tumors of oral cavity were included to the analysis, while other anatomical sites (larynx, hypopharynx, oropharynx and tonsil) were excluded. Transcriptomic data of patients with kidney renal clear cell carcinoma (n = 535), liver hepatocellular carcinoma (n = 374), lung adenocarcinoma (n = 527), and melanoma (n = 471) are based upon data generated by the TCGA Research Network: https://www.cancer.gov/tcga.

Mice

The following mice were purchased from the Jackson Laboratory, and bred and maintained at the University of Chicago under specific pathogen-free conditions: B6 (C57BL/6J) mice, Foxp3-DTR (B6.129(Cg)-*Foxp3*$^{tm3(DTR/GFP)Ayr}$/J) mice, *Tcrb* $^{-/-}$ *x Tcrd* $^{-/-}$ (B6.129P2-*Tcrb*^{tm1Mom} *Tcrd*^{tm1mom}/J) mice, *Ighm*$^{-/-}$ (B6.129S2-Ighm^{tm1Cgn}/J) mice, *Pdcd1-/-* (B6.Cg-Pdcd1$^{tm1.1Shr}$/J) mice, *Rag1*$^{-/-}$ (B6.129S7-*Rag1*^{tm1Mom}/J) mice, *Tcra*$^{-/-}$ (B6.129S2-*Tcra*^{tm1Mom}/J) mice, CD4-Cre (B6.Cg-Tg(Cd4-cre)1Cwi/BfluJ) mice, *Foxp3*^{GFP} (B6.Cg-*Foxp3*^{tm2Tch}/J) mice, and *Ifngr1-/-* (B6.129S7-Ifngr1^{tm1Agt}/J) mice. "TCRβtg" mice expressing a fixed TCRβ chain of sequence TRBV26-

[b] Much of this section is reproduced, with modifications, from Chao, J.L., Korzinkin, M., Zhavoronkov, A., Ozerov, I., Higgins, K., Lingen, M.W., Izumchenko, E., and Savage, P.A. "Effector T Cell Responses Unleashed by Regulatory T Cell Ablation Promote Progression of Oral Squamous Cell Carcinoma" *Submitted*.

ASSLGSSYEQY were generated as described previously[83]. All mice were generated on a pure B6 background or were fully backcrossed to the B6 background. All mice were bred and maintained under specific pathogen-free conditions in accordance with the animal care and use regulations of the University of Chicago. Mice for experiments were age-matched, cage-mates, and littermates when possible, and assigned to experimental groups randomly and based on genotype, when appropriate. Both male and female mice were used for experiments, as appropriate.

Cell lines and bacteria

Drosophila S2 cells were used for recombinant production of I-A^b; cells were transfected according to the Drosophila Expression System manual (Thermo Fisher) in Schneider's Drosophila medium supplemented with 10% FBS, 1X Pen/Strep (100 U/mL penicillin, 0.1 mg/mL streptomycin), and 20 μg/mL gentamicin, and maintained in stationary cultures at 27°C. S2 transfectants were selected with 25 μg/mL Blasticidin, and stable lines were expanded for expression in Express Five SFM supplemented with 25 μg/mL Blasticidin, 1X Pen/Strep, and 20 μg/mL gentamicin, in suspension culture shaking at 120 rpm and 27°C. Plat-E cells (Cell Biolabs) were used for retroviral packaging of TCRα-containing pMGflThy1.1 plasmid; cells were grown in Dulbecco's Modified Eagle's Medium 14 (Gibco) supplemented with 10% FBS, 1X Pen/Strep, 10 μg/mL Blasticidin, and 1 μg/mL Puromycin and maintained in stationary cultures at 37°C. Plat-E transfectants were cultured in the absence of Blasticidin and Puromycin. E. coli DH5α (New England Biolabs) was used for cloning and propagation of TCRα-containing pMGflThy1.1 plasmid.

Deconvolution of bulk transcriptomic profiles

Pre-processed gene expression data was loaded into the version of iPANDA algorithm[116,117] with disabled gene grouping and topological weights. The 'off' state of topology coefficients means that they are equal to 1 for all genes during the calculation. The 'off' state for the gene grouping means that all the genes are treated as individual genes. Deconvolution was performed using a collection of differentially expressed genes that facilitate annotation of the four T-cell subtypes as naive-like, regulatory, cytotoxic, and exhausted[118], and the estimated proportion of each subtype was calculated for each sample [119]. Activation signs for all the genes was obtained from Puram et al.[118] and iPANDA algorithm was used for the dimension reduction in gene expression data prior to the clustering and data visualization[117]. In order to validate the results, another deconvolution algorithm, xCell[120], was used. The "xCell" R package (version 1.12) was used to generate immune estimates for the xCell method[120]. A general immune estimation score for cases from TCGA cohort was already generated by xCell and is publicly available. For comparison purposes, only cell types which could be detected by both iPANDA and xCell were used for validation.

Administration of 4-NQO

For most experiments, 6-8 week old mice were administered 4-NQO in their drinking water for a continuous period of 20 weeks. In some experiments, mice were administered 4-NQO in their drinking water for a continuous period of 8 weeks, then supplied normal drinking water for an additional 12 weeks or 24 weeks, and mice were analyzed 20 weeks or 32 weeks, respectively, after start of 4-NQO treatment. For stock solution, 4-NQO powder (Sigma) was dissolved in DMSO at a 50 mg/mL concentration and stored at -20°C until use. Stock solution was dissolved

in propylene glycol (Sigma) and added to drinking water for a final concentration of 100 μg/mL 4-NQO in 0.6% propylene glycol. 4-NQO drinking water was replaced weekly.

Tongue tissue histology and immunohistochemistry

Tongues were isolated and fixed in 10% buffered formalin (Sigma) for 24-48 hours then longitudinally bisected and embedded in paraffin. Consecutive 5 μm sections were stained with hematoxylin and eosin (H&E) for blinded histopathological analysis or processed for immunohistochemical detection of CD3, Foxp3, pSTAT1, or Ki-67 antigens using anti-CD3 (clone SP162, Sigma-Aldrich), anti-Foxp3 (clone FJK-16s, Invitrogen), anti-pSTAT1 (Tyr701) (clone 58D6, Cell Signaling), anti-Ki-67 (clone SP6, Thermo Scientific) antibodies, respectively. Slides were scanned at 40X using the Aperio ScanScope XT and viewed and analyzed on the accompanying software ImageScope. Tissue processing, staining, and digital scanning was performed by the Human Tissue Resource Center at University of Chicago. To analyze histopathology incidence, each H&E slide was scored once based on the most severe grade present, using established criteria[108]: normal epithelium, hyperkeratosis, dysplasia, or invasive squamous cell carcinoma. To analyze histopathology burden, the epithelial perimeter of each tongue was outlined, and each region was scored as normal epithelium, hyperkeratosis, dysplasia, or invasive squamous cell carcinoma. In this way, each histological grade defined a certain percentage of the total perimeter of the sample. For immunohistochemistry quantification, images were captured at 40X and positive cells were counted in an automated fashion in ImageJ[121] using the following macro code (written to iterate over all images in a given directory):

```
dir = getDirectory("Choose a Directory to PROCESS");
list = getFileList(dir);
dir2 = getDirectory("Choose a Directory for SAVING");
//setBatchMode(true);
```

```
for (f=0; f<list.length; f++) {
path = dir+list[f];
if (!endsWith(path,"/")) open(path);
if (nImages>=1) {
if (endsWith(path,"f")) {

//dir=getDirectory("select folder to save images"); // Find
T=getTitle;
run("Properties...", "channels=1 slices=1 frames=1 unit=um pixel_width=0.249 pixel_height=0.249 voxel_depth=0.249 global");


run("Colour Deconvolution", "vectors=[H DAB]");
selectWindow(T+"-(Colour_2)");  // selecting the brown window, i.e. the one with the positive IHC stain

setAutoThreshold("Default");
setThreshold(0, 105);
// CD3 IHC = setThreshold(0, 105) ; Foxp3 and Ki-67 IHC = setThreshold(0, 100) ; pSTAT1 IHC = setThreshold(0, 150)
run("Convert to Mask");
run("Make Binary");
run("Fill Holes");
run("Despeckle");
run("Watershed");

rename(T + " IHC+ cells");
run("Analyze Particles...", "size=15-Infinity circularity=0.01-1.00 display exclude clear summarize add");
// Foxp3 and pSTAT1 IHC: "size=5-Infinity circularity=0.01-1.00 display exclude clear summarize add" ; CD3 IHC: "size=15-Infinity circularity=0.01-1.00 display exclude clear summarize add" ; Ki-67 IHC: "size=6-Infinity circularity=0.01-1.00 display exclude clear summarize add"
selectWindow(T);
roiManager("Show All without labels");
waitForUser("check outlines");

run("Flatten");

// next three lines are code to strip off the .tif extension from the filename
s=lastIndexOf(T, '.');
  T=substring(T, 0,s);
saveAs("Tiff", dir + T + "_Markup.tif");

run("Close All");
}
```

}
}

Treg cell depletion with diphtheria toxin (DT)

For late-stage Treg cell depletion, mice were treated with 1 μg DT (Sigma) via intraperitoneal (i.p.) injections on days 0, 1, 3, 5, and 7 during the 17th week of 4-NQO exposure. In some experiments, Treg cells were depleted in a periodic and transient manner, in which mice were treated with 1 μg DT on two consecutive days during the 9th, 12th, 15th, and 18th week of 4-NQO exposure.

Monoclonal antibody treatment

For immunotherapy treatment, mice were treated with 100 μg of the following monoclonal antibodies via i.p. injections twice weekly, starting during the 17th week of 4-NQO exposure: anti-CTLA-4 (clone 9D9), anti-PD-1 (clone RMP1-14), anti-PD-L1 (clone 10F.9G2), or control (clones MPC11, 2A3, or LTF-2). For neutrophil depletion, mice were treated with 200 μg of anti-Gr-1 (clone RB6-8C5) or control (clone LTF-2) monoclonal antibody via i.p. injection three times during the 17th week of 4-NQO exposure. For T cell depletion, mice were treated with 150 μg of the following monoclonal antibodies via i.p. injections twice during the first week, following by weekly treatments, starting during the 17th week of 4-NQO exposure: anti-CD4 (clone GK1.5), anti-CD8 (clone 2.43), or control (clone LTF-2). For IFN-γ neutralization, mice were treated with 500 μg of anti-IFN-γ (clone XMG1.2) or control (clone HRPN) monoclonal antibody via i.p. injections weekly, starting during the 17th week of 4-NQO exposure. All antibodies for *in vivo* use were purchased from BioXCell.

Immunization with peptide plus CFA

Mice were given a single subcutaneous (s.c.) injection on the flank of 100 μg of 2W1S peptide (GenScript) in 100 μL of CFA emulsion (InvivoGen) after 18 weeks of 4-NQO exposure. CFA emulsion consisted of a 1:1 ratio peptide:CFA. Mice were analyzed 2 weeks later.

Cell isolation, flow cytometry, and fluorescence-activated cell sorting

Cells from secondary lymphoid organs were isolated into single cell suspension in RPMI-1640 media supplemented with 10% FBS and 1% penicillin/streptomycin using a 70 μm filter. To harvest tongue-infiltrating lymphocytes, tongues were excised and injected and digested with 5 mM EDTA in RPMI-1640 for 15 minutes at 37°C, followed by digestion with Liberase TL (10 mg/mL, Roche) and DNase (20 mg/mL, Roche) in RPMI-1640 for 30 minutes at 37°C. Digested organ tissues were mechanically disrupted with frosted microscope slides and viable lymphocytes were enriched using Histopaque 1119 (Sigma). Cells were stained with conjugated antibodies specific for the following proteins (clone name in parentheses): B220 (RA3-6B2), CD11b (M1/70), CD11c (N418), CD127 (A7R34), CD25 (PC61.5), CD3ε (17A2), CD4 (RM4-5 or GK1.5), CD44 (IM7), CD45.1 (A20), CD45.2 (104), CD62L (MEL-14), CD69 (H1.2F3), CD8α (53-6.7), CD8β (YTS156.7.7), Egr2 (erongr2), F4/80 (BM8), Foxp3 (FJK-16s), Gata3 (TWAJ), Gr-1 (RB6-8C5), I-A/I-E (M5/114.15.2), IFN-γ (XMG1.2), IL-17A (eBio17B7), IL-4 (11B11), Ly6C (HK1.4), Ly6G (1A8), NK1.1 (PK136), PD-1 (RMP1-30), ROR□t (Q31-378), T-bet (4B10), TCRβ (H57-597), TCRγδ (GL3), Thy1.1 (OX-7), Thy1.2 (53-2.1), TNFα (MP6-XT22). Cells were stained for 20 minutes at 4°C in staining buffer (PBS with 2% FCS, 0.1 NaN_3, 5% normal rat serum, 5% normal mouse serum, 5% normal rabbit serum (all sera from The Jackson Laboratory), and 10 μg/mL 2.4G2 antibody). Overnight intracellular staining for Foxp3, T-bet,

Gata3, RORγt, IFN-γ, IL-17A, IL-4, and TNFα was performed using the Foxp3 Transcription Factor Staining Buffer Set (eBioscience). In experiments involving tetramer staining, cells were stained as previously described[122]. Briefly, cells were stained with PE- and APC-labeled 2W1S/I-A^b tetramers at a final concentration of 10 nM for 1 hour at room temperature, followed by enrichment using the EasySep™ PE Positive Selection Kit (StemCell Technologies). The resulting bound fraction was stained for surface and intracellular proteins as described above. Flow cytometry was performed on an LSR Fortessa (BD Biosciences) and data were analyzed using FlowJo software (TreeStar). Fluorescence-activated cell sorting (FACS) was preformed using a FACSAria (BD Biosciences).

In vitro T cell stimulation

Lymphocytes from tongues were isolated into single cell suspension as described above and plated into 96-well U-bottom plates, pooling 1-3 mice per well. Cells were stimulated with PMA (50 ng/mL, Sigma) and Ionomycin (500 ng/mL, Sigma) for 5 hours. Monensin (2 μM, eBioscience) was added to the culture during the last 4 hours of incubation. T cells were then stained to assess cytokine profile, as described above.

TCR sequence analysis

Foxp3^{GFP} x TCRβtg mice were treated with 4-NQO drinking water for 8 weeks, then supplied normal drinking water for an additional 24 weeks. Lymphocytes from whole tongues were isolated into single cell suspension as described above, and Foxp3-GFP$^+$ Treg cells were single-cell sorted into catch solution (sterile H_20 with TRIS (pH 8.0, Ambio) and RNase inhibitor (Promega)) in 96 well U-bottom plates and processed for TCRα sequencing analysis, as described in Dash et al.[123]

with modifications. Briefly, cDNA synthesis was performed directly from single cells using Maxima First Strand cDNA Synthesis Kit (Thermo Scientific) per manufacturer's instructions with minor modifications. The cDNA synthesis used 6 μL of reaction mix consisting of 3 μL 5X Reaction Mix, 0.5 μL Maxima Enzyme Mix, and 1.25% IGEPAL (Sigma). This was added to the 10 μL single cell-containing solution and incubated at 25°C for 10 minutes, 50°C for 50 minutes, and 85°C for 5 minutes. Following reverse transcription, multiplex PCR was performed to amplify the CDR3α transcripts in a 20 μL reaction mix containing 2 μL cDNA and DreamTaq Green Master Mix (Thermo Scientific). The first round of PCR used a mixture of 23 TRAV forward and 1 TRAC reverse primers. The PCR conditions were 94°C for 5 minutes followed by 45 cycles of 94°C for 30 seconds, 56°C for 30 seconds, and 72°C for 1 minute, with a final extension at 72°C for 8 minutes. The second round of PCR used the product from the first round of PCR as template and a mixture internal 23 TRAV forward and 1 TRAC reverse primers. The PCR conditions were similar to the first round but with 50 cycles. The nested PCR product was purified using EXOSap-IT (Applied Biosystems) per the manufacturer's instructions, and sequenced using the internal TRAC reverse primer. TCRα sequences were analyzed and assigned using the international ImMunoGeneTics information system (IMGT) database (http://www.imgt.org).

Retrovirus production, infection, and generation of TCR retrogenic (TCRrg) mice

TCRrg mice were generated as previously described[122,124]. In brief, the *Tcra* sequence that encodes a TCRα chain of interest was cloned into a modified retroviral construct. Plat-E cells were used to generate retrovirus. *Tcra*$^{-/-}$ CD4-Cre^{+} TCRβtg^{+} mice were injected with 5-fluorouracil (APP Pharmaceuticals) three days prior to bone marrow harvest. Bone marrow cells were then cultured for two days in X-Vivo 10 media (Lonza) supplemented with 15% FCS, 1%

penicillin/streptomycin, 100 ng/mL mouse SCF, 10 ng/mL mouse IL-3, and 20 ng/mL mouse IL-6 (BioLegend). Cells were infected with retrovirus by spinfection in the presence of 6 μg/mL polybrene (EMD Millipore) and cultured for an additional 24 hours. All spinfected cells were then mixed with 5 x 10^6 freshly harvested bone marrow "filler" cells from *Rag1*$^{-/-}$ mice and injected intravenously (i.v.) into lethally irradiated (800 rad) CD45$^{.1/.1}$ B6.SJL recipient mice to produce "primary TCRrg" mice. For "secondary TCRrg" mice, CD4$^+$ T cells were FACS-purified from primary TCRrg mice following CD4 MACS enrichment (Miltenyi Biotech) and 10^4 Thy1.1$^+$ CD4$^+$ T cells were transferred i.v. with 10^6 freshly harvested "filler" RBC-lysed splenocytes from CD45$^{.1/.1}$ mice into *Tcrb*$^{-/-}$ hosts. "Secondary TCRrg" mice were analyzed three weeks later.

Generation of *Pdcd1*$^{+/+}$ / *Pdcd1*$^{-/-}$ mixed bone marrow-chimeric mice

Bone marrow cells from *Pdcd1*$^{-/-}$ CD45$^{.2/.2}$ and B6.SJL CD45$^{.1/.1}$ mice were isolated and enumerated. A mixture consisting of 50% *Pdcd1*$^{-/-}$ CD45$^{.2/.2}$ and 50% B6.SJL CD45$^{.1/.1}$ was prepared and 5 x 10^6 cells were retro-orbitally injected into lethally (900 rads) irradiated B6.SJL CD45$^{.1/.1}$ host mice. 8 weeks post-engraftment, mice were placed on 4-NQO drinking water for 20 weeks then analyzed.

2W1S/I-A^b tetramer production

2W1S/I-A^b tetramers bearing the 2W1S peptide (EAWGALANWAVDSA) were produced using methods similar to those described previously[122,125]. I-A^b was expressed in *Drosophila* S2 cells, using separate plasmids to encode the alpha and beta chains, as described previously[122,125]. Constructs were co-transfected into *Drosophila* S2 cells together with a plasmid encoding the BirA biotin ligase. Protein expression was induced with the addition of 0.8 mM $CuSO_4$, in the presence

of 2 μg/mL biotin (Sigma-Aldrich). Biotinylated I-A^b protein was purified from culture supernatant by nickel affinity chromatography with His Bind Ni-IDA resin (EMD Millipore) and by avidin affinity chromatography with Pierce Monomeric Avidin UltraLink Resin (Thermo Fisher). Tetramers were formed by mixing biotinylated I-A^b with streptavidin-APC (Prozyme PJ27S) or streptavidin-PE (Prozyme PJRS34) at a slight molar excess of I-A^b to biotin binding sites. Saturation of the streptavidin conjugate was verified by non-reducing SDS-PAGE without boiling samples.

I-A^b Alpha Chain The extracellular domain of the I-A^b alpha chain (underlined) was fused at its N terminus to a secretion signal sequence (boundary denoted by "/"), and at its C terminus to an acidic leucine zipper, and a recognition sequence for the BirA biotin ligase.

MPCSRALILGVLALTTMLSLCGG/EDDIEADHVGTYGISVYQSPGDIGQYTFEFDGDELF
YVDLDKKETVWMLPEFGQLASFDPQGGLQNIAVVKHNLGVLTKRSNSTPATNEAPQAT
VFPKSPVLLGQPNTLICFVDNIFPPVINITWLRNSKSVADGVYETSFFVNRDYSFHKLSYL
TFIPSDDDIYDCKVEHWGLEEPVLKHWEPEIPAPMSELTETGGGGSTTAPSAQLEKELQA
LEKENAQLEWELQALEKELAQGGSGGSGLNDIFEAQKIEWHE.

I-A^b Beta Chain with 2W1S Peptide The extracellular domain of the I-A^b beta chain (underlined) was fused at its N terminus to a secretion signal sequence (boundary denoted by "/"), the 2W1S peptide (in **bold**) and a linker sequence, and at its C terminus to a basic leucine zipper and a 6xHis tag.

MALQIPSLLLSAAVVVLMVLSSPGTEG/GDS**EAWGALANWAVDSA**GGGGSLVPRGSG
GGGSERHFVYQFMGECYFTNGTQRIRYVTRYIYNREEYVRYDSDVGEHRAVTELGRPD
AEYWNSQPEILERTRAELDTVCRHNYEGPETHTSLRRLEQPNVVISLSRTEALNHHNTLV
CSVTDFYPAKIKVRWFRNGQEETVGVSSTQLIRNGDWTFQVLVMLEMTPRRGEVYTCH

VEHPSLKSPITVEWRAQSESAWSKGGGGSTTAPSAQLKKKLQALKKKNAQLKWKLQAL
KKKLAQHHHHHH.

Data and code availability

Source data for patient datasets used for Figure 3 and Figure 4 is available at https://doi.org/10.1038/nature14129 and https://www.cancer.gov/tcga. Source code used for analysis for Figure 3 and Figure 4 is available at https://doi.org/10.1038/ncomms13427 and http://doi.org/10.5281/zenodo.1004662. The single-cell TCRα sequence data generated in this study are available in Table S1. Source TCR sequence data and analysis used for $CD4^+$ $Foxp3^+$ Treg and $CD4^+$ $Foxp3^{neg}$ Tconv catalogs in Figure 8A-B is available at https://doi.org/10.1016/j.immuni.2016.02.009.

Quantification and statistical analysis

Data were analyzed using Prism software (GraphPad) and R (The R Project for Statistical Computing)[126]. Pairwise correlation statistics was performed using the Pearson correlation score. Significance testing was performed using the nonparametric Mann–Whitney test (two-tailed), one-way ANOVA with Bonferroni's multiple comparisons test (two-tailed), or Fisher's exact test, as specified in the figure legends. The number per group is indicated in the figure legends. A value of $p < 0.05$ was considered statistically significant.

Table 1. Key Resources Table

REAGENT or RESOURCE	SOURCE	IDENTIFIER
Antibodies		
Anti-CD3 antibody, Rabbit monoclonal, clone SP162	Sigma-Aldrich	Cat# SAB5500057
FOXP3 Monoclonal Antibody, clone FJK-16s	eBioscience	Cat# 14-5773-82, RRID: AB_467576
Rabbit Anti-Stat1, phospho (Tyr701) Monoclonal Antibody, clone 58D6, unconjugated	Cell Signaling	Cat# 9167, RRID:AB_561284
Rabbit Anti-Human Ki67 (Ki-67) Monoclonal Antibody, Unconjugated, Clone SP6	Thermo Fisher	Cat# RM-9106-S, RRID: AB_149707
anti-mouse/human CD45R/B220 antibody, clone RA3-6B2, APC conjugated	BioLegend	Cat# 103211, RRID:AB_312996
anti-mouse/human CD45R/B220 antibody, clone RA3-6B2, FITC conjugated	BioLegend	Cat# 103205, RRID:AB_312990
anti-mouse/human CD45R/B220 antibody, clone RA3-6B2, Pacific Blue conjugated	BioLegend	Cat# 103230, RRID:AB_492877
anti-mouse/human CD45R/B220 antibody, clone RA3-6B2, PE/Cy7 conjugated	BioLegend	Cat# 103221, RRID:AB_313004
anti-mouse/human CD11b antibody, clone M1/70, BV605 conjugated	BioLegend	Cat# 101237, RRID:AB_11126744
anti-mouse/human CD11b antibody, clone M1/70, Pacific Blue conjugated	BioLegend	Cat# 101223, RRID:AB_755985
anti-mouse CD11c antibody, clone N418, APC conjugated	BioLegend	Cat# 117310, RRID:AB_313779
anti-mouse CD11c antibody, clone N418, Pacific Blue conjugated	BioLegend	Cat# 117321, RRID:AB_755987
anti-mouse CD127 (IL-7Ralpha) antibody, clone A7R34, PE/Cy7 conjugated	BioLegend	Cat# 135013, RRID:AB_1937266
anti-mouse CD25 antibody, clone PC61, APC conjugated	BioLegend	Cat# 102011, RRID:AB_312860
anti-mouse CD3 antibody, clone 17A2, Alexa Fluor 700 conjugated	BioLegend	Cat# 100216, RRID:AB_493697
anti-mouse CD3 antibody, clone 17A2, APC/Cy7 conjugated	BioLegend	Cat# 100221, RRID:AB_2057374
anti-mouse CD3 antibody, clone 17A2, PE/Cy7 conjugated	BioLegend	Cat# 100219, RRID:AB_1732068
anti-mouse CD3 antibody, clone 17A2, FITC conjugated	BioLegend	Cat# 100203, RRID:AB_312660
anti-mouse CD4 antibody, clone RM4-5, BV605 conjugated	BioLegend	Cat# 100547, RRID:AB_11125962
CD4 Monoclonal Antibody, clone RM4-5, eFluor 450 conjugated	eBioscience	Cat# 48-0042-82, RRID:AB_1272194

Table 1, continued.

anti-mouse CD4 antibody, clone GK1.5, PerCP/Cy5.5 conjugated	BioLegend	Cat# 100434, RRID:AB_893324
anti-mouse/human CD44 antibody, clone IM7, APC/Cy7 conjugated	BioLegend	Cat# 103028, RRID:AB_830785
anti-mouse/human CD44 antibody, clone IM7, FITC conjugated	BioLegend	Cat# 103006, RRID:AB_312957
anti-mouse CD45.1 antibody, clone A20, Alexa Fluor 700 conjugated	BioLegend	Cat# 110724, RRID:AB_493733
anti-mouse CD45.1 antibody, clone A20, FITC conjugated	BioLegend	Cat# 110705, RRID:AB_313494
anti-mouse CD45.1 antibody, clone A20, Pacific Blue conjugated	BioLegend	Cat# 110721, RRID:AB_492867
anti-mouse CD45.2 antibody, clone 104, APC/Cy7 conjugated	BioLegend	Cat# 109823, RRID:AB_830788
anti-mouse CD45.2 antibody, clone 104, BV711 conjugated	BioLegend	Cat# 109847, RRID:AB_2616859
anti-mouse CD62L antibody, clone MEL-14, PE conjugate	BioLegend	Cat# 104408, RRID:AB_313095
anti-mouse CD69 antibody, clone H1.2F3, PE/Cy7 conjugated	BioLegend	Cat# 104512, RRID:AB_493564
anti-mouse CD8a antibody, clone 53-6.7, APC/Cy7 conjugated	BioLegend	Cat# 100714, RRID:AB_312753
anti-mouse CD8a antibody, clone 53-6.7, PE/Cy7 conjugated	BioLegend	Cat# 100721, RRID:AB_312760
anti-mouse CD8a antibody, clone 53-6.7, PerCP/Cy5.5 conjugated	BioLegend	Cat# 100733, RRID:AB_2075239
anti-mouse CD8b (Ly-3) antibody, clone YTS156.7.7, Alexa Fluor 700 conjugated	BioLegend	Cat# 126618, RRID:AB_2563949
anti-mouse CD8b (Ly-3) antibody, clone YTS156.7.7, APC/Cy7 conjugated	BioLegend	Cat# 126619, RRID:AB_2563950
anti-mouse CD8b (Ly-3) antibody, clone YTS156.7.7, PerCP/Cy5.5 conjugated	BioLegend	Cat# 126609, RRID:AB_961304
EGR2 Monoclonal Antibody, clone erongr2, APC conjugated	eBioscience	Cat# 17-6691-80, RRID:AB_11150966
anti-mouse F4/80 antibody, clone BM8, Pacific Blue conjugated	BioLegend	Cat# 123124, RRID:AB_893475
FOXP3 Monoclonal Antibody, clone FJK-16s, APC conjugated	eBioscience	Cat# 17-5773-82, RRID:AB_469457
FOXP3 Monoclonal Antibody, clone FJK-16s, eFluor 450 conjugated	eBioscience	Cat# 48-5773-82, RRID:AB_1518812
FOXP3 Monoclonal Antibody, clone FJK-16s, FITC conjugated	eBioscience	Cat# 11-5773-82, RRID:AB_465243
FOXP3 Monoclonal Antibody, clone FJK-16s, PE conjugated	eBioscience	Cat# 12-5773-82, RRID:AB_465936

Table 1, continued.

FOXP3 Monoclonal Antibody, clone FJK-16s, PE/Cy7 conjugated	eBioscience	Cat# 25-5773-82, RRID:AB_891552
Gata-3 Monoclonal Antibody, clone TWAJ, PE conjugated	eBioscience	Cat# 12-9966-41, RRID:AB_1963601
Gata-3 Monoclonal Antibody, clone TWAJ, PerCP-eFluor 710 conjugated	eBioscience	Cat# 46-9966-42, RRID:AB_10804487
anti-mouse Ly-6G/Ly-6C (Gr-1) antibody, clone RB6-8C5, APC/Cy7 conjugated	BioLegend	Cat# 108424, RRID:AB_2137485
anti-mouse I-A/I-E antibody, clone M5/114.15.2, Pacific Blue conjugated	BioLegend	Cat# 107620, RRID:AB_493527
anti-mouse IFN-g antibody, clone XMG1.2, APC conjugated	BD Biosciences	Cat# 562018, RRID:AB_10896992
IL-17A Monoclonal Antibody, clone eBio17B7, PE conjugated	eBioscience	Cat# 12-7177-81, RRID:AB_763582
anti-mouse IL-4 antibody, clone 11B11, BV421 conjugated	BioLegend	Cat# 504119, RRID:AB_10896945
Rat Anti-Mouse IL-4 Antibody, clone 11B11, BV650 conjugated	BD Biosciences	Cat# 564004, RRID:AB_2687569
anti-mouse Ly-6C antibody, clone HK1.4, PE conjugated	BioLegend	Cat# 128007, RRID:AB_1186133
anti-mouse NK1.1 antiody, clone PK136, APC conjugated	BD Biosciences	Cat# 550627, RRID:AB_398463
anti-mouse CD279 (PD-1) antibody, clone RMP1-30, PE/Cyanine7 conjugated	BioLegend	Cat# 109109, RRID:AB_572016
anti-mouse Ly-6G antibody, clone 1A8, FITC conjugated	BioLegend	Cat# 127606, RRID:AB_1236494
Mouse Anti-Mouse RORgt, clone Q31-378, BV786 conjugated	BD Biosciences	Cat# 564723, RRID:AB_2738916
anti-T-bet antibody, clone 4B10, BV421 conjugated	BioLegend	Cat# 644816, RRID:AB_10959653
anti-mouse TCR beta chain antibody, clone H57-597, BV510 conjugated	BioLegend	Cat# 109234, RRID:AB_2562350
anti-mouse TCR beta chain antibody, clone H57-597, PE conjugated	BioLegend	Cat# 109207, RRID:AB_313430
anti-mouse TCR beta chain antibody, clone H57-597, PE/Cy7 conjugated	BioLegend	Cat# 109221, RRID:AB_893627
anti-mouse TCR gamma/delta antibody, clone GL3, APC conjugated	BioLegend	Cat# 118116, RRID:AB_1731813
anti-mouse TCR gamma/delta antibody, clone GL3, PE/Cy7 conjugated	BioLegend	Cat# 118123, RRID:AB_11203530
anti-rat CD90/mouse CD90.1 (Thy-1.1) antibody, clone OX-7, PE conjugated	BioLegend	Cat# 202524, RRID:AB_1595524
anti-mouse CD90.2 (Thy1.2) antibody, clone 53-2.1, FITC conjugated	BioLegend	Cat# 140304, RRID:AB_10642812

Table 1, continued.

anti-mouse TNF-alpha antibody, clone MP6-XT22, BV421 conjugated	BioLegend	Cat# 506327, RRID:AB_10900823
2W1S/I-A^b tetramer, APC conjugated	Laboratory of P.A.S.	[122]
2W1S/I-A^b tetramer, PE conjugated	Laboratory of P.A.S.	[122]
InVivoPlus anti-mouse CTLA-4 (CD152) antibody, clone 9D9	BioXCell	Cat# BE0164, RRID:AB_10949609
InVivoPlus anti-mouse PD-1 (CD279) antibody, clone RMP1-14	BioXCell	Cat# BE0146, RRID:AB_10949053
InVivoPlus anti-mouse PD-L1 (B7-H1) antibody, clone 10F.9G2	BioXCell	Cat# BE0101, RRID:AB_10949073
InVivoPlus anti-mouse Ly6G/Ly6C (Gr-1) antibody, clone RB6-8C5	BioXCell	Cat# BE0075, RRID:AB_10312146
InVivoPlus anti-mouse CD4 antibody, clone GK1.5	BioXCell	Cat# BE0003-1, RRID:AB_1107636
InVivoPlus anti-mouse CD8a antibody, clone 2.43	BioXCell	Cat# BE0061, RRID:AB_1125541
InVivoPlus anti-mouse IFNγ antibody, clone XMG1.2	BioXCell	Cat# BE0055, RRID:AB_1107694
InVivoPlus mouse IgG2b isotype control antibody, clone MPC-11	BioXCell	Cat# BE0086, RRID:AB_1107791
InVivoPlus rat IgG2a isotype control antibody, clone 2A3	BioXCell	Cat# BE0089, RRID:AB_1107769
InVivoPlus rat IgG2b isotype control antibody, clone LTF-2	BioXCell	Cat# BE0090, RRID:AB_1107780
InVivoPlus rat IgG1 isotype control antibody, clone HRPN	BioXCell	Cat# BE0088, RRID:AB_1107775
Bacterial and Virus Strains		
E. coli DH5a	New England Biolabs	Cat# C2987H
Biological Samples		
Chemicals, Peptides, and Recombinant Proteins		
4-Nitroquinoline *N*-oxide	Sigma-Aldrich	Cat# N8141
Dimethyl sulfoxide	Sigma-Aldrich	Cat# D4540
Propylene Glycol	Fisher Scientific	Cat# P355-1
Formalin solution, neutral buffered, 10%	Sigma-Aldrich	Cat# HT501128
Diphtheria Toxin from *Corynebacterium diphtheriae*	Sigma-Aldrich	Cat# D0564
Complete Freund's Adjuvant (CFA)	InvivoGen	Cat# vac-cfa-10
Custom 2W1S peptide (EAWGALANWAVDSA), >98% pure	GenScript	N/A
Liberase TL Research Grade	Roche	Cat# 5401020001
DNase I, grade II, from bovine pancreas	Roche	Cat# 10104159001
Phorbol 12-myristate 13-acetate (PMA)	Sigma-Aldrich	Cat# 79346

Table 1, continued.

Ionomycin calcium salt from *Streptomyces conglobatus*	Sigma-Aldrich	Cat# I0634
Monensin Solution (1000X)	eBioscience	Cat# 00-4505-51
5-Fluorouracil	APP Pharmaceuticals	Cat# 101710
Recombinant Mouse M-CSF (carrier free)	BioLegend	Cat# 576406
Recombinant Mouse IL-3 (carrier free)	BioLegend	Cat# 575504
Recombinant Mouse IL-6 (carrier free)	BioLegend	Cat# 575706
Polybrene Infection / Transfection Reagent	EMD Millipore	Cat# TR-1003-G
Critical Commercial Assays		
CD4 $^{+}$ T Cell Isolation Kit, mouse	Miltenyi Biotec	Cat# 130-104-454
EasySep PE Positive Selection Kit	Stem Cell Technologies	Cat# 18557
EasySep APC Positive Selection Kit	Stem Cell Technologies	Cat# 18453
Foxp3 / Transcription Factor Staining Buffer Set	eBioscience	Cat# 00-5523-00
Maxima First Strand cDNA Synthesis Kit for RT-qPCR	Thermo Scientific	Cat# K1641
DreamTaq Green PCR Master Mix (2X)	Thermo Scientific	Cat# K1081
Deposited Data		
TCRa sequence dataset	This paper	Table S1
TCRa catalogs	Malchow et al., 2016[127]	N/A
TCGA-HNSCC dataset	Cancer Genome Atlas Network, 2015[96]	N/A
CHGC dataset	Keck et al., 2015[97]	N/A
TCGA datasets (kidney renal clear cell carcinoma, liver hepatocellular carcinoma, lung adenocarcinoma, melanoma)	https://www.cancer.gov/tcga	N/A
Experimental Models: Cell Lines		
Plat-E Retroviral Packaging Cell Line	Cell Biolabs	Cat# RV-101
Experimental Models: Organisms/Strains		
Mouse: B6: C57BL/6J	Jackson Laboratories	JAX: 000664
Mouse: Foxp3-DTR: B6.129(Cg)-*Foxp3$^{tm3(DTR/GFP)Ayr}$*/J	Jackson Laboratories	JAX: 016958
Mouse: *Tcrb$^{-/-}$ x Tcrd$^{-/-}$*-: B6.129P2-*Tcrb^{tm1Mom} Tcrd^{tm1mom}*/J	Jackson Laboratories	JAX: 002122
Mouse: *Ighm$^{-/-}$* (B6.129S2-Ighm^{tm1Cgn}/J)	Jackson Laboratories	JAX: 002288
Mouse: *Pdcd1-/-* (B6.Cg-Pdcd1$^{tm1.1Shr}$/J)	Jackson Laboratories	JAX: 028276
Mouse: *Rag1$^{-/-}$* (B6.129S7-*Rag1^{tm1Mom}*/J)	Jackson Laboratories	JAX: 002216
Mouse: *Tcra$^{-/-}$* (B6.129S2-*Tcra^{tm1Mom}*/J)	Jackson Laboratories	JAX: 002116

Table 1, continued.

Mouse: CD4-Cre (B6.Cg-Tg(Cd4-cre)1Cwi/BfluJ)	Jackson Laboratories	JAX: 022071
Mouse: *Foxp3*^{GFP} (B6.Cg-*Foxp3*^{tm2Tch}/J)	Jackson Laboratories	JAX: 006772
Mouse: *Ifngr1*$^{-/-}$ (B6.129S7-Ifngr1^{tm1Agt}/J)	Jackson Laboratories	JAX: 003288
Mouse: TCRbtg: transgenic mouse expressing (TRBV26)- ASSLGSSYEQY TCRβ chain	Laboratory of P.A.S.	Malchow et al., 2013[83]
Oligonucleotides		
Recombinant DNA		
I-A ^{b} alpha chain in pRMHa3	Laboratory of E.J. Adams	Leonard et al. 2017[122]
I-A ^{b} beta chain (2W1S peptide) in pRMHa3	Laboratory of E.J. Adams	Leonard et al. 2017[122]
pMGflThy1.1	Laboratory of A. Bendelac	McDonald et al., 2015[128]
Software and Algorithms		
Prism (v9.0.0)	GraphPad	http://www.graphpad.com
FlowJo v10.7.1	BD Biosciences	http://www.flowjo.com
R v4.0.2	R Core Team, 2020	https://www.r-project.org/
Fiji	Schindelin et al., 2012[121]	https://fiji.sc/
iPANDA	Ozerov et al., 2016[116]	
xCell R package (version 1.12)	Aran et al., 2017[120]	https://github.com/dviraran/xCell
Aperio ImageScope	Leica	https://www.leicabiosystems.com/
Other		
Aperio ScanScope XT	Leica	
LSR Fortessa	BD Biosciences	
FACSAria	BD Biosciences	

RESULTS[c]

Introduction

In recent years, a broad conceptual framework has emerged for understanding the endogenous immune response to cancer and factors impacting the success or failure of immune-based cancer therapies[19]. The genetic and epigenetic changes associated with tumorigenesis can lead to tumor cell expression of mutated or aberrantly expressed proteins, which serve as the source of short peptide antigens that can be complexed with MHC molecules and displayed at the cell surface for recognition by $CD4^+$ and $CD8^+$ T cells. Antigen presenting cells acquire tumor-derived constituents and present peptide antigens to T cells in the draining lymph nodes. In cases in which productive T cell priming occurs, T cells undergo activation, proliferation, and differentiation, followed by exit from the lymph nodes and trafficking to the tumor site. There, effector T cells have the potential to induce tumor control via directed production of cytolytic effectors or local production of modulatory factors.

For many cancer types, a major fraction of tumors lack a substantial T cell infiltrate[19,32,129], implying the lack of effective T cell priming in the lymph nodes, the exclusion of primed T cells from the tumor parenchyma, or limited survival of T cells within the tumor microenvironment. Clinical studies demonstrate that a paucity of intratumoral T cells is a major factor restricting the efficacy of checkpoint blockade antibodies targeting the PD-1 or CTLA-4 axes, as objective responses are largely restricted to "T cell-inflamed" tumors that harbor a high-density T cell infiltrate at baseline[32–35]. This has sparked considerable interest in understanding the mechanisms

[c] Much of this section is reproduced, with modifications, from Chao, J.L., Korzinkin, M., Zhavoronkov, A., Ozerov, I., Higgins, K., Lingen, M.W., Izumchenko, E., and Savage, P.A. "Effector T Cell Responses Unleashed by Regulatory T Cell Ablation Promote Progression of Oral Squamous Cell Carcinoma" *Submitted*.

restricting T cell density within tumors, and devising new strategies to induce a T cell-inflamed phenotype in otherwise "cold" neoplasms.

In this regard, a major focus has centered on understanding the biology of $CD4^+$ $FOXP3^+$ regulatory T (Treg) cells in the tumor setting. Treg cells are found at elevated densities within many human cancers, and are thought to facilitate cancer progression and therapeutic resistance by suppressing the priming and activity of tumor-reactive effector T cells[1,130,131]. Consistent with these observations, intratumoral Treg cell density has been correlated with a poor prognosis for some cancer types[54,57]. However, studies in mice have demonstrated that Treg cells may serve diverse tissue-specific functions that are unrelated to effector T cell suppression, including metabolic regulation[84,85], the promotion of tissue repair[88,89], and the regulation of stem cell differentiation[91], suggestive of multifaceted functions of intratumoral Treg cells within the tumor microenvironment. Importantly, intratumoral Treg cells express a panoply of cell-surface receptors that are targeted by current and emerging antibody-based therapies, including PD-1, CTLA-4, OX40, 4-1BB, TIM-3, Lag3, and GITR[1,78,80–82,132], suggesting that tumor-infiltrating Treg cells are likely to be directly impacted by therapeutic antibodies and are therefore key determinants of therapeutic outcome.

Smoking-associated human papilloma virus (HPV)-negative head-and-neck squamous cell carcinomas (HNSCCs), which include many OSCCs, represent an archetypal cancer that exhibits cardinal features of response or resistance to immune-based therapy, making it a compelling system for understanding the immunological forces that shape cancer development and response to therapy. Most HNSCCs harbor an elevated density of somatic point mutations[99–101] with potential to encode peptide neo-antigens. Notably, HPV-negative HNSCCs may arise from different anatomical sites and exhibit substantial genomic, phenotypic, and therapeutic

heterogeneity, with the fraction of advanced HNSCCs that are responsive to anti-PD-1 and anti-PD-L1 checkpoint blockade largely restricted to those with a T cell-inflamed phenotype at baseline[104]. However, HPV-negative HNSCCs also exhibit compelling properties that are not aligned with the common conceptual framework of anti-tumor immunity. First, numerous prognostic studies reveal that high Treg cell density within the tumor center or tumor stroma is associated with a favorable prognosis in a subset of HNSCC patients[56,105,106], a finding inconsistent with the notion that intratumoral Treg cells promote HNSCC and negatively impact clinical outcome by suppressing tumor-reactive effector T cells. Second, a study of HNSCC patients treated with anti-PD-1 or anti-PD-L1 therapy reported that over 25% of patients experienced "hyper-progression" characterized by accelerated tumor growth kinetics following therapy[53], suggesting that checkpoint blockade may accelerate disease in a fraction of patients. These reports demonstrate that the processes governing endogenous anti-tumor immunity and the response to therapy are likely to vary based on host genetics, cancer genetics, the microbiota, the cell type of cancer origin, as well as the local tissue environment, and highlight a critical need for mechanistic insight in tractable animal models that accurately mimic carcinogen-induced HNSCC development and progression.

Here, we utilize deconvolution-based profiling of human transcriptional data and mechanistic studies in a mouse model of autochthonous carcinogen-induced OSCC to investigate the relationship between two major determinants of response to immunotherapy - immune suppression by $Foxp3^+$ Treg cells and tumor infiltration by $CD4^+$ and $CD8^+$ effector T cells. Transcriptional profiling of human HPV-negative oral squamous cell carcinoma (OSCC), the most common type of HNSCC, and other cancers identified polarized clusters enriched for either $CD8^+$ T cells or $CD4^+$ Treg and conventional T cells, implying that the factors dictating the intratumoral

density of $CD8^+$ T cells are distinct from those driving the density of Treg cells in many patients. In a mouse model of carcinogen-induced OSCC of the tongue, we found that induction of a strong T cell-inflamed phenotype via late-stage depletion of Treg cells did not induce tumor regression, but instead induced rapid emergence of OSCCs via a process that was dependent on effector T cells. These mechanistic insights suggest that therapeutic intervention to manipulate intratumoral Treg cells or augment a T cell-inflamed phenotype may induce unexpected tumor-promoting effects, highlighting the importance of defining the mechanisms driving these effects and delineating biomarkers to identify HNSCC patients at risk of such adverse events.

In human subjects, the density of OSCC-infiltrating Treg cells does not correlate with $CD8^+$ T cell density in a subset of human tumors

Previous studies have suggested that the influx or expansion of $FOXP3^+$ Treg cells in human solid malignancies may be triggered in response to $CD8^+$ effector T cell infiltration and effector activity[34,133]. To examine this relationship in human HPV-negative OSCC and other cancers, we used previously defined T cell type-specific reference gene expression profiles from single-cell RNA sequencing[118] to estimate the relative abundance of $CD4^+$ Treg cells, $CD4^+$ conventional T cells, cytotoxic $CD8^+$ T cells, and exhausted $CD8^+$ T cells from bulk gene expression data derived from The Cancer Genome Atlas (TCGA) and Chicago Head and Neck Genomics Cohort (CHGC) data sets[97] by mathematical deconvolution using the iPANDA algorithm[116,117,134]. This analysis revealed that human HPV-negative OSCCs are associated with a range of predicted densities of exhausted and cytotoxic $CD8^+$ T cells (Figure 3A, C), highlighting the known variability of $CD8^+$ T cell infiltration in OSCCs[101,102,105,117,135–137]. The analysis also demonstrated that the predicted density of $CD4^+$ Treg cells correlated with the density of $CD4^+$

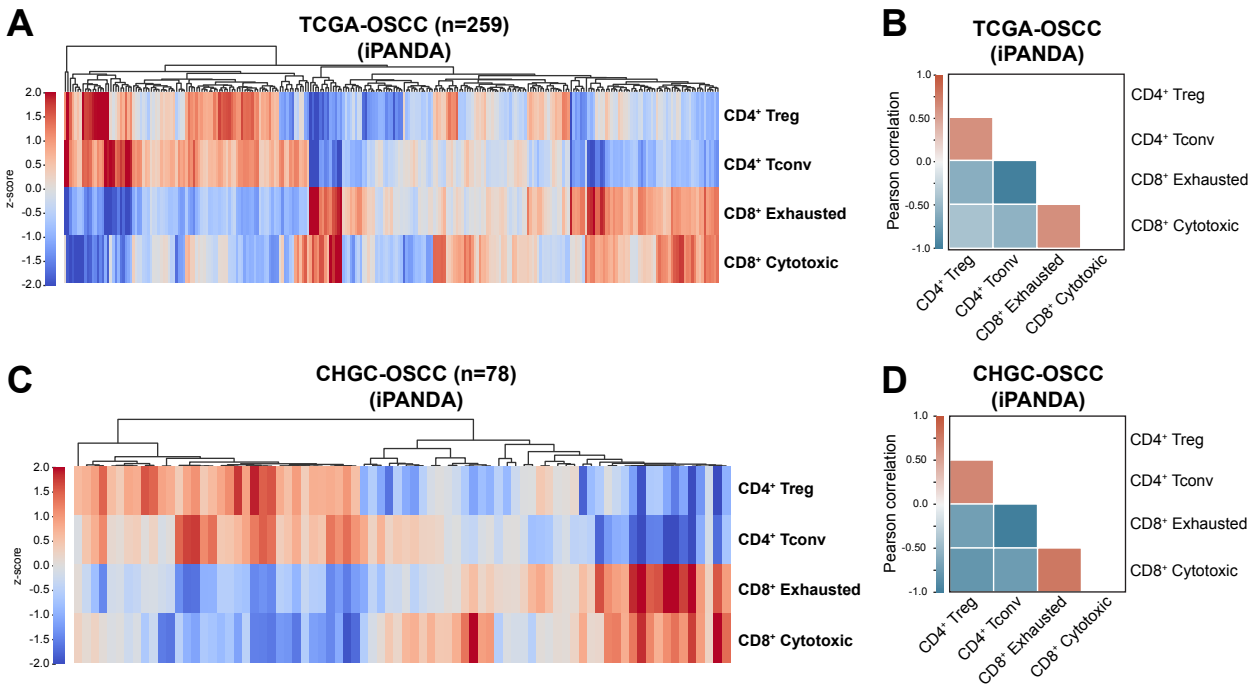

Figure 3. In human subjects, the density of OSCC-infiltrating Treg cells does not correlate with CD8$^+$ T cell density in a subset of tumors

Heat map of z-scores depicting the relative abundance of CD4$^+$ Treg cells, CD4$^+$ conventional T cells, cytotoxic CD8$^+$ T cells, and exhausted CD8$^+$ T cells from bulk gene expression data using the iPANDA algorithm.

A, C) Heat maps of HPV-negative OSCC datasets derived from (A) The Cancer Genome Atlas (TCGA) or (C) Chicago Head and Neck Genomics Cohort (CHGC) displaying the normalized z-scores of the relative abundance of CD4$^+$ Treg cells, CD4$^+$ conventional T cells, cytotoxic CD8$^+$ T cells, and exhausted CD8$^+$ T cells. Each column represents an individual patient sample. Color denotes the normalized z-score. Unsupervised clustering is used.

B, D) Correlation plots displaying pairwise comparisons of each T cell subset from (B) TCGA or (D) CHGC datasets. Color denotes the Pearson correlation score.

n = 329 samples (TCGA), 78 samples (CHGC).

conventional T cells (Figure 3A-D). Notably, unsupervised clustering based on the relative densities of the four T cell subtypes revealed polarized OSCC clusters enriched for either $CD8^+$ T cells or $CD4^+$ Treg and conventional T cells (Figure 3A, C). Similar clusters enriched for either $CD8^+$ T cells or Treg cells were also identified using the xCell cell type enrichment analysis platform[120] (Figure 4A), and were observed using iPANDA to analyze other human solid cancer types that are amenable to immune-based therapy (Figure 4B-I). Interestingly, the anti-correlation between $CD8^+$ T cells and $CD4^+$ T cells is most pronounced in OSCC (Figure 3B, D), compared to other solid cancer types analyzed (Figure 4C, E, G, I). These findings indicate that in some tumors, the factors dictating the density of intratumoral $CD4^+$ T cells (Treg cells and/or $CD4^+$ T conventional cells) are likely to be distinct from the determinants of $CD8^+$ T cell density, and suggest that tumor infiltration by $CD8^+$ T cells is unlikely to be a primary determinant of intratumoral Treg cell density in such cancers.

Characterization of a mouse model of carcinogen-induced oral squamous cell carcinoma

The above findings, paired with prognostic studies indicating that high Treg cell density is associated with a favorable prognosis in OSCCs and some other human cancers[54,56,57,101,105,106,135,137–140], illustrate compelling correlates that may have functional significance for understanding anti-tumor immunity and response to immunotherapy. A clear understanding of the significance of these relationships requires mechanistic loss- and gain-of-function experiments in animal models that accurately recapitulate the biology of OSCC. With this in mind, we utilized a mouse model of carcinogen-induced OSCC to gain a better understanding of the nature of Treg cells associated with these neoplasms, and to define the relationship between Treg cells and effector T cells in this setting. In this model, mice are exposed to drinking water

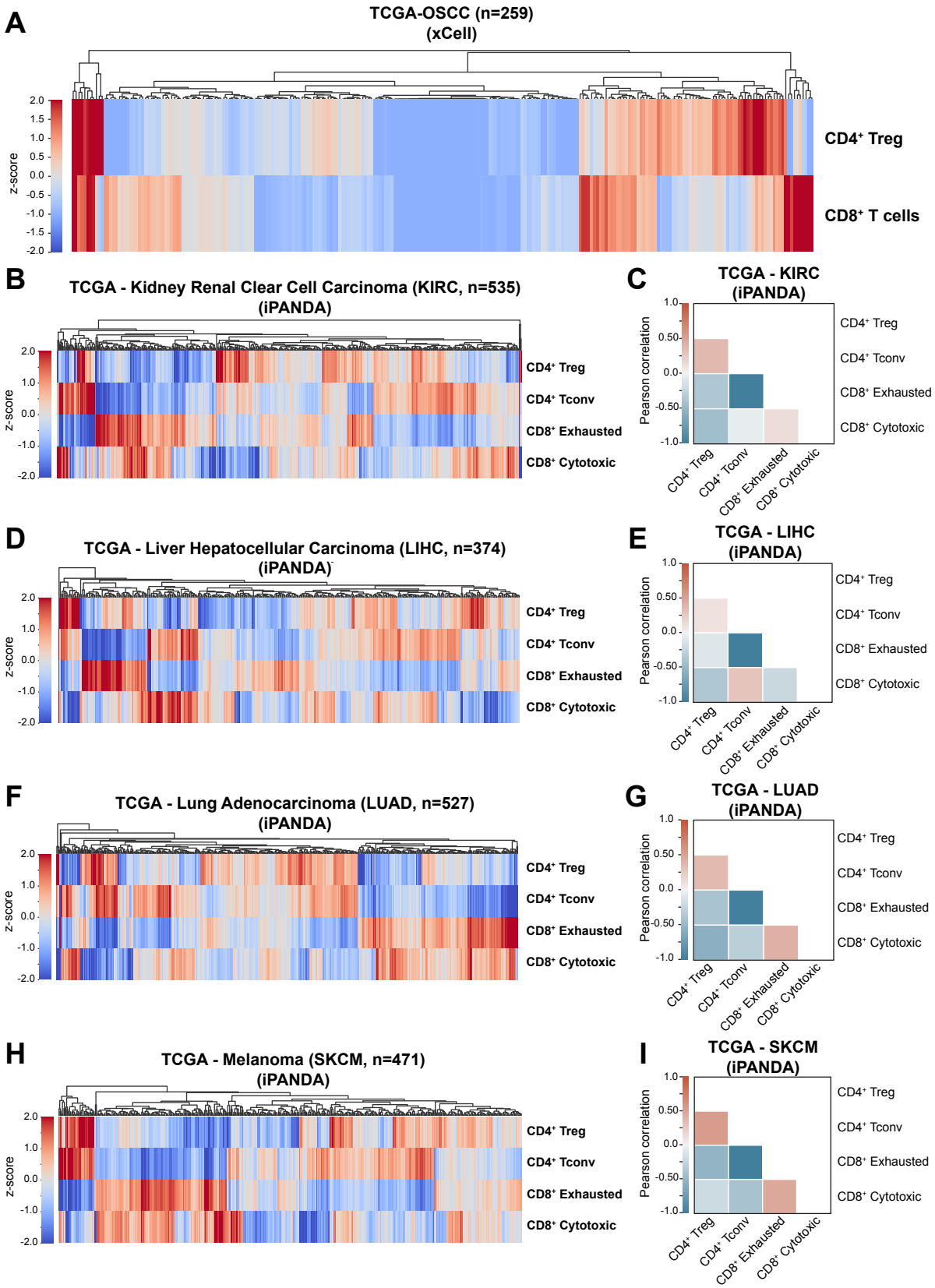

Figure 4. The density of tumor-infiltrating Treg cells does not correlate with CD8$^+$ T cell density in a subset of human solid tumors *(Legend on next page)*

Figure 4, continued.
Heat maps of the relative abundance of T cell populations from bulk gene expression data using the xCell or iPANDA algorithm.
A) Heat map of HPV-negative OSCC dataset derived from The Cancer Genome Atlas (TCGA) displaying the normalized z-scores of the relative abundance of $CD4^+$ Treg cells and $CD8^+$ T cells, using xCell. Each column represents an individual patient sample. Color denotes the normalized z-score. Unsupervised clustering was used. n = 259 samples.
B, D, F, H) Heat maps of indicated solid tumor datasets derived from TCGA displaying the normalized z-scores of the relative abundance of $CD4^+$ Treg cells, $CD4^+$ conventional T cells, cytotoxic $CD8^+$ T cells, and exhausted $CD8^+$ T cells, using iPANDA. Each column represents an individual patient sample. Color denotes the normalized z-score. Unsupervised clustering was used.
C, E, G, I) Correlation plots displaying pairwise comparisons of each T cell subset of indicated solid tumor datasets derived from TCGA. Color denotes the Pearson correlation score.
n = 535 samples (kidney renal clear cell carcinoma (KIRC)), 374 samples (liver hepatocellular carcinoma (LIHC)), 527 samples (lung adenocarcinoma (LUAD)), 471 samples (melanoma (SKCM)).

containing the chemical carcinogen 4-nitroquinoline N-oxide (4-NQO) for 20 weeks to induce oral lesions in the tongue epithelium[108–112]. Notably, the progression and histopathology of 4-NQO-induced lesions in mice closely mirrors that of human HPV-negative OSCC, including characteristic progression from pre-neoplastic dysplasia to invasive OSCC[108,111,113–115]. Previous studies using this model report an OSCC incidence ranging from 10-50%, depending on the duration and dose of 4-NQO exposure[110,112]. We developed an approach to quantitatively assess 4-NQO-induced lesions of the tongue with respect to the incidence and burden of lesions of distinct histological grades. Following longitudinal tongue bisection, tissue sections from the mid-plane were stained with H&E and blinded. The epithelial perimeter of each tongue section was then traced, and the fraction of the perimeter characterized by distinct histological grades (normal epithelium, hyperkeratosis, dysplasia, or invasive OSCC, Figure 5A) was quantified and plotted for each mouse using two approaches. Using this approach, we can quantify the histopathology burden per mouse, as well as assess distinct asynchronous lesions within an individual mouse. As illustrated for a cohort of twenty-nine 4-NQO-treated mice in Figure 5B, all mice developed hyperkeratosis and dysplastic lesions by 20 weeks of carcinogen exposure, with 11 mice developing invasive OSCC (Figure 5B). Importantly, 4-NQO exposure for 20 weeks induced dysplasia and invasive OSCC to a similar extent in male and female mice (Figure 5C-D), demonstrating no significant sex-based differences to susceptibility to carcinogen-induced OSCC.

Next, we compared the 20 week continuous 4-NQO exposure regimen described above to an alternative 4-NQO treatment regimen in which 4-NQO is provided in the drinking water for 8 weeks, followed by a "rest" period for the remaining 12 weeks in which mice are supplied normal drinking water not containing the carcinogen[108–112]. Although not statistically significant, mice exposed to 4-NQO for a full 20-week schedule trended towards an increased incidence of OSCC

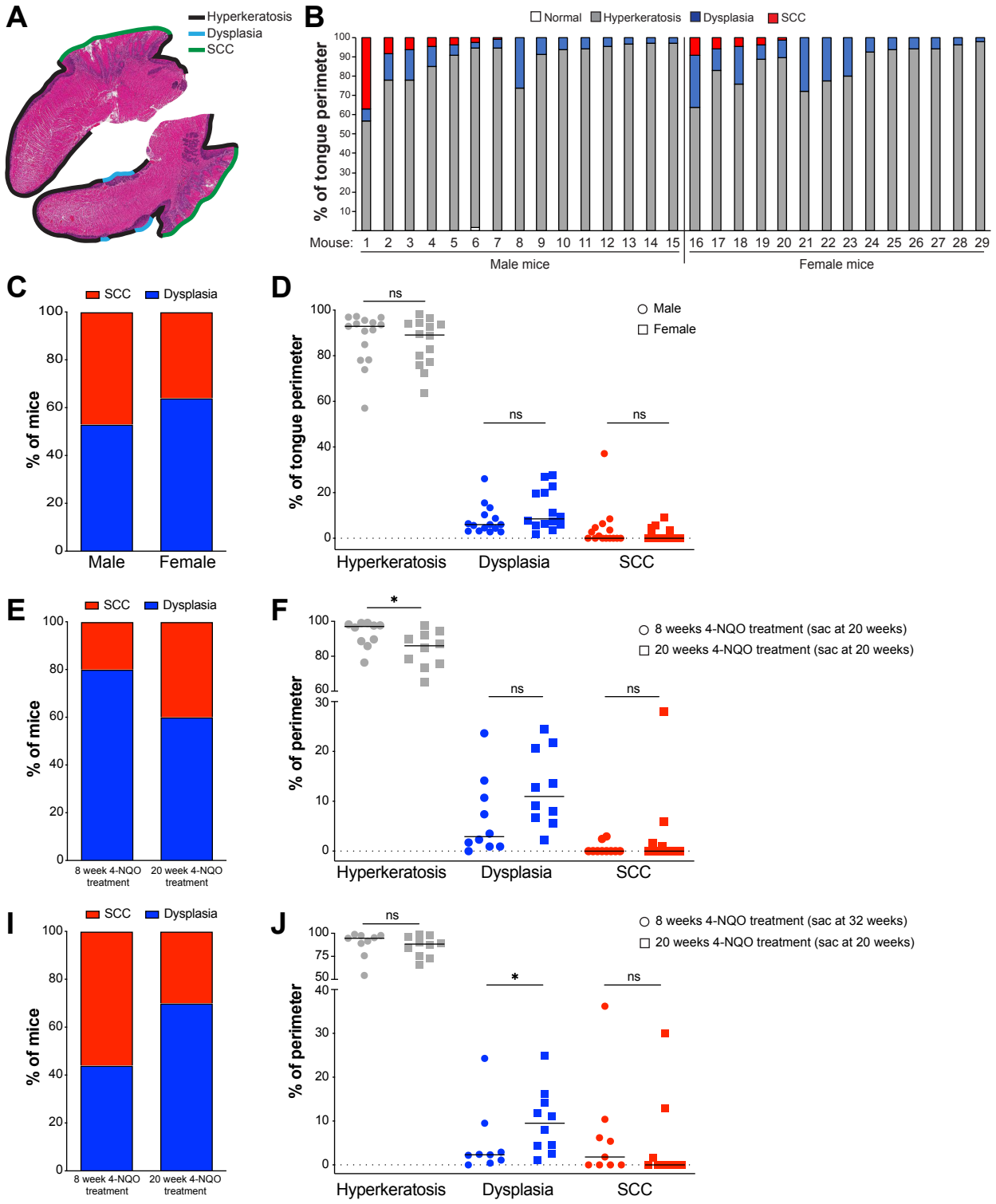

Figure 5. The chemical carcinogen 4-NQO induces the development of pre-neoplastic dysplasia and invasive oral squamous cell carcinoma

A) Quantification of histopathology. 6- to 8-week-old C57Bl/6 mice were exposed to drinking water containing 100 µg/mL 4-NQO for 20 weeks. After 20 weeks since the start of 4-NQO exposure, tongues were dissected, fixed in 10% formalin, bisected longitudinally, and stained

Figure 5, continued.
with H&E. The perimeter of each tongue is outlined and categorized base on histology grade: hyperkeratosis (black), dysplasia (blue), or SCC (green). Shown is a representative H&E stain of FFPE tongue after longitudinal bisection of 4-NQO-treated mouse, perimeter traced based on histology grades noted above.
B) Summary plot of 4-NQO-induced histopathology, showing the percentage of tongue perimeter defined as indicated histology grade. Each bar represents an individual tongue from a single mouse treated with 4-NQO drinking water for 20 weeks, separated by sex.
C, E, I) Tumor incidence, where each mouse was scored once based on most severe histology grade observed. Summary plot of pooled data, showing the percentage of mice scored as indicated histology grade. Each bar represents the cumulative data for mice of the indicated sex (C), or indicated 4-NQO exposure experimental setup (E, I). Mice were treated with 4-NQO drinking water for a continuous 20 week period (C, E, I), treated for 8 weeks followed by 12 weeks of rest on normal drinking water (E), or treated for 8 weeks followed by 24 weeks of rest on normal drinking water (I).
D, F, J) Tumor burden. Summary plots of pooled data, showing the percentage of tongue perimeter defined as hyperkeratosis, dysplasia, or SCC. Each symbol represents an individual tongue from a single mouse of the indicated sex (D), or indicated 4-NQO-exposure experimental set up (E, I). Median is indicated. Mice were treated with 4-NQO drinking water for a continuous 20 week period (D, F, J), treated for 8 weeks followed by 12 weeks of rest on normal drinking water (F), or treated for 8 weeks followed by 24 weeks of rest on normal drinking water (J).
Data are pooled from multiple independent experiments. n = 10 – 15 mice per group. Fisher t-test (C, E, I), two-tailed nonparametric Mann Whitney test (D, F, J). NS = not significant, * = $p < 0.01$.

(Figure 5E) and increased burden of dysplasia (Figure 5F) when compared to mice exposed to 4-NQO for 8 weeks. We also evaluated a third 4-NQO treatment schedule in which mice are provided with 4-NQO drinking water for 8 weeks, followed by a "rest" period of 24 weeks and analysis at 32 weeks after the initiation of 4-NQO exposure. It is important to note that this alternative treatment schedule translates to analyzing mice at ~9.5 months of age. In this setting, there were no significant differences in OSCC incidence and burden compared to mice exposed to 4-NQO for 20 weeks (Figure 5I-J). Together, these data demonstrate that the incidence and burden of dysplasia and invasive OSCC are comparable for the various 4-NQO treatment regimens utilized. To maximize OSCC incidence and burden while avoiding the need to analyze aged mice, the experiments presented in this thesis focused on the 20-week continuous 4-NQO exposure regimen, unless otherwise noted.

Murine carcinogen-induced oral lesions are associated with a low-density T cell infiltrate polarized towards enrichment of $CD4^+$ T cells

To understand the endogenous immune response in this model, we analyzed the nature of immune cell subsets infiltrating 4-NQO-induced oral lesions. Tongue-associated innate immune cells, including dendritic cells and various subsets of myeloid cells, were readily detected in the tongues of 4-NQO-treated mice by flow cytometry (Figure 6A-C). Next, we looked for the presence of infiltrating T cells. Of note, control experiments demonstrated that exposure to 4-NQO did not impair the T cell response elicited by immunization with a foreign peptide plus adjuvant (Figure 6D-E), indicating that 4-NQO exposure does not induce broad immune suppression. Analysis using immunohistochemistry (IHC) revealed that $CD3^+$ T cells were detected at low densities within most 4-NQO-induced dysplasias and OSCCs, and that these densities were slightly

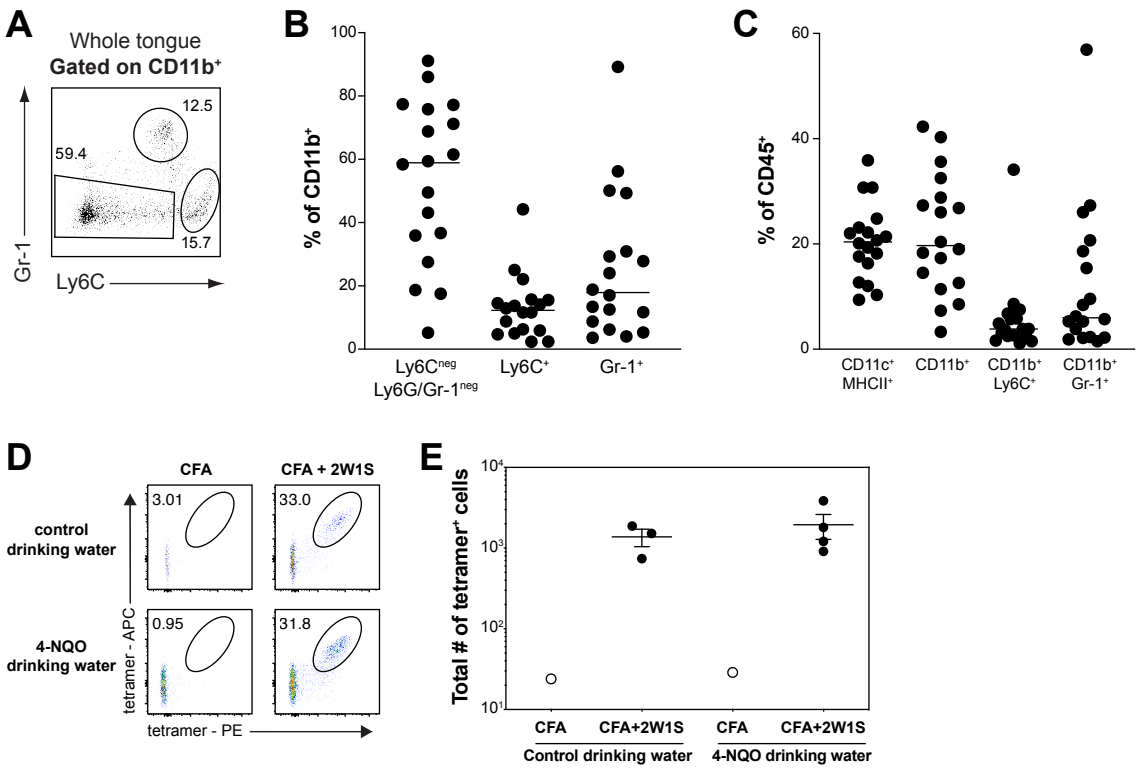

Figure 6. Murine carcinogen-induced oral lesions harbor innate immune cells

A-C) 6- to 8-week-old female C57Bl/6 mice were exposed to 4-NQO drinking water for 8 weeks followed by 24 weeks on normal drinking water. Mice were analyzed 32 weeks after the start of 4-NQO treatment. Data are pooled from three independent experiments.

A) Representative flow cytometric analysis of Ly6C vs. Gr-1 expression by $CD11b^+$ cells isolated from tongues of 4-NQO-treated mice. The frequency of cells within the indicated gates is denoted.

B) Summary plot of pooled data from (A), showing the frequency of $Ly6C^{neg}$ $Ly6G/Gr\text{-}1^{neg}$ cells, $Ly6C^+$ cells, and $Gr\text{-}1^+$ cells amongst $CD11b^+$ cells isolated from whole tongues of 4-NQO-treated mice. Each symbol represents an individual mouse. Mean is indicated. n = 18 mice.

C) Summary plot of pooled data, showing the frequency of $CD11c^+$ $MHCII^{hi}$ cells, $CD11b^+$ cells, $CD11b^+$ $Ly6C^+$ cells, and $CD11b^+$ $Gr\text{-}1^+$ cells amongst $CD45^+$ cells isolated from whole tongues of 4-NQO-treated mice. Mean is indicated. n = 18 mice.

D-E) 6-week-old female C57Bl/6 mice were exposed to 4-NQO drinking water for 20 weeks. After 18 weeks of 4-NQO exposure, mice were immunized subcutaneously with 100 μg 2W1S peptide emulsified in CFA. Two weeks after immunization, after 20 weeks of 4-NQO exposure, $CD4^+$ T cells were isolated and 2W1S/I-A^b tetramer-binding cells were enriched from pooled SLOs and analyzed by flow cytometry. Age-matched C57Bl/6 female mice not exposed to 4-NQO were used as controls. Data from one experiment. n = 1 – 4 mice per group.

D) Representative flow cytometric analysis of $CD4^+$ T cells isolated from pooled SLOs of immunized mice. Plots depict dual 2W1S/I-A^b tetramer staining on $CD4^+$ T cells. The frequency of cells within the indicated gates is denoted.

E) Summary plot of pooled data from (D), showing the total number of dual 2W1S/I-A^b tetramer-binding $CD4^+$ T cells, enriched from SLOs of immunized mice. Each symbol represents an individual mouse. Mean ± SEM is indicated.

elevated relative to normal epithelium and regions of hyperkeratosis (Figure 7A-B). T cells were sparse and typically localized near the basal epithelium or interspersed within the parenchyma of dysplastic and OSCC lesions (Figure 7A). Analysis of tongue-associated T cells from either the whole tongue or from excised lesions of 4-NQO-treated mice using flow cytometry revealed a preponderance of $CD4^+$ αβ T cells (Figure 7C-E), similar to published reports assessing immune populations resident in the oral cavity[141,142]. $CD8^+$ αβ T cells were also readily detectable but were typically found at lower densities (Figure 7C-E), and γδ T cells were uncommon (data not shown and Figure 14G-H). On average, $Foxp3^+$ Treg cells accounted for 54%±18 of tongue-associated $CD4^+$ T cells isolated from 4-NQO-treated mice (Figure 7F), consistent with reports showing that human OSCCs harbor elevated percentages of $FOXP3^+$ Treg cells[101,105,135]. These Treg cells did not express lineage-defining transcription factors of differentiated helper T cell subsets, including T-bet, Gata3, and RORγt (Figure 7G), as has been described in some murine tumor models and human cancer patients[47,48,143,144]. Furthermore, the elevated frequency of $Foxp3^+$ Tregs was specific to 4-NQO exposure and was more pronounced in the draining cervical lymph nodes (Figure 7H), suggesting enhanced Treg cell abundance in response to 4-NQO-induced lesions. Together, these data reveal that 4-NQO-induced lesions are characterized by low-density T cell infiltration polarized towards enrichment of $CD4^+$ Treg and conventional T cells.

A fraction of tongue-associated Treg cells exhibit clonal expansion and reactivity to regional antigens

To gain insight into the antigen specificity of tongue-associated Treg cells in this model, we performed single-cell sorting of Treg cells isolated from whole tongues of 4-NQO-treated mice, followed by nested PCR amplification and sequencing of rearranged TCR genes[123]. To facilitate

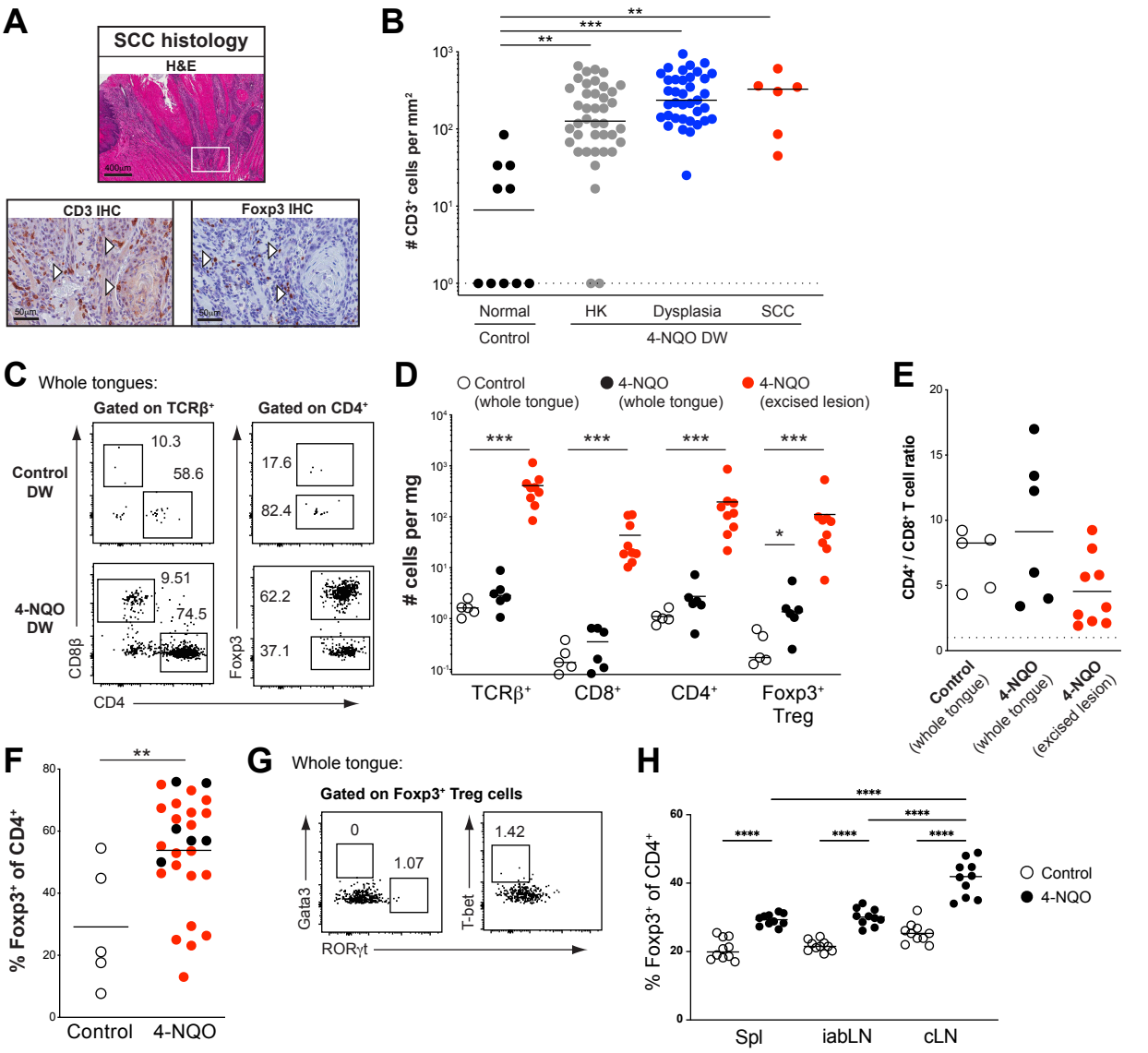

Figure 7. Murine carcinogen-induced oral lesions are enriched for CD4⁺ Treg and conventional T cells

6- to 8-weekd old C57Bl/6 mice were exposed to 4-NQO drinking water for 20 weeks.

A) (Top) Representative H&E image of SCC region of tongue epithelium. (Bottom) Representative CD3 (left) and Foxp3 (right) IHC images of adjacent sections of depicted SCC region denoted by white box in H&E image. White arrows denote $CD3^+$ or $Foxp3^+$ cells. Scale bar represents 400 μm (H&E) or 50 μm (IHC).

B) Summary plot of pooled data from CD3 IHC density analysis, showing the number of $CD3^+$ cells per mm^2 for each lesion. Each symbol represents an individual lesion. Median is indicated. n = 10 regions from 1 mouse (control), n = 6 – 40 lesions from 10 mice (4-NQO).

C) Representative flow cytometric analysis of $CD8^+$ and $CD4^+$ T cells isolated from tongues of 4-NQO-treated or vehicle-treated mice. Left plots depict CD4 vs. CD8β expression by $TCR\beta^+$ cells, whereas the right plots depict CD4 vs. Foxp3 expression by $CD4^+$ T cells. The frequency of cells within the indicated gates is denoted.

D-F) Summary plot of pooled data from (C), showing the number of $TCR\beta^+$, $CD8^+$, $CD4^+$, or

Figure 7, continued.
Foxp3$^+$ T cells per mg of tissue (D), the ratio of CD4$^+$ to CD8$^+$ T cells (E), or the frequency of Foxp3$^+$ cells amongst CD4$^+$ T cells (F) isolated from whole tongues of vehicle-treated mice (open circles), whole tongues from 4-NQO-treated mice (black circles), or excised tongue lesions from 4-NQO-treated mice (red circles). Each symbol represents an individual mouse (open and black circles) or an individual lesion (red circles). Mean is indicated. Dotted line represents ratio = 1 (E). n = 5 (control whole tongues), n = 6 (4-NQO whole tongues), n = 9 – 21 (4-NQO excised lesions). **G)** Representative flow cytometric analysis of Foxp3$^+$ Treg cells isolated from tongue of 4-NQO-treated mouse. Left plot depicts RORγt vs. Gata3 expression, whereas the right plot depicts RORγt vs. T-bet expression. The frequency of cells within the indicated gates is denoted. **H)** Summary plot of pooled data, showing the frequency of Foxp3$^+$ cells amongst CD4$^+$ T cells isolated from spleen or lymph nodes of 4-NQO treated mice. Mean is indicated. n = 10 mice per group. Spl = spleen, iabLN = axial, inguinal, and brachial lymph nodes, cLN = cervical lymph node.
Data are pooled from multiple independent experiments. HK = hyperkeratosis, SCC = squamous cell carcinoma, DW = drinking water. One-way ANOVA with Dunn's post-test analysis, comparing all pairs in column (B, H, adjusted p-values from Dunn's post-test are depicted), two-tailed nonparametric Mann Whitney test (D, F). ** = $p < 0.01$, *** = $p < 0.001$, **** = $p < 0.0001$.

this analysis, we utilized mice expressing a *Foxp3*^{GFP} reporter allele and a fixed transgenic TCRβ (TCRβtg) chain[83], which enables the analysis of TCR specificity and diversity by sequencing of the TCRα chain alone[124,127]. Our survey of Treg cells from five 4-NQO-treated *Foxp3*^{GFP} TCRβtg mice demonstrated that tongue-associated Treg cells from each mouse expressed a diverse array of TCRα chains (Figure 8A). While the overall repertoire was diverse, a small fraction of tongue-associated Treg cell clones were found recurrently in multiple mice; seven clones were found in at least three of the five animals analyzed (Figure 8B). These recurrent clones expressed distinct CDR3α sequences and utilized diverse Vα and Jα elements (Table 2). Analysis of the representation of these TCRs in previously published TCRα data sets of T cells from the pooled secondary lymphoid organs (SLOs) of untreated tumor-free *Foxp3*^{GFP} TCRβtg mice[127] revealed that most TCRs expressed by tongue-associated Treg cells were preferentially expressed by Treg cells found in tumor-free mice (Figure 8A-B), suggesting that tongue-associated Treg cell clones in 4-NQO-treated mice were likely drawn from a pre-existing Treg cell pool.

To define the nature of antigens recognized by these recurrent Treg cell clones, we generated monoclonal TCR "retrogenic" (TCRrg) mice[124,128] expressing single recurrent tongue-associated Treg cell TCRs identified above. CD4$^+$ T cells from TCRrg mice were purified and co-transferred with congenically disparate polyclonal splenocytes into T cell-deficient *Tcrb*$^{-/-}$ recipient mice that had not been exposed to 4-NQO, and the distribution and activation status of donor TCRrg cells was assessed. For three of the four clones, TCRrg CD4$^+$ T cells exhibited preferential activation and/or accumulation in the tongue-draining cervical lymph nodes (cLNs) (Figure 8C-D), suggestive of reactivity to regional antigens that are presented in tumor-free animals, irrespective of tumor status and 4-NQO exposure.

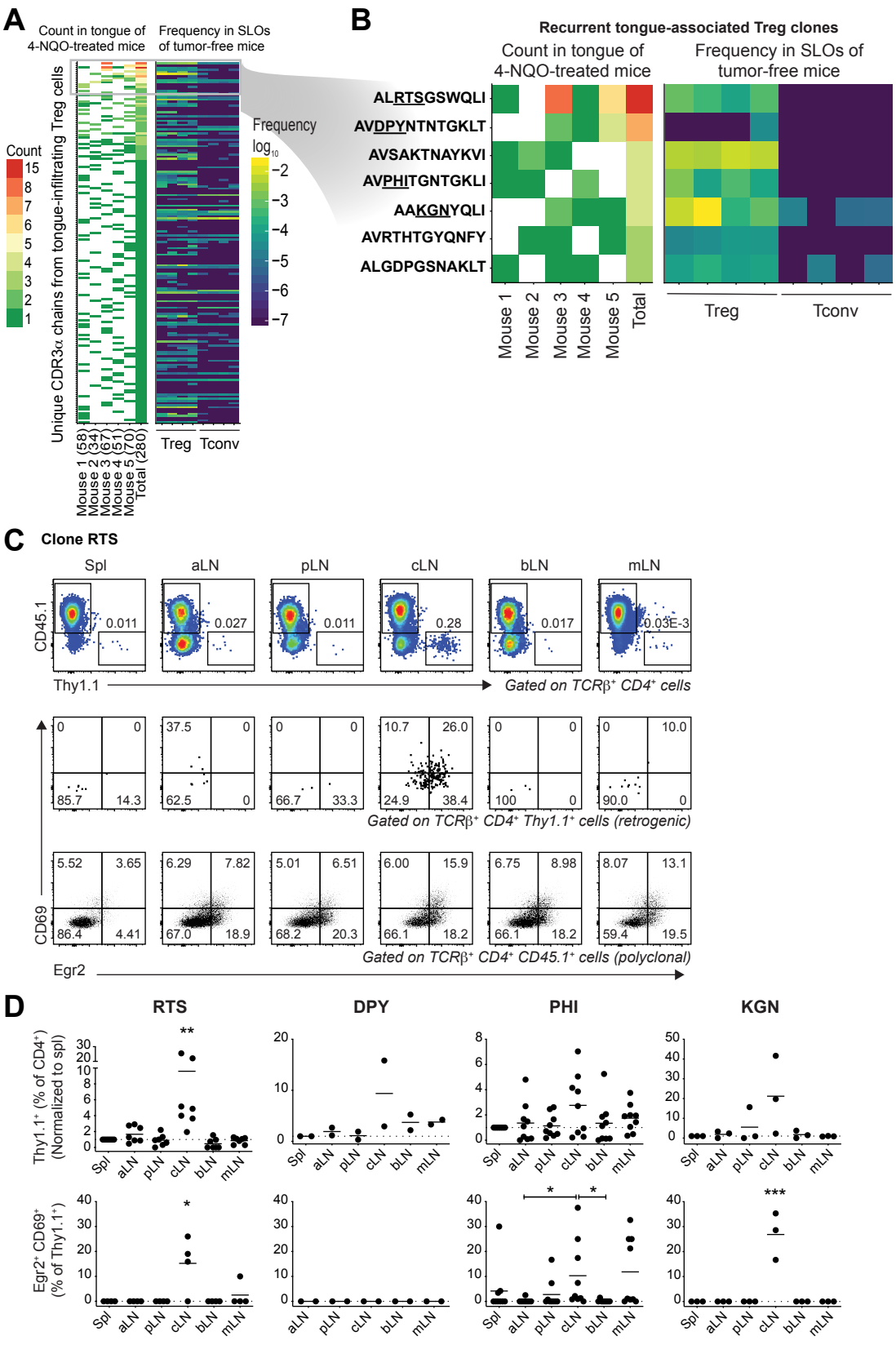

Figure 8. A fraction of tongue-associated Treg cell clones exhibit clonal expansion and reactivity to regional antigens *(Legend on next page)*

Figure 8, continued.
A-B) 6- to 8-week-old Foxp3^{GFP} TCRβtg^{+} mice were placed on 4-NQO drinking water for 8 weeks, followed by 24 weeks of normal drinking water. Treg cells were subsequently isolated from tongues, single-cell sorted by FACS, and TCRβ chains were amplified by nested PCR and subjected to Sanger sequencing (see methods). n = 5 mice.
A) Heatmap depicting all CDR3α sequences identified among all single-cell sorted Treg cells. Each row represents a unique CDR3α sequence. (Left) The number of occurrences each CDR3α sequence appears in tongue-associated Treg datasets from individual 4-NQO-treated mice. Each column represents an individual mouse, with the number of cells sequenced per mouse noted in parenthesis. The last column represents the cumulative data. Color denotes the total number each CDR3α sequence appears in dataset. (Right) The frequency each CDR3α sequence appears in published datasets of CD4^{+} Foxp3^{+} Treg cells or CD4^{+} Foxp3^{neg} Tconv cells isolated from pooled secondary lymphoid organs (SLOs) of untreated, non-tumor-bearing Foxp3^{GFP} TCRβtg^{+} mice[83]. Each column represents dataset from an individual mouse. Color denotes the frequency of each CDR3α sequence in dataset.
B) Select CDR3α sequences from (A), depicting those recurrent among at least three 4-NQO-treated mice. Underlined amino acid sequence refers to the 3-letter ID used to reference each TCR clone in (C-D).
C-D) 10^4 Thy1.1^{+} CD4^{+} TCR retrogenic (TCRrg) T cells were isolated from pooled SLOs of primary retrogenic mice and co-transferred with 10^6 RBC-lysed splenocytes from CD45$^{.1/.1}$ mice intravenously into *Tcrb*$^{-/-}$ secondary recipients (see methods). 3 weeks after transfer, the fate of transferred T cells was assessed in SLOs.
C) Representative flow cytometric analysis of CD4^{+} T cells isolated from indicated organs of secondary recipients that received RTSrg donor T cells. The top plots depict Thy1.1 vs. CD45.1 expression by CD4^{+} cells, whereas the middle and bottom plots depict Egr2 vs. CD69 expression by donor Thy1.1^{+} RTSrg or CD45.1^{+} polyclonal CD4^{+} T cells, respectively. The frequency of cells within the indicated gates is denoted.
D) Summary plots of pooled data from (C), showing the frequency of Thy1.1^{+} CD4^{+} TCRrg T cells amongst total CD4^{+} T cells (top), and the frequency of Thy1.1^{+} CD4^{+} TCRrg T cells expressing Egr2 and CD69 (bottom), isolated from indicated organs of secondary recipient mice. TCR clone names depicted refer to the 3rd – 5th amino acids of the CDR3α sequence, underlined in (B). Mean is indicated. Dotted line denotes y-axis = 1 (top) or y-axis = 0 (bottom). n = 4 – 7 mice (RTS TCRrg), n = 2 mice (DPY TCRrg), n = 9 mice (PHI TCRrg), n = 3 mice (KGN TCRrg).
Data are pooled from multiple independent experiments. Spl = spleen, aLN = axial lymph node, pLN = periaortic lymph node, cLN = cervical lymph node, bLN = brachial lymph node, mLN = mesenteric lymph node. One-way ANOVA with Tukey's post-test analysis, comparing all pairs in column (D, adjusted p-values from Tukey's post-test are depicted). * = $p < 0.0.5$, ** = $p < 0.01$, *** = $p < 0.001$.

CDR3α	V-region	J-region
AL**RTS**GSWQLI	mTRAV12-1	mTRAV22
AV**DPY**NTNTGKLT	mTRAV7-5	mTRAV27
AV**SAK**TNAYKVI	mTRAV9-3	mTRAJ30
AV**PHI**TGNTGKLI	mTRAV3-4	mTRAV37
AA**KGN**YQLI	mTRAV14D-3/DV8	mTRAV33
AV**RTH**TGYQNFY	mTRAV3-4	mTRAJ49
AL**GDP**GSNAKLT	mTRAV6D-6	mTRAJ42

Table 2. Recurrent tongue-associated Treg TCRs isolated from 4-NQO-treated mice
CDR3α sequences depicted in Figure 8B, representing the 7 recurrent TCR clones found in at least three 4-NQO-treated mice. Bold amino acid sequence of CDR3α refers to the 3-letter ID used to reference each TCR clone. TRAV and TRAJ usage for each clone is depicted. Clones RTS, DPY, PHI, and KGN, representing a range of TRAV and TRAJ usage, were selected for retrogenic mouse generation and downstream characterization for Figure 8C-D.

4-NQO-induced lesions are not significantly impacted by the endogenous adaptive immune response

Given that 4-NQO-induced lesions mimic genetic heterogeneity of human tobacco-associated OSCC[145], and harbor a high density of point mutations with potential to encode tumor-specific neo-antigens[114,115] we hypothesized that the endogenous T cell response may restrict the emergence of dysplasia or OSCC, as has been suggested for cancers exhibiting a high mutational load[146]. However, our data revealed that the incidence and burden of dysplasias and OSCCs were not significantly altered in αβ T cell-deficient *Tcrb*$^{-/-}$ mice or γδ T cell-deficient *Tcrd*$^{-/-}$ mice relative to wild-type littermates (Figure 9A-B), indicating that T cells do not measurably impact the emergence of 4-NQO-induced lesions in the absence of immune-based therapy. Similarly, the incidence and burden of dysplasias and OSCCs were not significantly altered in B cell-deficient *Ighm*$^{-/-}$ mice compared to wild-type littermates (Figure 9C-D), demonstrating that B cells also do not measurably impact the emergence of 4-NQO-induced lesions in the absence of immune-based therapy. Together, these data demonstrate that the endogenous adaptive immune response does not impact the development or progression of 4-NQO-induced OSCC at steady-state, in the absence of any perturbations.

Tongue-associated PD-1-deficient T cells have a competitive advantage in 4-NQO-treated mice

Given the role of PD-1 as an important negative regulator of T cells[25], we generated mixed bone marrow chimeras by engrafting equal ratios of wild-type and congenically disparate PD-1-deficient *Pdcd1*$^{-/-}$ bone marrow into lethally irradiated wild-type hosts to assess the role of PD-1 expression on T cell infiltration in 4-NQO-induced lesions. After 20 weeks of 4-NQO exposure,

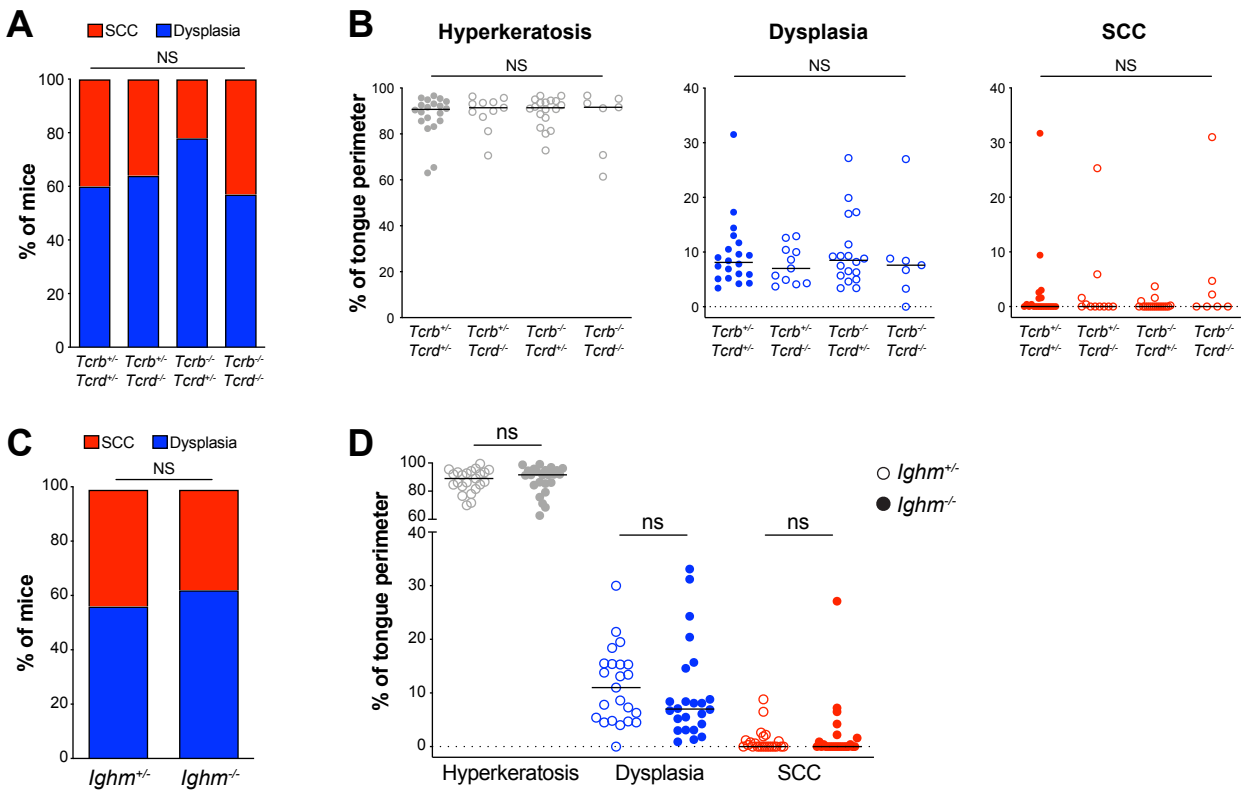

Figure 9. 4-NQO-induced lesions are not significantly impacted by the endogenous adaptive immune response

6- to 8-week-old littermates of indicated genotype were exposed to 4-NQO drinking water for 20 weeks, and tongues were subsequently excised, and histopathology was quantified as in Figure 5A.

A, C) Tumor incidence, where each mouse was scored once based on most severe histology grade observed. Summary plot of pooled data, showing the percentage of mice scored as indicated histology grade. Each bar represents the cumulative data for mice of the indicated genotype.

B, D) Tumor burden. Summary plots of pooled data, showing the percentage of tongue perimeter defined as hyperkeratosis, dysplasia, or SCC. Each symbol represents an individual tongue from a single mouse of the indicated genotype. Median is indicated.

Data are pooled from multiple independent experiments. SCC = squamous cell carcinoma. n = 20 mice (*Tcrb*$^{+/-}$ *Tcrd*$^{+/-}$), n = 11 mice (*Tcrb*$^{+/-}$ *Tcrd*$^{-/-}$), n = 18 mice (*Tcrb*$^{-/-}$ *Tcrd*$^{+/-}$), n = 7 mice (*Tcrb*$^{-/-}$ *Tcrd*$^{-/-}$), n = 23 mice (*Ighm*$^{+/-}$), n = 24 mice (*Ighm*$^{-/-}$). Fisher t test (A, C), one-way ANOVA, comparing all pairs in column (B), two-tailed nonparametric Mann Whitney test (D). NS = not significant.

tongue-associated T cells were largely derived from the *Pdcd1*$^{-/-}$ bone marrow compartment (Figure 10A-D). This was true for all T cell subsets analyzed, including CD8^{+} T cells (Figure 10A, B), CD4^{+} Foxp3^{neg} Tconv cells (Figure 10A, C), and CD4^{+} Foxp3^{+} Treg cells (Figure 10A, D). Furthermore, the overrepresentation of *Pdcd1*$^{-/-}$ T cells was unique to tongue-associated T cells, as this was not observed in spleen or lymph nodes (Figure 10B-D). Together, these data demonstrate that PD-1-deficient T cells have a competitive advantage compared to wild-type T cells in the tongues of 4-NQO-treated mice, and suggest that targeting PD-1 via checkpoint blockade may promote T cell infiltration and/or survival within carcinogen-induced lesions.

4-NQO-induced lesions are not significantly impacted by treatment with checkpoint blockade therapies

To define the extent to which 4-NQO-induced lesions are responsive to established antibody-mediated checkpoint blockade immunotherapies, we treated 4-NQO-exposed mice with monotherapy using anti-CTLA-4, anti-PD-1, or anti-PD-L1 antibody, each paired with appropriate isotype control groups. As shown in Figure 11, these monotherapies did not significantly alter the burden or incidence of pre-neoplastic lesions or OSCCs (Figure 11A-B, E-F, H-I), and failed to significantly alter the density of infiltrating T cells (Figure 11C-D, G, J), suggesting that 4-NQO-induced lesions were largely resistant to these T cell-directed checkpoint blockade monotherapies in the animal cohorts examined.

To further test whether 4-NQO-induced lesions are responsive to checkpoint blockade immunotherapies, we next treated 4-NQO-exposed mice that were depleted of neutrophils with a combination of anti-PD-L1 and anti-CTLA-4 antibodies. We wondered if this strong treatment strategy would lead to tumor regression. Depleting neutrophils using an anti-Gr-1 monoclonal

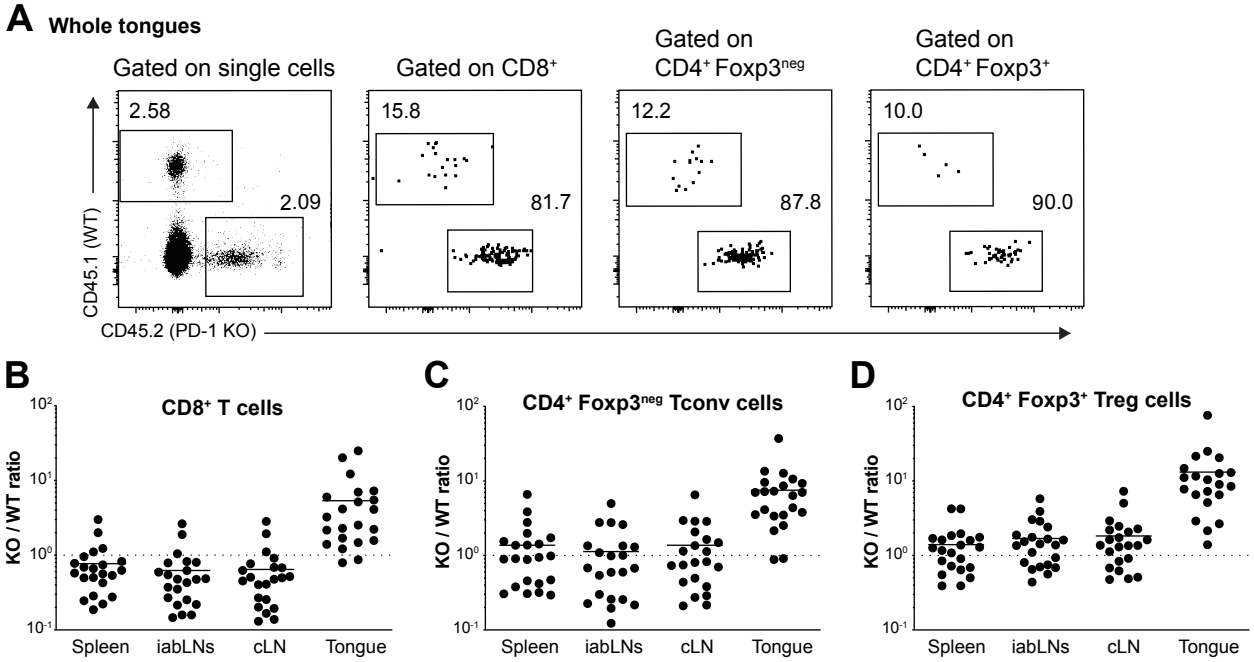

Figure 10. Tongue-associated PD-1-deficient T cells have a competitive advantage in 4-NQO-treated mice

B6.SJL ($CD45^{.1/.1}$) littermates were lethally irradiated and reconstituted with a 1:1 mixture of *Pdcd1*$^{+/+}$ (CD45.1) and *Pdcd1*$^{-/-}$ (CD45.2) bone marrow. 8 weeks post-engraftment, mice were placed on 4-NQO drinking water for 20 weeks.

A) Representative flow cytometric analysis of cells isolated from tongue of 4-NQO-treated mixed bone marrow chimera mouse. Plots depict CD45.2 vs. CD45.1 expression by all single cells (leftmost plot), $CD8^+$ T cells (left-center plot), $CD4^+$ $Foxp3^{neg}$ Tconv cells (right-center plot), and $CD4^+$ $Foxp3^+$ Treg cells (rightmost plot). The frequency of cells within the indicated gates is denoted.

B-C) Summary plot of pooled data from (A), showing the ratio of *Pdcd1*$^{-/-}$ to *Pdcd1*$^{+/+}$ cells amongst $CD8^+$ T cells (B), $CD4^+$ $Foxp3^{neg}$ Tconv cells (C), or $CD4^+$ $Foxp3^+$ Treg cells (D). Each symbol represents an individual mouse. Mean is indicated. Dotted line represents ratio = 1.

Data are pooled from three independent experiments. iabLNs = inguinal, axial, and brachial lymph nodes, cLN = cervical LN. n = 22 mice.

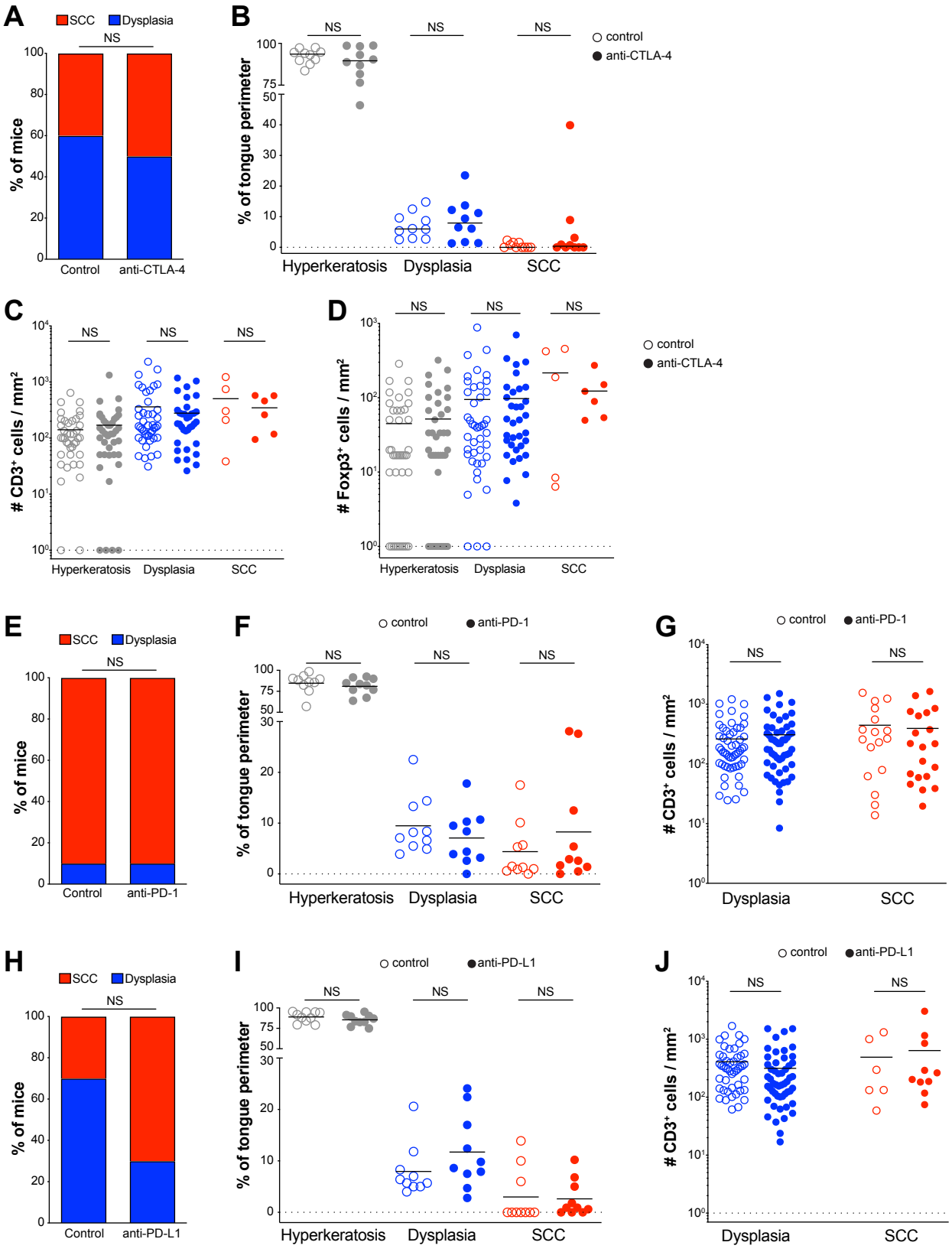

Figure 11. 4-NQO-induced lesions are not significantly impacted by treatment with checkpoint blockade monotherapies *(Legend on next page)*

Figure 11, continued.
6- to 8-week-old C57Bl/6 mice were exposed to 4-NQO drinking water for 20 weeks. During the last 4 weeks of 4-NQO exposure, mice were treated intraperitoneally twice weekly with 100 μg anti-CTLA-4 (A-D), anti-PD-1 (E-G), anti-PD-L1 (H-J) or isotype control monoclonal antibody. Tongues were excised at endpoint, and histopathology and IHC staining was performed and quantified. n = 10 mice per group.
A, E, H) Tumor incidence, where each mouse was scored once based on most severe histology grade observed. Summary plot of pooled data, showing the percentage of mice scored as indicated histology grade. Each bar represents the cumulative data for mice that received control antibody or anti-CTLA-4 (A), anti-PD-1 (E), or anti-PD-L1 (H) monoclonal antibody.
B, F, I) Tumor burden. Summary plot of pooled data, showing the percentage of tongue perimeter defined as the indicated histology grade. Each symbol represents an individual tongue from a single mouse that received control antibody or anti-CTLA-4 (B), anti-PD-1 (F), or anti-PD-L1 (I) monoclonal antibody. Median is indicated.
C, G, J) Summary plot of pooled data from CD3 IHC density analysis, showing the number of $CD3^+$ cells per mm^2 for each lesion from mice that received control antibody or anti-CTLA-4 (C), anti-PD-1 (G), or anti-PD-L1 (J) monoclonal antibody. Each symbol represents an individual lesion. Median is indicated. n = 5 – 54 lesions from 10 mice per group.
D) Summary plot of pooled data from Foxp3 IHC density analysis, showing the number of $Foxp3^+$ cells per mm^2 for each lesion. Each symbol represents an individual lesion. Median is indicated. n = 5 – 43 lesions from 10 mice per group.
Data are pooled from multiple independent experiments. SCC = squamous cell carcinoma. Fisher t test (A, E, H), two-tailed nonparametric Mann Whitney test (B-D, F-G, I-J). NS = not significant.

antibody (Figure 12A) did not significantly alter the incidence or burden of dysplasias or OSCCs alone or in combination with anti-PD-L1 and anti-CTLA-4 treatment (Figure 12B-C). These data demonstrate that neutrophils do not measurably impact 4-NQO-induced lesions, whether or not in the context of combination checkpoint blockade therapy.

Together, these data demonstrate that 4-NQO-induced lesions are largely resistant to checkpoint blockade therapies, both as monotherapies and as combination therapies, and neutrophils do not significantly impact tumorigenesis. While the factors underlying the negligible impact of checkpoint blockade therapy remain undefined, we hypothesized that a lack of a high-density tumor-infiltrating effector T cell response and a preponderance of suppressive Foxp3$^+$ Treg cells observed in Figure 7 may promote therapeutic resistance.

Late-stage Treg cell depletion enhances the emergence of invasive OSCC

The above results suggest that the 4-NQO-induced model of OSCC mirrors a substantial fraction of human OSCCs and other common human malignancies, in which cancer lesions are associated with a low-density of infiltrating T cells and do not exhibit robust responses following checkpoint blockade therapy[32,33,35,104,147]. In this regard, a major therapeutic goal is to develop novel approaches to drive increased densities of tumor-infiltrating T cells, thereby turning non-T cell-inflamed "cold" tumors into T cell-inflamed "hot" tumors[32–35]. To examine this idea mechanistically, we aimed to augment effector T cell infiltration of 4-NQO-induced lesions by transiently ablating Foxp3$^+$ Treg cells, which has been previously shown to enhance intratumoral T cell density and promote tumor regression in some murine cancer models[61,62,148,149]. To this end, we utilized *Foxp3*$^{DTR/y}$ mice in which the human diphtheria toxin receptor (DTR) is expressed by all Foxp3-expressing cells, enabling inducible ablation of Treg cells via intraperitoneal

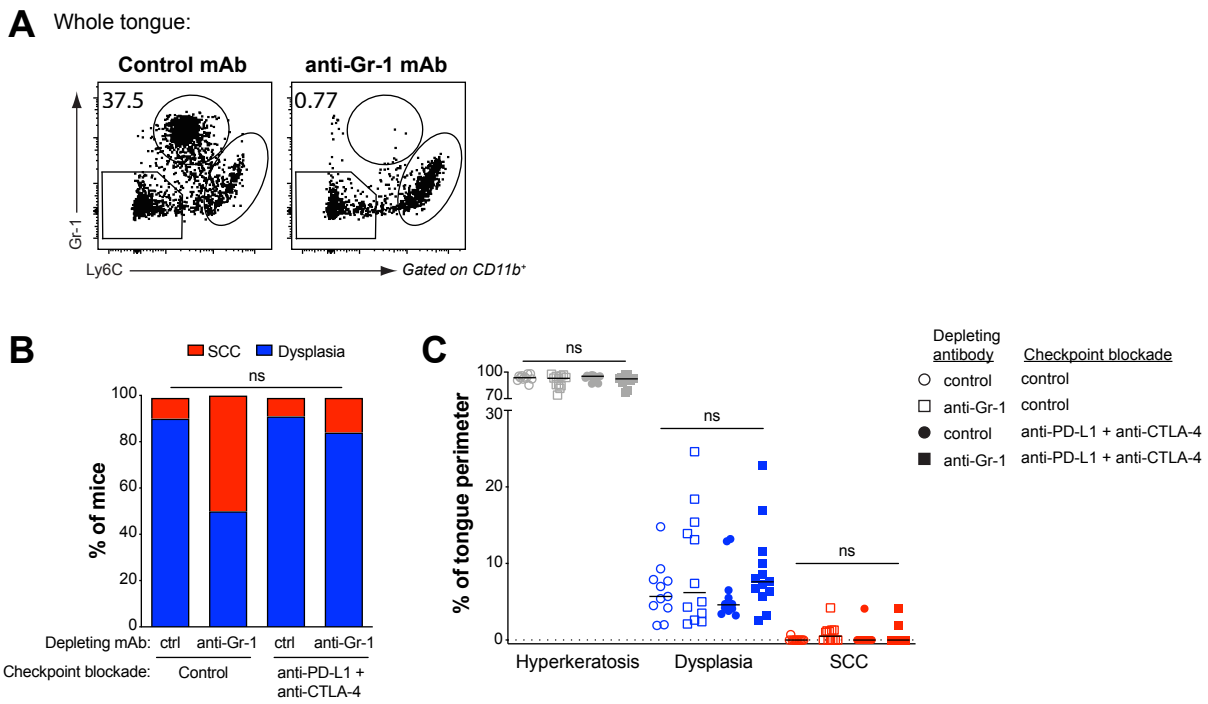

Figure 12. 4-NQO-induced lesions are not significantly impacted by neutrophil depletion or combination checkpoint blockade treatment

6- to 8-week-old female C57Bl/6 mice were exposed to 4-NQO drinking water for 20 weeks. During the last 4 weeks of 4-NQO exposure, mice were treated intraperitoneally with 200 μg anti-Gr-1 depleting or isotype control antibody, plus 100 μg each of anti-CTLA-4 and anti-PD-L1 or isotype control monoclonal antibodies (see methods). Tongues were excised at endpoint, and histopathology staining was performed and quantified as in Figure 5A. n = 11 – 13 mice per group.

A) Representative flow cytometric analysis of $CD11b^+$ cells isolated from tongues of 4-NQO-treated mice treated with isotype control or anti-Gr-1 neutrophil depleting monoclonal antibody. Plots depict Ly6C vs. Gr-1 expression by $CD11b^+$ cells. The frequency of $Gr\text{-}1^+$ neutrophils within the indicated gates is denoted.

B) Tumor incidence, where each mouse was scored once based on most severe histology grade observed. Summary plot of pooled data, showing the percentage of mice scored as indicated histology grade. Each bar represents the cumulative data for mice that received indicated depleting antibody and indicated combination checkpoint blockade antibodies.

C) Tumor burden. Summary plot of pooled data, showing the percentage of tongue perimeter defined as the indicated histology grade. Each symbol represents an individual tongue from a single mouse that received indicated depleting antibody and indicated combination checkpoint blockade antibodies. Median is indicated.

Data are pooled from multiple independent experiments. mAb = monoclonal antibody, ctrl = control monoclonal antibody, SCC = squamous cell carcinoma. Fisher t test (B, adjusted p-values from Bonferroni correction are depicted), one-way ANOVA with Dunn's post-test analysis, comparing all pairs in column (C, adjusted p-values from Dunn's post-test are depicted). NS = not significant.

administration of diphtheria toxin (DT). We exposed *Foxp3*$^{DTR/y}$ and control *Foxp3*$^{WT/y}$ male littermates to 4-NQO for 20 weeks. Starting at 16 weeks of 4-NQO exposure, Treg cells were ablated via DT administration for one week, and mice were then given three weeks to recover (Figure 13A). Of note, while DT-mediated Treg cell depletion was systemic[63], mice did not develop adverse autoimmune reactions in non-lymphoid organs (data not shown), similar to previously reported results using a similar regimen[61].

Unexpectedly, depletion of Treg cells at this late stage did not trigger regression of dysplastic lesions or OSCCs, but instead induced increased incidence and burden of OSCCs within the short four-week period following initiation of Treg cell ablation (Figure 13B-C). By IHC, increased OSCC incidence and burden were associated with a >2.5-fold increase in the densities of CD3$^+$ T cells in both dysplasias and OSCCs at endpoint (Figure 14A-B). In Treg-depleted *Foxp3*$^{DTR/y}$ mice, CD3$^+$ T cells were found in distinct clusters in both the basal epithelium and within the tumor parenchyma, compared to the sparse localization in lesions from *Foxp3*$^{WT/y}$ littermates (Figure 14A). Notably, Foxp3$^+$ Treg cell densities within 4-NQO-induced lesions returned to baseline levels at the 20 week endpoint (4 weeks after initiation of Treg cell ablation, Figure 14C), highlighting the robust mechanisms driving Treg cell recovery following inducible depletion. Flow cytometry-based analysis of the whole tongues of treated mice revealed that Foxp3^{neg}CD4$^+$ and CD8$^+$ αβ effector T cells were the major immune cell populations to increase in the tongues following Treg cell depletion (Figure 14D-F), with other tongue-infiltrating CD45$^+$ cell populations remaining largely unaltered (Figure 14G-H). To determine if Treg cell depletion had a similar impact during the earlier stages of carcinogenesis, we depleted Treg cells in a transient and periodic manner by administrating DT on consecutive days starting at 8 weeks of 4-NQO exposure and repeated every 3 weeks (Figure 15A). We found that this regimen induced

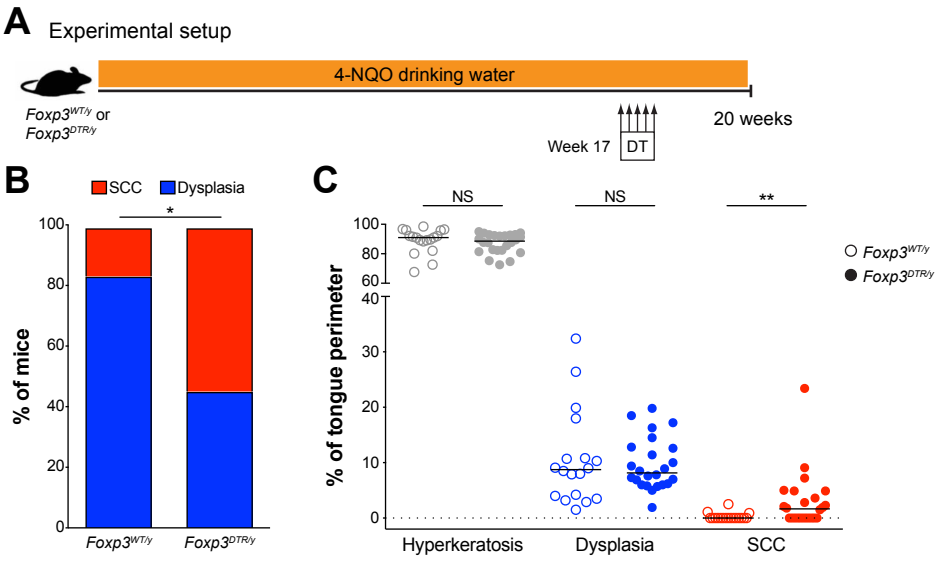

Figure 13. Late-stage Treg cell depletion enhances the emergence of invasive OSCC

A) Experimental setup. 6- to 8-week-old *Foxp3*$^{WT/y}$ and *Foxp3*$^{DTR/y}$ littermates were exposed to 4-NQO drinking water for 20 weeks. During the 17th week of 4-NQO exposure, all mice were treated intraperitoneally every other day with diphtheria toxin (DT) for 1 week. Mice were sacrificed either 3 weeks later, at the 20 week endpoint, for histopathology analysis.

B) Tumor incidence at 20 week endpoint, where each mouse was scored once based on most severe histology grade observed. Summary plot of pooled data, showing the percentage of mice scored as indicated histology grade. Each bar represents the cumulative data for mice of the indicated genotype. n = 18 mice (*Foxp3*$^{WT/y}$), n = 24 mice (*Foxp3*$^{DTR/y}$).

C) Tumor burden at 20 week endpoint. Summary plot of pooled data, showing the percentage of tongue perimeter defined as the indicated histology grade. Each symbol represents an individual tongue from a single mouse of the indicated genotype. Median is indicated. n = 18 mice (*Foxp3*$^{WT/y}$), n = 24 mice (*Foxp3*$^{DTR/y}$).

Data are pooled from multiple independent experiments. SCC = squamous cell carcinoma. Fisher t test (B), two-tailed nonparametric Mann Whitney test (C). NS = not significant, * = $p < 0.0.5$, ** = $p < 0.01$, *** = $p < 0.001$, **** = $p < 0.0001$.

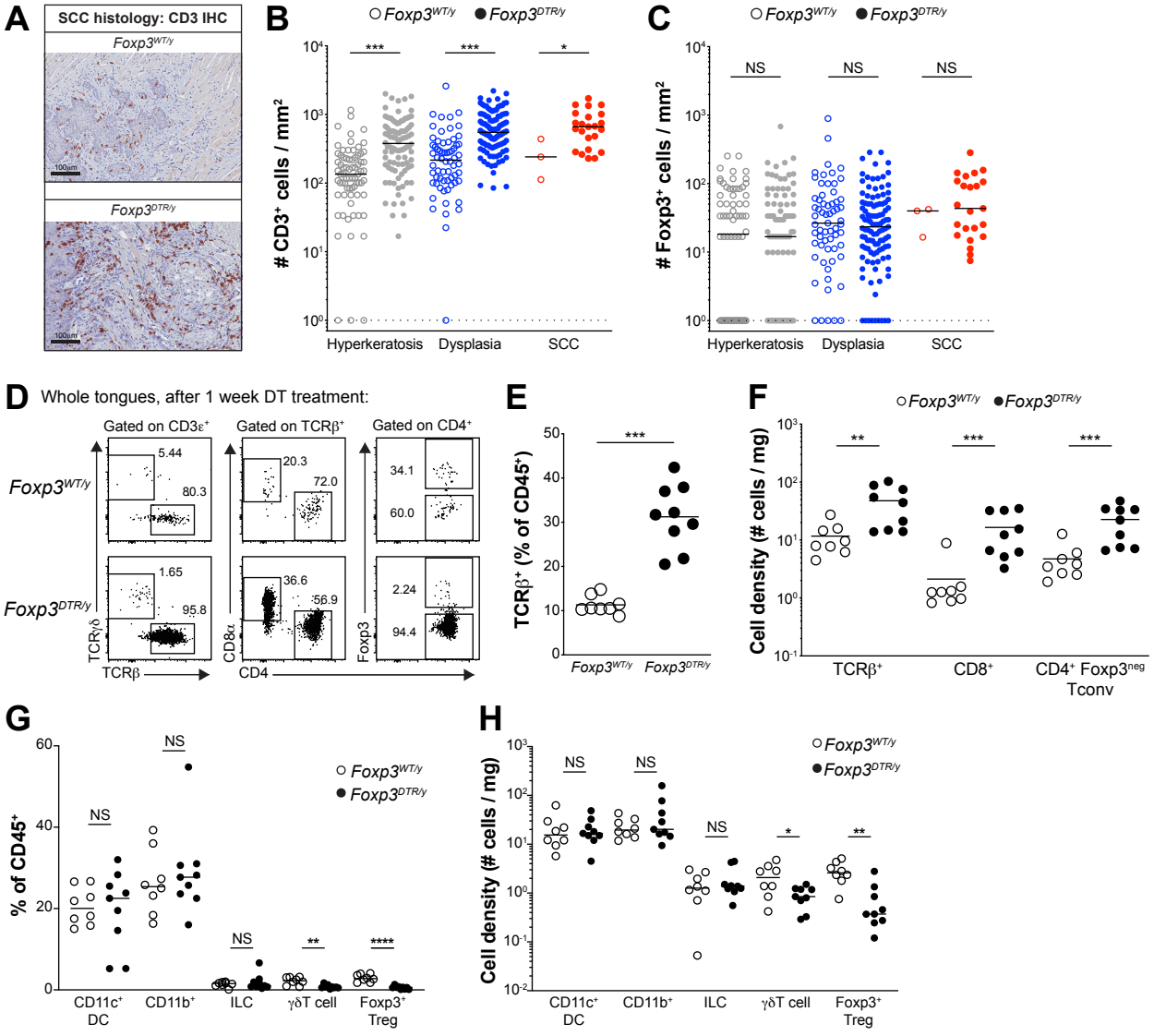

Figure 14. Late-stage Treg cell depletion is associated with an increase in effector T cell density

6- to 8-week-old *Foxp3*$^{WT/y}$ and *Foxp3*$^{DTR/y}$ littermates were exposed to 4-NQO drinking water for 20 weeks. During the 17th week of 4-NQO exposure, all mice were treated intraperitoneally every other day with diphtheria toxin (DT) for 1 week. Mice were sacrificed either 3 weeks later, at the 20 week endpoint, for IHC staining (A-C), or after the 1 week DT treatment, at the 17 week endpoint, for flow cytometry analysis (D-H).

A) Representative CD3 IHC image of SCC region of tongue isolated from mice of the indicated genotype, at 20 week endpoint. Scale bar represents 100 μm.

B) Summary plot of pooled data from CD3 IHC density analysis at 20 week endpoint, showing the number of CD3$^+$ cells per mm^2 for each lesion. Each symbol represents an individual lesion. Median is indicated. n = 3 – 110 lesions from 18 – 24 mice per group.

C) Summary plot of pooled data from Foxp3 IHC density analysis at 20 week endpoint, showing the number of Foxp3$^+$ cells per mm^2 for each lesion. Each symbol represents an individual lesion. Median is indicated. n = 3 – 110 lesions from 18 – 24 mice per group.

Figure 14, continued.
D) Representative flow cytometric analysis of T cells isolated from whole tongues of 4-NQO-treated mice of indicated genotype at 17 week endpoint, after 1 week of DT treatment. Left plots depict TCRβ vs. TCRγδ expression by $CD3^+$ T cells, middle plots depict CD4 vs CD8α expression by αβ T cells, and right plots depict CD4 vs. Foxp3 expression by $CD4^+$ T cells. The frequency of cells within the indicated gates is denoted.
E-F) Summary plots of pooled data from (D), showing the frequency of $TCR\beta^+$ T cells amongst $CD45^+$ cells (E), or number of $TCR\beta^+$, $CD8^+$, or $CD4^+$ $Foxp3^{neg}$ T cells per mg of tissue (F), isolated from whole tongues of 4-NQO-treated mice of indicated genotype. Each symbol represents an individual mouse. Mean is indicated. n = 8 mice (*Foxp3*$^{WT/y}$), n = 9 mice (*Foxp3*$^{DTR/y}$).
G) Summary plots of pooled data, showing the frequency of $CD11c^+$ DCs, $CD11b^+$ myeloid cells, ILCs, γδ T cells, and $Foxp3^+$ Treg cells amongst $CD45^+$ cells. Each symbol represents an individual mouse. Mean is indicated. n = 8 mice (*Foxp3*$^{WT/y}$), n = 9 mice, (*Foxp3*$^{DTR/y}$).
H) Summary plot of pooled data, showing the number of $CD11c^+$ DCs, $CD11b^+$ myeloid cells, ILCs, γδ T cells, and $Foxp3^+$ Treg cells per mg of tissue. Each symbol represents an individual mouse. Mean is indicated. n = 8 mice (*Foxp3*$^{WT/y}$), n = 9 mice, (*Foxp3*$^{DTR/y}$).
Data are pooled from multiple independent experiments. SCC = squamous cell carcinoma, DC = dendritic cell, ILC = innate lymphoid cell = $CD3^{neg}$ $Thy1^+$ $CD127^+$. Two-tailed nonparametric Mann Whitney test (B-C, E-H). NS = not significant, * = $p < 0.0.5$, ** = $p < 0.01$, *** = $p < 0.001$, **** = $p < 0.0001$.

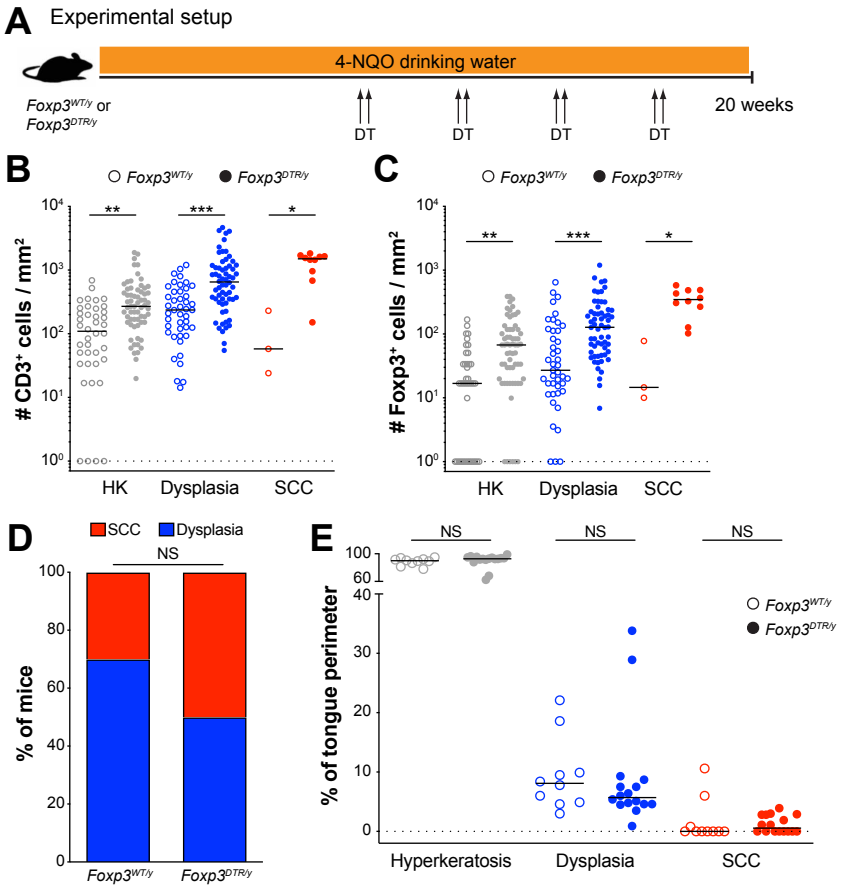

Figure 15. Early-stage transient and periodic Treg cell depletion does not impact OSCC incidence and burden

A) Experimental setup. 6- to 8-week-old *Foxp3*$^{WT/y}$ and *Foxp3*$^{DTR/y}$ littermates were exposed to 4-NQO drinking water for 20 weeks. During the 9th, 12th, 15th, and 18th weeks of 4-NQO exposure, all mice were treated intraperitoneally with diphtheria toxin (DT) on two consecutive days. At the 20 week endpoint, tongues were excised, and histopathology and IHC staining was performed and quantified. n = 10 mice (*Foxp3*$^{WT/y}$), n = 16 mice (*Foxp3*$^{DTR/y}$).

B) Summary plot of pooled data from CD3 IHC density analysis, showing the number of CD3$^+$ cells per mm^2 for each lesion. Each symbol represents an individual lesion. Median is indicated. n = 3 – 64 lesions from 10 – 16 mice per group.

C) Summary plot of pooled data from Foxp3 IHC density analysis, showing the number of Foxp3$^+$ cells per mm^2 for each lesion. Each symbol represents an individual lesion. Median is indicated. n = 3 – 64 lesions from 10 – 16 mice per group.

D) Tumor incidence, where each mouse was scored once based on most severe histology grade observed. Summary plot of pooled data, showing the percentage of mice scored as indicated histology grade. Each bar represents the cumulative data for mice of the indicated genotype.

E) Tumor burden. Summary plot of pooled data, showing the percentage of tongue perimeter defined as the indicated histology grade. Each symbol represents an individual tongue from a single mouse of the indicated genotype. Median is indicated.

Data are pooled from multiple independent experiments. HK = hyperkeratosis, SCC = squamous cell carcinoma. Two-tailed nonparametric Mann Whitney test (A-B, D-E, G), Fisher t test (F). NS = not significant. * = p < 0.0.5, ** = p < 0.01, *** = p < 0.001.

elevated densities of $CD3^+$ T cells and $Foxp3^+$ Treg cells at the endpoint (Figure 15B-C), but did not have a significant effect on OSCC incidence or burden (Figure 15D-E), suggesting that the impact of Treg cell ablation is dependent on the time of depletion along the continuum of cancer progression. Cumulatively, these data reveal the unexpected finding that transient Treg cell depletion at the later stages of carcinogenesis enhances the emergence of OSCC.

Increased incidence and burden of OSCC following late-stage Treg cell depletion is dependent on effector T cells

Given that αβ effector T cells were the major immune population to significantly expand following Treg cell depletion (Figure 14D-H), we next asked if effector T cells were required for the enhanced emergence of OSCC in this setting. To test this, starting at 16 weeks of 4-NQO exposure, $Foxp3^{WT/y}$ and $Foxp3^{DTR/y}$ mice were treated with DT for one week to transiently ablate Treg cells, plus concurrent anti-CD4 and anti-CD8 depleting antibodies or isotype control antibodies (Figure 16A). In mice treated with DT plus isotype control antibodies, Treg cell ablation led to elevated incidence and burden of OSCCs compared to non-depleted controls (Figure 16B-C, compare data columns 1 and 2), consistent with data presented in Figure 13B-C. However, in $Foxp3^{DTR/y}$ mice treated with DT plus anti-CD4 and anti-CD8 depleting antibodies, the impact of Treg cell ablation was abrogated, as OSCC incidence and burden remained at baseline (Figure 16B-C, compare data columns 2 and 4). In $Foxp3^{DTR/y}$ mice, DT plus anti-CD8 depleting antibody alone had no impact on OSCC incidence or burden compared to DT plus isotype control antibody (Figure 17A-C), demonstrating that effector $CD4^+$ $Foxp3^{neg}$ T cells alone are sufficient to promote the emergence of OSCC following Treg cell ablation. Of note, analysis of $Foxp3^{WT/y}$ mice revealed that the depletion of all $CD4^+$ and $CD8^+$ T cells had no impact on the incidence of 4-NQO-induced

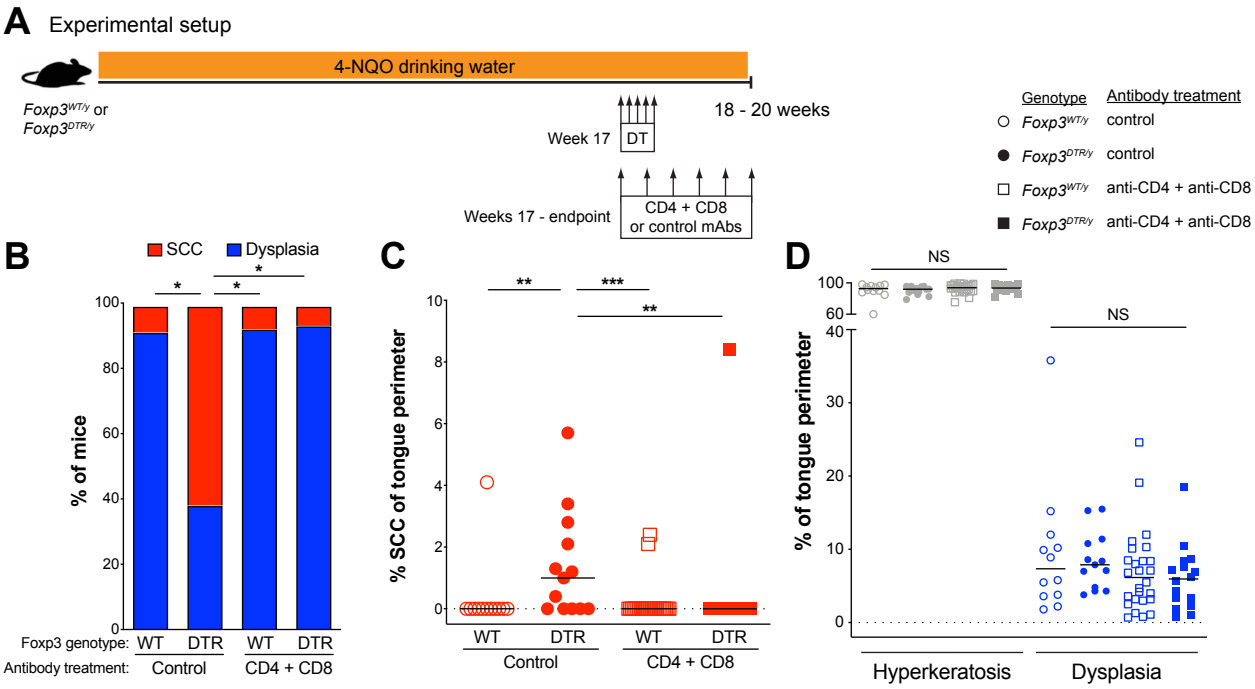

Figure 16. Increased incidence and burden of OSCC following late-stage Treg cell depletion is dependent on effector T cells

A) Experimental setup. 6- to 8-week-old *Foxp3*$^{DTR/y}$ and *Foxp3*$^{WT/y}$ littermates were exposed to 4-NQO drinking water for 20 weeks. During the 17th week of 4-NQO exposure, all mice were treated with diphtheria toxin (DT) for 1 week, as in Figure 13A. During weeks 17 through endpoint, mice were concomitantly injected intraperitoneally with 150 μg each of anti-CD4 + anti-CD8 depleting or isotype control antibodies (see methods). Tongues were excised at endpoint and histopathology was quantified as in Figure 5A. n = 12 mice (*Foxp3*$^{WT/y}$, control antibodies), n = 13 mice (*Foxp3*$^{DTR/y}$, control antibodies), n = 26 mice (*Foxp3*$^{WT/y}$, anti-CD4 + anti-CD8 antibodies), n = 16 mice (*Foxp3*$^{DTR/y}$, anti-CD4 + anti-CD8 antibodies).

B) Tumor incidence, where each mouse was scored once based on most severe histology grade observed. Summary plot of pooled data, showing the percentage of mice scored as indicated histology grade. Each bar represents the cumulative data for mice of the indicated genotype and antibody treatment.

C-D) Tumor burden. Summary plot of pooled data, showing the percentage of tongue perimeter defined as SCC (C) or defined as hyperkeratosis and dysplasia (D). Each symbol represents an individual tongue from a single mouse of the indicated genotype and antibody treatment. Median is indicated.

Data are pooled from multiple independent experiments. mAb = monoclonal antibody, SCC = squamous cell carcinoma. Fisher t test (B, adjusted p-values from Bonferroni correction are depicted), one-way ANOVA with Dunn's post-test analysis, comparing all pairs in column (C-D, adjusted p-values from Dunn's post-test are depicted). NS = not significant, * = $p < 0.0.5$, ** = $p < 0.01$, *** = $p < 0.001$.

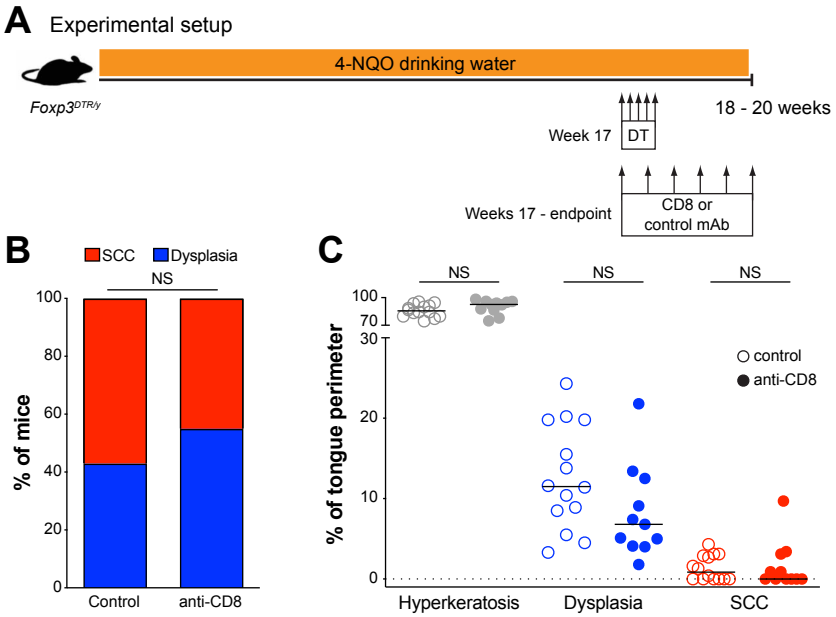

Figure 17. Depletion of CD8$^+$ T cells alone is not sufficient to abrogate the increased incidence and burden of OSCC following late-stage Treg cell depletion

A) Experimental setup. 6- to 8-week-old *Foxp3$^{DTR/y}$* mice were exposed to 4-NQO drinking water for 20 weeks. During the 17th week of 4-NQO exposure, all mice were treated with diphtheria toxin (DT) for 1 week, as in Figure 13A. During weeks 17 through endpoint, mice were injected intraperitoneally with 150 μg of anti-CD8 depleting or isotype control antibody (see methods). Tongues were excised at endpoint and histopathology was quantified as in Figure 5A. n = 14 mice (isotype control antibody), n = 11 mice (anti-CD8 antibody).

B) Tumor incidence, where each mouse was scored once based on most severe histology grade observed. Summary plot of pooled data, showing the percentage of mice scored as indicated histology grade. Each bar represents the cumulative data for mice that received indicated antibody treatment. Fisher t test.

C) Tumor burden. Summary plot of pooled data, showing the percentage of tongue perimeter defined as SCC. Each symbol represents an individual tongue from a single mouse that received the indicated antibody treatment. Median is indicated. Two-tailed nonparametric Mann Whitney test.

Data are pooled from multiple independent experiments. SCC = squamous cell carcinoma. NS = not significant.

lesions compared to isotype control antibody (Figure 16B-D, compare data columns 1 and 3), consistent with our findings in αβ T cell-deficient *Tcrb*$^{-/-}$ mice (Figure 9A-B). These collective findings demonstrate that the rapid emergence of OSCCs following late-stage Treg cell ablation is dependent on the presence of effector T cells, implying that the observed effects are dependent on a factor or factors produced by conventional T cells.

To better understand the mechanisms driving the rapid emergence of OSCCs following Treg cell ablation, we analyzed tissue sections for expression of the proliferation marker Ki-67. Density analysis revealed that in lesions from non-Treg-depleted control mice, a substantial fraction of cells exhibiting a basal cell morphology stained positive for Ki-67 (Figure 18A). In lesions of Treg cell-ablated mice, the percentage of cells staining positive for Ki-67 was comparable to controls (Figure 18B). In an effort to identify potential effector T cell-expressed factors that may contribute to the enhanced emergence of OSCC following Treg cell depletion, we analyzed T cell production of common effector cytokines by flow cytometry. These data revealed that Treg cell-depleted mice harbored a greater fraction of tongue-associated $CD3^+$ T cells (primarily $CD4^+$ $Foxp3^{neg}$ Tconv cells) that produced IFN-γ (Figure 18C-E). In contrast, the fraction of T cells producing IL-17A and IL-4 was not elevated in Treg cell-ablated mice (Figure 18C-E). The increase in IFN-γ-producing effector T cells was associated with elevated tissue staining for phospho-STAT1, an intracellular readout of IFN-γ sensing (Figure 18F-G). Of note, cells of both lymphocyte and epithelial cell morphology stained positive for pSTAT1, suggesting that both immune cells and carcinoma cells were responding to cues in the local environment.

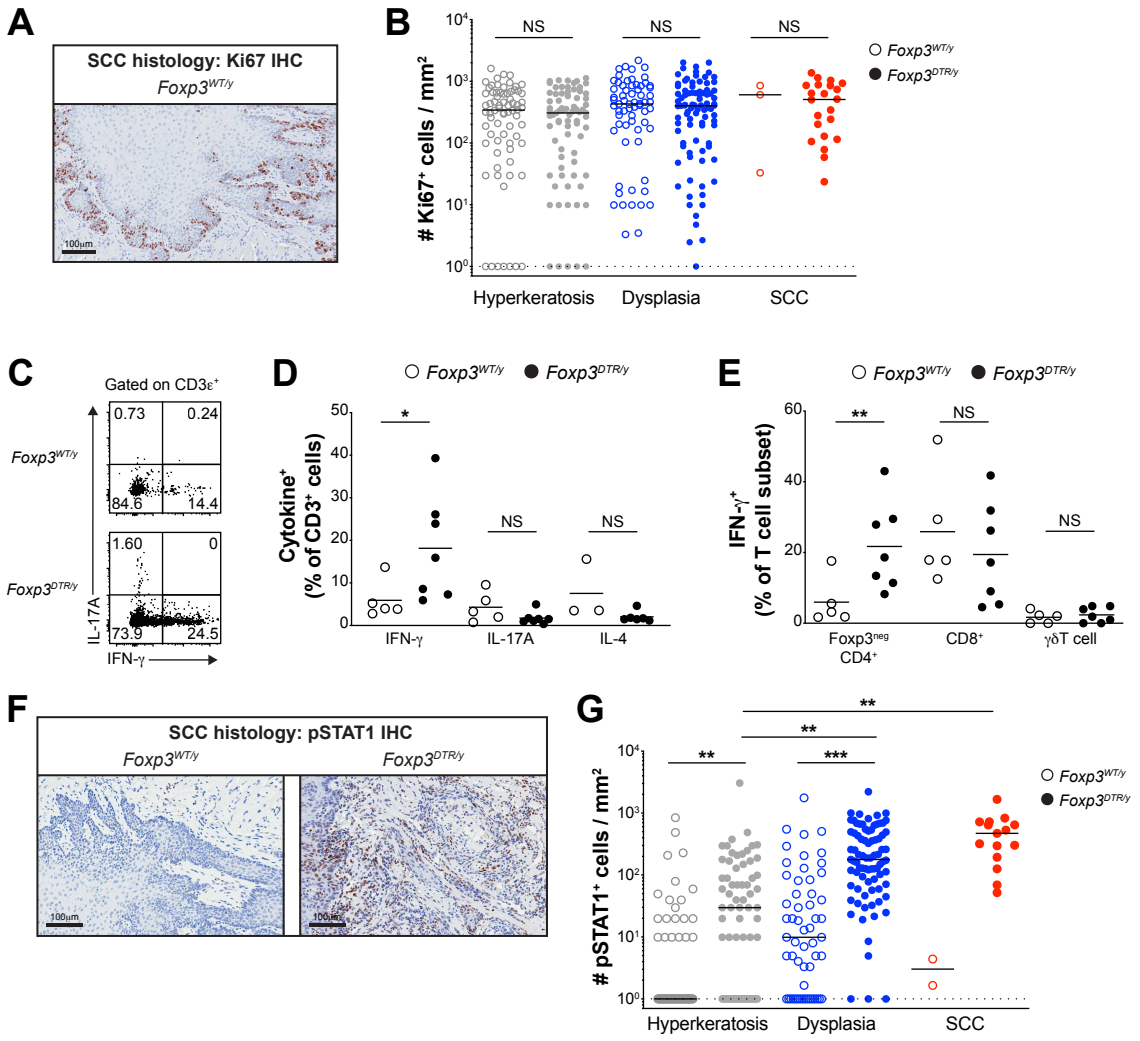

Figure 18. Increase in IFN-γ$^+$ effector T cells following late-stage Treg cell depletion

6- to 8-week-old *Foxp3$^{DTR/y}$* and *Foxp3$^{WT/y}$* littermates were exposed to 4-NQO drinking water for 20 weeks. During the 17th week of 4-NQO exposure, all mice were treated with diphtheria toxin (DT) for 1 week, as in Figure 13A. Mice were sacrificed either 3 weeks later, at the 20 week endpoint, for IHC staining (A-B, F-G), or after the 1 week DT treatment, at 17 week endpoint, for flow cytometry analysis (C-E).

A) At the 20 week endpoint, tongues were excised and Ki-67 IHC staining was performed and quantified. Representative Ki-67 IHC image of SCC region of tongue isolated from a *Foxp3$^{WT/y}$* mouse. Scale bar represents 100 μm.

B) Summary plot of pooled data from Ki-67 IHC density analysis, showing the number of Ki-67$^+$ cells per mm^2 for each lesion. Each symbol represents an individual lesion. Median is indicated. n = 3 – 89 lesions from 18 – 19 mice per group.

C) Following 1 week DT treatment, at the 17 week endpoint, lymphocytes from 1-3 tongues were pooled, stimulated with PMA and ionomycin for 5 hours, and analyzed by flow cytometry. Representative flow cytometric analysis of IFN-γ vs. IL-17A expression by CD3$^+$ T cells isolated from tongues of mice of the indicated genotype. The frequency of cells within the indicated gates is denoted.

Figure 18, continued.
D) Summary plot of pooled data from (C), showing the frequency of $CD3^+$ T cell that are positive for IFN-γ, IL-17, or IL-4, isolated from pooled tongues of 4-NQO-treated mice of indicated genotype at the 17 week endpoint, after 1 week of DT treatment. Each symbol represents a pooled sample. Mean is indicated. n = 5 pooled samples from 11 mice (*Foxp3*$^{WT/y}$, IFN-γ and IL-17A), n = 7 pooled samples from 13 mice (*Foxp3*$^{DTR/y}$, IFN-γ and IL-17A), n = 3 pooled samples from 7 mice (*Foxp3*$^{WT/y}$, IL-4), n = 6 pooled samples from 11 mice (*Foxp3*$^{DTR/y}$, IL-4).
E) Summary plot of pooled data from (C), showing the frequency of IFN-γ^+ cells amongst $CD4^+$ $Foxp3^{neg}$ T cells, $CD8^+$ T cells, or γδ T cells, isolated from pooled tongues of 4-NQO-treated mice of indicated genotype at the 17 week endpoint, after 1 week of DT treatment. Each symbol represents a pooled sample. Mean is indicated. n = 5 pooled samples from 11 mice (*Foxp3*$^{WT/y}$, IFN-γ and IL-17A), n = 7 pooled samples from 13 mice (*Foxp3*$^{DTR/y}$, IFN-γ and IL-17A), n = 3 pooled samples from 7 mice (*Foxp3*$^{WT/y}$, IL-4), n = 6 pooled samples from 11 mice (*Foxp3*$^{DTR/y}$, IL-4).
F) At the 20 week endpoint, tongues were excised and pSTAT1 IHC staining was performed and quantified. Representative pSTAT1 IHC image of SCC region of tongues isolated from mice of the indicated genotype. Scale bar represents 100 μm.
G) Summary plot of pooled data from pSTAT1 IHC density analysis, showing the number of $pSTAT1^+$ cells per mm^2 for each lesion. Each symbol represents an individual lesion. Median is indicated. n = 2 – 81 lesions from 16 – 17 mice per group.
Data are pooled from multiple independent experiments. SCC = squamous cell carcinoma. Two-tailed nonparametric Mann Whitney test (B, D-E), one-way ANOVA with Dunn's post-test analysis, comparing all pairs in column (G adjusted p-values from Dunn's post-test are depicted). NS = not significant, * = $p < 0.0.5$, ** = $p < 0.01$, *** = $p < 0.001$.

Increased incidence and burden of OSCC following late-stage Treg cell depletion is not dependent on IFN-γ sensing

Given the increase in incidence and burden of OSCC following late-stage Treg cell ablation is: 1) dependent on effector T cells (Figure 16B-C); 2) associated with an upregulation of IFN-γ^+ effector T cells (Figure 18C-E); and 3) associated with an increase in pSTAT1$^+$ cell density (Figure 18F-G), we hypothesized that IFN-γ plays a key role in promoting the progression of OSCC upon late-stage Treg cell ablation. To test this hypothesis, we took a two-pronged approach. First, starting at 16 weeks of 4-NQO exposure, *Foxp3*$^{DTR/y}$ mice were treated with DT for one week plus anti-IFN-γ neutralizing antibody or isotype control antibody (Figure 19A). Treatment with anti-IFN-γ neutralizing antibody did not have a significant impact on the incidence or burden of OSCC (Figure 19B-C). However, there was also no observable change in the pSTAT1$^+$ cell density with anti-IFN-γ treatment (Figure 19D), suggesting that anti-IFN-γ neutralization was not effective within carcinogen-induced lesions *in vivo*. As a second approach, *Ifngr1*$^{-/-}$ mice were crossed to *Foxp3*^{DTR} mice, allowing for DT-mediated Treg cell depletion in mice that are not able to sense IFN-γ due to the genetic loss of IFN-γR1. Similar to previous experiments, starting at 16 weeks of 4-NQO exposure, *Foxp3*$^{DTR/y}$ *Ifngr1*$^{+/+}$ or *Ifngr1*$^{+/-}$ and *Foxp3*$^{DTR/y}$ *Ifngr1*$^{-/-}$ littermates were treated with DT for one week to transiently ablate Treg cells, and then rested for up to 3 additional weeks (Figure 19E). In this setting, the density of pSTAT1$^+$ cells was reduced in lesions in *Foxp3*$^{DTR/y}$ *Ifngr1*$^{-/-}$ mice after Treg cell ablation, compared to *Foxp3*$^{DTR/y}$ IFN-γR1-sufficient littermates (Figure 19H), supporting the notion that STAT1 phosphorylation is at least partially dependent on IFN-γ sensing in this model. However, loss of IFN-γ sensing in *Foxp3*$^{DTR/y}$ *Ifngr1*$^{-/-}$ mice did not have a significant effect on OSCC incidence or burden (Figure 19F-G). Cumulatively, these data

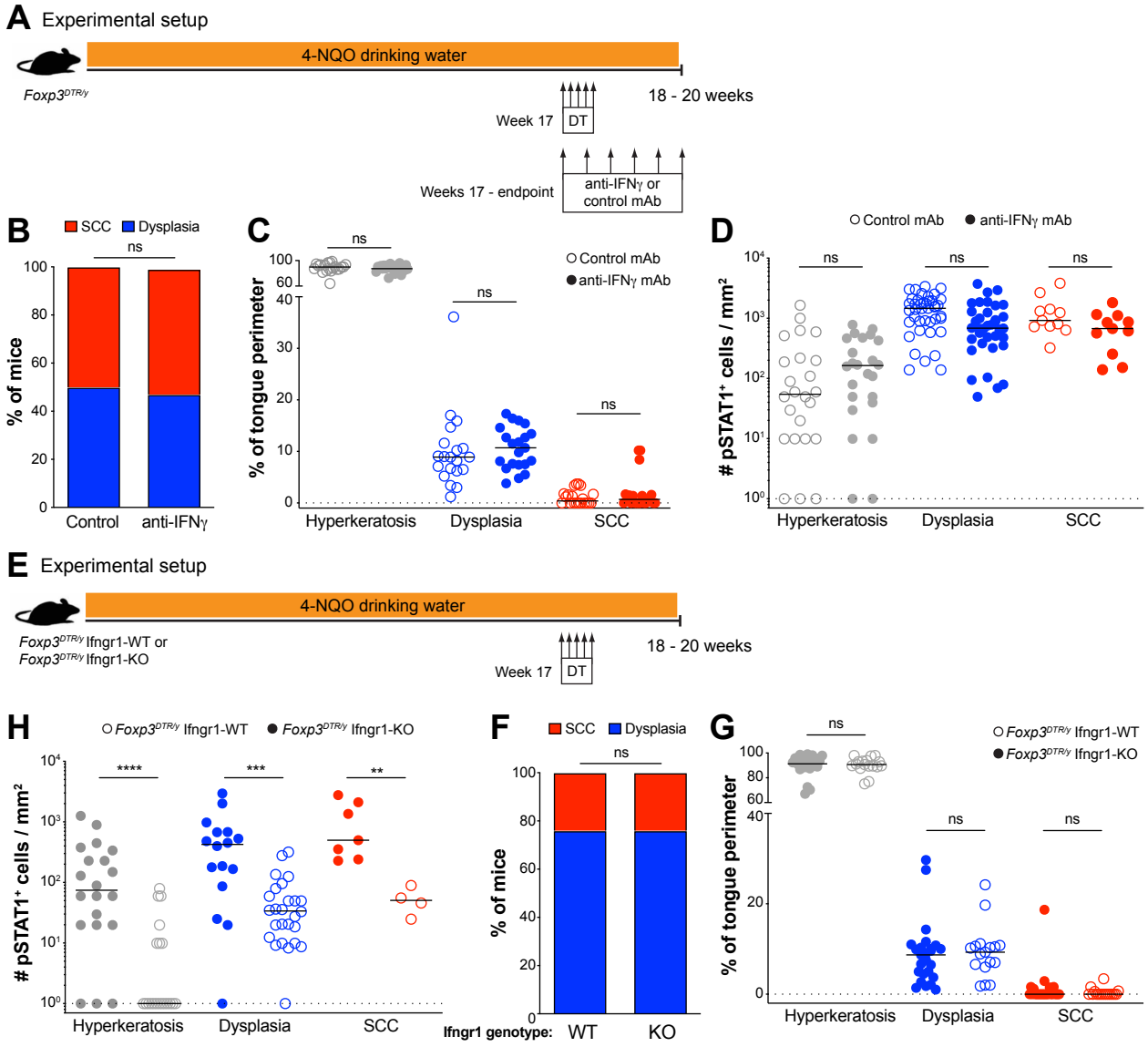

Figure 19. Increased incidence and burden of OSCC following late-stage Treg cell depletion is not dependent on IFN-γ sensing

A) Experimental setup for panels B-D. 6- to 8-week-old *Foxp3*$^{DTR/y}$ mice were exposed to 4-NQO drinking water for 20 weeks. During the 17th week of 4-NQO exposure, all mice were treated with diphtheria toxin (DT) for 1 week, as in Figure 13A. During weeks 17 through endpoint, mice were injected intraperitoneally weekly with 500 μg of anti-IFN-γ neutralizing or isotype control antibody. Tongues were excised at endpoint and histopathology was quantified as in Figure 5A. n = 20 mice (isotype control antibody), n = 21 mice (anti-IFN-γ antibody).

B) Tumor incidence, where each was mouse scored once based on most severe histology grade observed. Summary plot of pooled data, showing the percentage of mice scored as indicated histology grade. Each bar represents the cumulative data for mice that received indicated antibody treatment.

C) Tumor burden. Summary plot of pooled data, showing the percentage of tongue perimeter defined as SCC. Each symbol represents an individual tongue from a single mouse that received the indicated antibody treatment. Median is indicated.

Figure 19, continued.
D) Summary plot of pooled data from pSTAT1 IHC density analysis, showing the number of $pSTAT1^+$ cells per mm^2 for each lesion. Each symbol represents an individual lesion. Median is indicated. n = 11 – 41 lesions from 6 mice per group.
E) Experimental setup for panels H-G. 6- to 8-week-old *Foxp3*$^{DTR/y}$ *Ifngr*$^{+/+}$, *Foxp3*$^{DTR/y}$ *Ifngr1*$^{+/-}$, and *Foxp3*$^{DTR/y}$ *Ifngr1*$^{-/-}$ mice were exposed to 4-NQO drinking water for 20 weeks. During the 17th week of 4-NQO exposure, all mice were treated with diphtheria toxin (DT) for 1 week, as in Figure 12A. Tongues were excised at endpoint and histopathology was quantified as in Figure 4A. Ifngr1-WT = *Ifngr1*$^{+/+}$ or *Ifngr1*$^{+/-}$, Ifngr1-KO = *Ifngr1*$^{-/-}$. n = 24 mice (*Foxp3*$^{DTR/y}$ Ifngr1-WT), n = 17 mice (*Foxp3*$^{DTR/y}$ Ifngr1-KO).
H) Summary plot of pooled data from pSTAT1 IHC density analysis, showing the number of $pSTAT1^+$ cells per mm^2 for each lesion. Each symbol represents an individual lesion. Median is indicated. n = 4 – 26 lesions from 5 mice per group.
F) Tumor incidence, where each was mouse scored once based on most severe histology grade observed. Summary plot of pooled data, showing the percentage of mice scored as indicated histology grade. Each bar represents the cumulative data for mice of indicated genotype.
G) Tumor burden. Summary plot of pooled data, showing the percentage of tongue perimeter defined as SCC. Each symbol represents an individual tongue from a single mouse of indicated genotype. Median is indicated.
Data are pooled from multiple independent experiments. mAb = monoclonal antibody, SCC = squamous cell carcinoma. Fisher t test (B, F), two-tailed nonparametric Mann Whitney test (C-D, H, G). NS = not significant, ** = $p < 0.01$, *** = $p < 0.001$, **** = $p < 0.0001$.

suggest that the increase in OSCC incidence and burden following late-stage Treg cell depletion is not dependent on IFN-γ.

Future studies will be key to determine the precise mechanism(s) of effector T cell-dependent increase in OSCC incidence and burden following late-stage Treg cell depletion. Current ongoing studies include an unbiased RNA-sequencing approach, where bulk RNA-sequencing and analysis will be performed from select micro-dissected dysplasias and OSCCs lesions from DT-treated *Foxp3*$^{WT/y}$ and *Foxp3*$^{DTR/y}$ littermates. The goal of this approach is to provide transcriptomic insight into the cellular and molecular changes induced by late-stage Treg cell ablation in an unbiased manner.

Discussion

Our finding that late-stage Treg cell ablation enhances the incidence and burden of carcinogen-induced OSCCs suggests that strategies to promote *de novo* T cell infiltration in a subset of tumors that lack a substantial T cell infiltrate at baseline may yield unintended tumor-promoting effects. In this regard, Foxp3^{+} Treg cells may sit at the fulcrum of such reactions, given their abundance within many human cancers (including OSCC), their potent regulatory functions, and the fact that Treg cells express high densities of many cell-surface receptors that are targeted by approved and emerging therapeutic antibodies. The potential for adverse consequences induced by immune-based therapy is also suggested by recent reports documenting patients with solid cancers, including those with HNSCC, that experience "hyper-progressive" disease following immunotherapy, characterized by accelerated tumor growth kinetics following therapy[49,51–53]. These collective findings highlight the importance of understanding the mechanisms driving accelerated disease following immunotherapy, and delineating predictive biomarkers to identify

patients who are at risk of such adverse events. The nature of the response to immune-based therapy is likely to be context-dependent and impacted by a multitude of factors, including host and cancer genetics, the microbiota, the histological site of cancer origin, the stage of disease, and the local tissue environment. Moreover, due to heterogeneity in tumor biology and the composition of immune cells within the tumor environment, the response to immunotherapy may reflect a mixture of immune-mediated tumor control coupled with immune-mediated tumor promotion, depending on the state of distinct lesions at the time of therapy.

Early studies using transplantable tumor models suggested that Treg cell depletion can promote immune-mediated tumor control[61,62,149]. In contrast, an expanding body of studies in autochthonous mouse cancer models reveal evidence that Treg cell ablation can have tumor-promoting effects, consistent with our current findings. In a mouse model of pancreatic cancer driven by oncogenic Kras activation, Zhang et al. demonstrated that Treg cell ablation accelerated tumor progression, and that this effect was abolished upon co-depletion of conventional $CD4^+$ T cells[150]. In other studies, Martinez et al. used an autochthonous model of polyoma middle-T oncogene-driven mammary carcinoma to demonstrate that Treg cell depletion at the pre-invasive ductal carcinoma in situ stage promoted progression to an early invasive carcinoma[151]. Intriguingly, earlier research from the same group using orthotopic implantation of polyoma middle-T-driven tumors showed that Treg cell ablation in mice bearing advanced primary tumors deterred tumor outgrowth[61], demonstrating that the impact of Treg cell ablation can be stage-specific for a given cancer model. These collective findings, coupled with our current work, highlight the importance of utilizing animal models that accurately recapitulate the biology and pathogenesis of OSCC development and progression in humans, in which tumors arise in situ and progress from pre-neoplastic to invasive lesions.

At this time, the mechanisms driving the enhanced emergence of OSCC following late-stage Treg cell ablation remain incompletely defined. Our results to date suggest that a factor or factors expressed by effector T cells are required to drive rapid emergence of OSCC in this setting. It is possible that this phenomenon is due to indirect effects such as local modulation of the inflammatory milieu, or due to direct interactions between T cells and tumor cells or their progenitors. It is also conceivable that other stromal cell types contribute to the observed reaction, including fibroblasts, endothelial cells, and non-transformed epithelial cells. Notably, previous work has demonstrated that tumor-associated conventional T cell populations can promote tumor progression in distinct contexts. This evidence includes the demonstration that IL-4-producing $CD4^+$ T cells promote metastasis in a murine model of mammary carcinoma[43], and the demonstration that $CD4^+$ T cells exhibiting a PD-1^+ T follicular helper-like phenotype are associated with diminished response to anti-PD-1 checkpoint blockade therapy[152]. Such findings are consistent with the notion that effector T cell subsets may promote cancer progression and that immune-based therapies have the potential to unleash undesirable tumor-promoting cascades in a subpopulation of patients. Our findings also provide a potential explanation for prognostic studies showing that high intratumoral Treg cell density is predictive of improved clinical outcome in OSCC and other HNSCCs[56,101,105,106,135,138,140]. In this scenario, intratumoral Treg cells may restrict tumor infiltration by tumor-promoting effector T cells, thereby contributing to the observed prognostic correlates. Moving forward, a key unresolved question in the 4-NQO-induced OSCC model is whether the enhanced emergence of carcinoma following Treg cell depletion is due to progression of dysplastic lesions to OSCC, and/or rapid expansion of pre-existing OSCCs. In our studies, late-stage Treg cell depletion enhanced the emergence of OSCC whereas earlier Treg cell ablation induced no measurable changes, suggesting that the observed effects are stage-specific.

Lastly, our identification of polarized clusters of OSCC enriched for either $CD8^+$ T cells or $CD4^+$ Treg and conventional T cells demonstrates that the density of Treg cells does not correlate with that of $CD8^+$ T cells in many OSCCs and tumors of other solid cancer types. This finding implies that the factors driving intratumoral $CD4^+$ T cell abundance are likely distinct from those driving intratumoral $CD8^+$ T cell density in many tumors, and indicates that the notion that Treg cell density largely "shadows" the density of tumor-infiltrating $CD8^+$ T cells[34,133,153] is not a universal principle applicable to all human cancers. This also suggests that in some cases, categorization of tumors as "T cell-inflamed" vs. "T cell non-inflamed" lacks the resolution to articulate the immune landscape of a given tumor with respect to the relative representation of $CD8^+$ effector T cells, $CD4^+$ effector T cells, and $CD4^+$ $Foxp3^+$ Treg cells. Future work aimed at understanding the differential mechanisms driving $CD4^+$ vs. $CD8^+$ T cell infiltration may reveal new approaches to selectively manipulate each T cell class within the tumor environment.

DISCUSSION

Overview

In this work, we analyzed the impact of the immune response to OSCC in both patient samples and in a mouse model of carcinogen-induced OSCC. By utilizing a deconvolution-based approach to interrogate the transcriptional profiles of human HPV-negative OSCCs, unsupervised clustering analysis revealed polarized clusters enriched for either $CD4^+$ T cells or $CD8^+$ T cells, demonstrating that the density of $CD4^+$ T cells, both $FOXP3^+$ Treg cells and Tconv cells, does not correlate with the density of $CD8^+$ T cells in many tumors (Figure 20A).

In an autochthonous mouse model of carcinogen-induced OSCC, we detected the presence of an infiltrating T cell population over-represented by $CD4^+$ T cells, suggesting that this model may represent the fraction of patients observed to have tumors with a high $CD4^+$ T cell density (Figure 20B). Despite the presence of infiltrating T cells, mice were largely resistant to checkpoint blockade monotherapies, suggesting the existence of endogenous resistance mechanisms. We hypothesized that tumor-associated $Foxp3^+$ Treg cells, which displayed a diverse TCR repertoire with a fraction of clones exhibiting clonal expansion and reactivity to regional antigens, play a major role in restricting anti-tumor immunity. However, late-stage Treg cell ablation did not induce tumor regression, but instead exacerbated disease and induced the emergence of OSCC, a process that was dependent on effector T cells. Together, our studies demonstrate that in this setting, induction of strong effector T cell responses can promote tumor development and progression (Figure 20C).

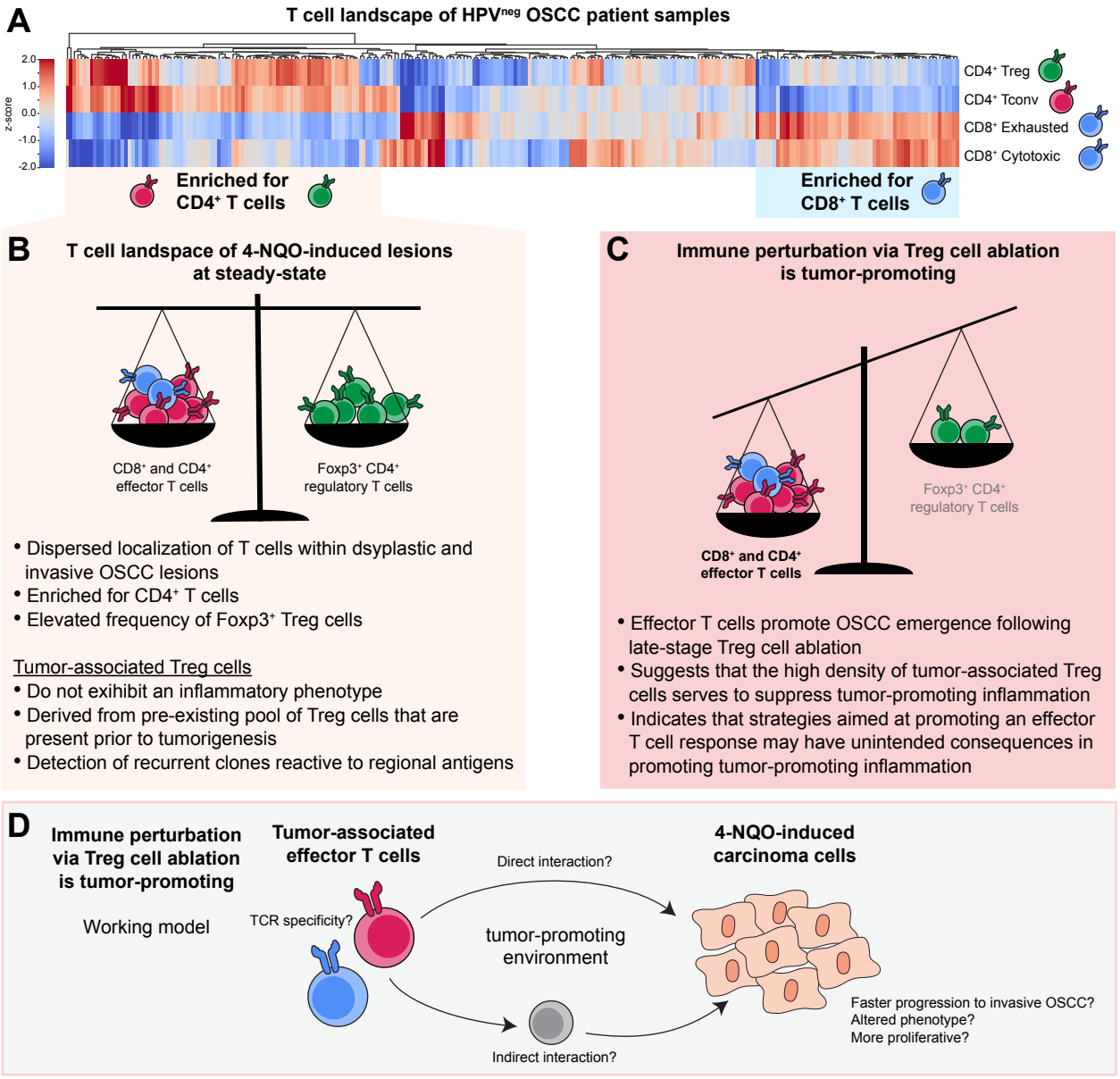

Figure 20. Working model of effector T cell-dependent emergence of OSCC following late-stage Treg cell depletion

A) Deconvolution-based profiling of human transcriptional data revealed OSCC clusters enriched for either CD4$^+$ Treg cells (green cells) and CD4$^+$ Tconv cells (pink cells) or CD8$^+$ T cells (blue cells).

B) In an autochthonous mouse model of OSCC, carcinogen-induced lesions are enriched for CD4$^+$ T cells at homeostasis

C) Perturbation to immune homeostasis via late-stage Treg cell ablation promotes the emergence of OSCC, an effect dependent on effector T cells.

D) Following late-stage Treg cell ablation, effector T cells exert a tumor-promoting environment. Effector T cells of unknown specificity may release a factor or factors that directly or indirectly interact with carcinoma cells to promote tumor progression, alter tumor cell phenotype, or induce tumor cell proliferation.

Strategies to promote a robust inflammatory response within the tumor environment may yield unintended adverse consequences

Ongoing efforts to improve therapeutic efficacy of immunotherapy has been focused on promoting a T cell response in the tumor environment, particularly for those tumors with a non-T cell-inflamed phenotype at baseline. Strategies for improving treatment options for patients include targeting effector T cells to promote an inflammatory immune response and targeting tumor-associated Treg cells for depletion or de-stabilization. Our findings that late-stage Treg cell ablation enhances the incidence and burden of carcinogen-induced OSCCs suggests that strategies that promote *de novo* T cell infiltration and effector T cell responses in tumors that lack a substantial T cell infiltrate at baseline may yield unintended consequences.

Adverse consequences beyond auto-immune related outcomes have been observed in a subset of patients treated with immunotherapy. In HNSCC, up to 25% of patients treated with anti-PD-1 or anti-PD-L1 experienced "hyper-progressive" disease, which is defined as accelerated tumor growth kinetics following start of treatment[53]. Hyper-progressive disease has also been reported in other solid tumors[49–52], suggesting that immune-based therapy can accelerate disease in multiple tumor types. The cellular and molecular mechanisms driving hyper-progression remain incompletely understand. In distinct settings, hyper-progression was associated with specific tumor cell genomic mutations or alterations[51], suggesting a tumor cell-intrinsic effect. Other studies suggest patient age[49] or metastatic disease[50] are associated with elevated risk of hyper-progression. Based on our finding that depletion of effector $CD8^+$ T cells alone was not sufficient to abrogate the emergence of OSCC following Treg cell ablation, we hypothesize that $CD4^+$ Tconv cells serve a critical role in this phenomenon. While experiments are currently ongoing to test this hypothesis, it is possible that hyper-progressive disease is restricted to those patients who harbor

tumors enriched for $CD4^+$ T cells, whereas response to immunotherapy is preferentially observed in tumors enriched for $CD8^+$ T cells.

It is important to note that the occurrence of hyper-pressive disease is currently controversial. The studies highlighted above were retrospective studies, whereas properly controlled phase 3 clinical trials are required to better understand the proportion of patients at risk for hyper-progressive disease, and to address the mechanism of hyper-progressive disease. These properly controlled, double-blinded studies, which would include a control group that does not receive immunotherapy, will require knowledge of tumor growth rate before and after start of immunotherapy to be able to better characterize the patient group defined as "non-responders." Currently, non-responders are a heterogenous group comprised of patients who maintain stable tumor growth kinetics, and therefore experience no benefit nor harm with immunotherapy, as well as patients who may be experiencing hyper-progression, and therefore suffer adverse consequences of immunotherapy treatment. The ability to distinguish between the "true" non-responder patient cohort and the cohort of patients experiencing hyper-progression due to immunotherapy treatment will be necessary to better understand the molecular and cellular mechanisms driving these unwanted effects. Furthermore, analysis of those patients who experience hyper-progression will allow for the identification of predictive biomarkers to stratify patients who may benefit with immunotherapy, versus those at risk of unwanted and detrimental effects of immunotherapy treatment.

Importance of studying the immune response in physiologically accurate mouse models

While our finding that late-stage Treg cell ablation promotes OSCC goes against current paradigm that tumor-associated Treg cells inhibit the anti-tumor immune response, two recent studies report similar observations that Treg cell ablation can be tumor-promoting. First, Zhang et al. found that in an autochthonous mouse model of pancreatic cancer driven by oncogenic Kras activation, Treg cell ablation accelerated tumor progression, which was associated with an increase in tumor-infiltrating IFN-γ^+ $CD4^+$ Tconv cells[150], similar to our observations in carcinogen-induced OSCC. Interestingly, the authors demonstrated that the tumor progression was abrogated when $CD4^+$ Tconv cells were depleted, consistent with our finding that $CD8^+$ T cell depletion alone was not sufficient to abrogate effects of Treg cell ablation. Although the mechanism remains incompletely defined in the pancreatic tumor model, the authors demonstrated that the chemokine receptor CCR1 played a critical role, and fibroblasts and epithelial cells in the tumor environment had an altered phenotype following Treg cell ablation. Together, the authors propose a model involving a cellular and molecular network between $CD4^+$ Tconv cells, CCR1 ligands, and tumor-associated macrophages and epithelial cells in promoting tumor progression upon Treg cell ablation.

In a separate study, Martinez et al. found that early-stage Treg cell ablation led to accelerated progression to invasive carcinoma in an autochthonous mouse model of polyoma middle-T oncogene-driven mammary carcinoma[151]. Similar to our findings, the authors observed accelerated tumor progression just two weeks after Treg cell ablation, demonstrating that the impact of Treg cell ablation can occur rapidly. While the mechanism also remains unknown, the authors observed elevated IL-4 and IL-5, but not IFN-γ, as well as an increase in tumor-associated macrophages upon Treg cell ablation, which is unlike the observations from Zhang et al. and our

studies. Together, these studies demonstrate that Treg cell ablation can be tumor-promoting across different autochthonous mouse models of cancer, and highlight how the cellular and molecular mechanisms driving this effect may be distinct depending on the tumor context.

Interestingly, the same group published a previous study in an orthotopic model of breast cancer, and found that Treg cell ablation led to slowed tumor outgrowth in the orthotopic setting[61]. The differential impact of Treg cell ablation at early-stage in the autochthonous breast cancer model compared to the orthotopic model may reflect stage-specific outcomes, as demonstrated in the 4-NQO-induced OSCC mouse model. It is also possible that the differential impact of Treg cell ablation is reflective of the differences between transplantable tumor models, which are fast growing and do not progress from pre-neoplasia to invasive carcinoma, and autochthonous tumor models, which more accurately recapitulate the biology of tumorigenesis. Early studies in mice demonstrating that Treg cell depletion promotes tumor regression relied on the use of transplantable tumor models[61,62]. However, the use of autochthonous tumor models, where tumors develop in situ, progress from pre-neoplasia to invasive carcinoma, and potentially have multiple heterogeneous lesions evolving in parallel, may reveal previously un-explored or under-appreciated interactions and observations, such as our findings that effector T cell expansion or infiltration triggered by late-stage Treg cell ablation exacerbates disease.

Given that autochthonous tumor models recapitulate many aspects of tumor biology highlighted above, the use of an autochthonous tumor is key to understanding how effector T cells promote OSCC emergence following late-stage Treg cell ablation. An effector T cell-derived factor or molecule may have a direct effect on transformed tongue epithelial cells, or could indirectly promote OSCC by altering other cell types in the tumor environment, such as innate immune cells, stromal cells, or non-transformed epithelial cells (Figure 20D). Similarly, it is

unclear if the increased incidence and burden of OSCC following late-stage Treg cell ablation is due to faster progression from dysplasia to invasive OSCC, in situ proliferation of carcinoma cells, or an altered phenotype of carcinoma cells (Figure 20D). A better understanding of the cellular and molecular mechanisms dictating OSCC emergence following late-stage Treg cell ablation is critical to gain insight into the tumor-promoting role of effector T cells, and may reveal novel biomarkers or therapeutic targets.

T cell deficiency does not impact tumor development or progression

Our findings that the incidence and burden of both dysplasia and invasive OSCC are unaltered in T cell-deficient, as well as in *Foxp3*$^{WT/y}$ mice treated with depleting anti-CD4 and anti-CD8 antibodies at late-stage, demonstrate that T cell deficiency does not significantly impact the kinetics of tumor development or progression. These findings suggest that immunoediting may not occur to a measurable extent in this mouse model of carcinogen-induced OSCC. While immunoediting has been demonstrated in the methylcholanthrene (MCA)-induced mouse model[15], in which mice are injected subcutaneously with the carcinogen MCA to induce sarcoma development, the extent to which this process is operative in other tumor models or in humans remains unclear. The evidence that immunoediting occurs in patients remain limited, particularly for HNSCCs. In a computational survey predicting neo-antigen density across an array of human cancers, putative immunoediting, as measured by depletion of predicted neoepitopes generated per non-silent point mutation, was only observed in two human cancer types analyzed: colorectal cancer and kidney clear cell cancer[16]. Notably, despite the fact that HPV-negative HNSCCs harbor a relatively high density of somatic mutations in protein-coding regions[99–101], this same approach

revealed that the depletion of putative neoepitopes was not statistically significant in HPV-negative HNSCC, suggesting that immunoediting may be uncommon in this cancer type.

While attempts to observe immunoediting have focused on the identification and quantification of predicted neo-antigens, other forms of immunoediting have been documented. Studies probing the genomic landscape of lung cancers isolated from patients observed the loss of heterozygosity at the HLA loci[17], implying selection against distinct HLA alleles. Loss of HLA heterozygosity was found to correlate with immune infiltration and neo-antigen burden. Furthermore, the authors found that a fraction of neo-antigens were predicted to bind more frequently to the lost HLA, providing a mechanism for immune evasion and clonal evolution of tumor cells. In a separate study, McGranahan et al. demonstrated that both lung adenocarcinomas and lung squamous cell carcinomas display a range of heterogeneity with regards to predicted neo-antigen expression[18]. The authors saw that tumors that expressed a more homogenous panel of mutations, and therefore the cancer was more clonal, were associated with an T cell-inflamed tumor phenotype and durable response to anti-PD-1 checkpoint blockade therapy, particularly for lung adenocarcinomas, highlighting tumor clonality as a key characteristic to T cell infiltration and immunotherapy efficacy. Together, these studies provide evidence that some tumors are under immune-mediated selective pressures, and that selective pressures can result in the loss of HLA heterozygosity or restrict clonal tumor outgrowth. Future studies probing the presentation of neo-antigens as well as alterations in genomic features of tumor lesions, such as tumor clonality and mutations within the MHC loci, in the presence or absence of T cells will be necessary to fully assess the extent to which immunoediting occurs in 4-NQO-induced OSCC.

Finally, it is important to note that T cell deficiency and T cell depletion leads to the loss of both effector T cell and Treg cell populations. Studies presented in this work suggests that a

delicate balance between effector T cells and Treg cells is established during tumor development and progression (Figure 20B). An impact on OSCC incidence and burden was only observed when a strong perturbation was imposed on this balance, such as systemic Treg cell ablation and subsequent expansion of effector T cells (Figure 20C). However, no impact on OSCC incidence and burden was observed when both sides of the scale were absent, such as in T cell-deficient mice and mice depleted of all T cells. Future studies aimed at expanding the tumor-associated Treg cell population will be critical to test this emerging concept.

A fraction of tumor-associated Treg cells exhibit clonal expansion and reactivity to regional antigens

Analysis of the TCR repertoire of Treg cells isolated from the tongues of 4-NQO-exposed mice revealed that the overall repertoire of tongue-associated Treg cells in 4-NQO-treated mice was diverse. We detected a handful of recurrent clones present across different mice, suggestive of clonal expansion. While the factor or factors that promote clonal expansion and clonal maintenance of Treg cells within the tumor remain to be determined, our studies utilizing TCR retrogenic mice revealed insights into the specificity of recurrent Treg TCR clones. Three of the four recurrent Treg cell clones analyzed exhibited enrichment patterns suggestive of reactivity to regional antigens present in tumor-free mice, consistent with previous studies from our lab identifying predominant tumor-infiltrating Treg cell clones reactive to organ-specific self-antigens[83]. Furthermore, TCR repertoire analysis of Treg cells isolated from human tumors have demonstrated that Treg cells in breast cancer were oligoclonal[78], and Treg cells isolated from liver tumors were more clonal than Treg cells isolated from peripheral blood[81]. Together, these data

demonstrate that tumors drive the selective oligoclonal enrichment of distinct Treg cell clones, implying a role for antigen-specificity.

Our data demonstrated that a fraction of recurrent Treg cell clones associated with oral lesions display reactivity to regional antigens presented in the draining cervical lymph nodes, irrespective of tumor or carcinogen exposure. Therefore, the antigens recognized by these clones are likely derived from organ-specific self-antigens or microbial-derived antigens that are present in the microbial community resident in the oral cavity. However, it is also possible that a fraction of tumor-associated Treg cell TCR clones have specificity to neo-antigens, particularly for those clones that were not found recurrent across mice analyzed, since each mouse likely harbors a unique set of expressed and presented neo-antigens. Consistent with this idea, Treg cell specificity to neo-antigens has been demonstrated for some dominant Treg TCRs isolated from human cancers[154].

Comparison of tumor-associated Treg cell TCRs to TCR repertoires of Treg cells isolated from pooled spleen and lymph nodes of non-tumor-bearing mice suggests that the majority of tumor-associated Treg cells are pulled from the pre-existing pool of Tregs present in the periphery before tumorigenesis, suggesting that the high preponderance of Treg cells in tumors may be co-opted from the regional environment. This concept is in agreement with previous reports in mice[83] and humans[154], which observed clonal overlap between the repertoires of Treg cells isolated from tumor and peripheral blood. Furthermore, a study that analyzed the TCRβ CDR3 clonotypes of Treg cells and $CD4^+$ Tconv cells isolated from human breast cancer demonstrated that the overall repertoires were dissimilar[78], suggesting that the intratumoral Treg cell and Tconv cell compartments are largely distinct.

Currently, it is unknown if the tumor-associated Treg cells are thymic-derived tTregs or peripherally induced pTregs, or a mixture of both. Given that pTregs are estimated to make up 15-25% of the peripheral Treg cell compartment at steady-state[155], it is possible that a fraction of Treg cells isolated from 4-NQO-induced oral lesions are pTregs present at steady-state and reactive to microbial antigens derived from the oral cavity microbiome. Another possibility is that a fraction of tumor-associated Treg cells is derived from the steady-state $CD4^+$ Tconv compartment and differentiate into pTreg during carcinogenesis. While Plitas et al. observed that the tumor-associated Treg and Tconv repertoires were largely dissimilar in human breast cancer[78], a small survey of three breast cancer patients observed clonotype overlap between tumor-associated Treg cells and $CD4^+$ Tconv cells[156]. Ahmadzadeh et al. also observed that a small fraction of tumor-associated Treg clonotypes overlapped with tumor-associated CD4+ Tconv clonotypes in patients with metastatic melanoma, gastrointestinal cancer, and ovarian cancer[154]. Together, the studies documenting shared repertoires between a fraction of tumor-associated Treg cells and $CD4^+$ Tconv cells suggest that some intratumoral Treg cells may be generated via pTreg cell differentiation in the tumor context.

Future studies utilizing TCR retrogenic mice will be key in understanding the developmental origins of tumor-associated Treg cells. We can perform intrathymic injections, where thymocytes isolated from retrogenic mice are intrathymically injected into thymi of secondary hosts that harbor polyclonal thymocytes, to assess tTreg development for clones of interest. Likewise, transfer of retrogenic $CD4^+$ Tconv cells into secondary hosts can be performed in parallel to assess the pTreg potential of tumor-associated Treg clones. Moreover, a better understanding of the TCR repertoire and specificity of tumor-associated effector T cell populations, particularly for $CD4^+$ Tconv cells, will be critical to understand the relationship

between Treg cells and effector T cells. Do the TCR repertoires overlap? Do Treg cells and effector T cells share reactivity to similar antigens, or do they recognize distinct sets of antigens? The answer to these questions will provide important insights to the development of antigen-based cancer vaccines, and the impact of directing the effector T cell or Treg cell response to specific tumor-associated antigens of interest.

Density of tumor-associated $CD8^+$ T cells does not correlate with density of tumor-associated $CD4^+$ T cells

Our observations from deconvolution-based transcriptional analysis suggest distinct factors dictate $CD8^+$ or $CD4^+$ T cell density within tumors. Our findings indicate that the notion that Treg cell infiltration and density within the tumor largely "shadows" that of $CD8^+$ T cells and inflammation may not be a universal principle applicable to all human cancers. Instead, our findings suggest that the characterization of "T cell-inflamed" tumor phenotype requires a more nuanced definition to more accurately reflect the immune landscape of a given tumor with respect to the relative representation of distinct T cell types. While the factors driving a $CD4^+$ T cell-biased versus a $CD8^+$ T cell-biased tumor environment remain unclear, it is possible that tumor cell-intrinsic mechanisms promote or inhibit either $CD4^+$ T cell or $CD8^+$ T cell infiltration into the tumor. Given that the enrichment for either $CD4^+$ or $CD8^+$ T cells was observed for a subset of tumor samples, perhaps a unique set of genomic alterations in tumor cells promote infiltration and survival of either $CD4^+$ or $CD8^+$ T cells, similar to the tumor cell-intrinsic role that has been described for β-catenin-driven immune exclusion in melanoma[157]. It is also possible that other factors within the tumor milieu, such as cytokines, chemokines, and nutrients, influence the infiltration and survival of $CD4^+$ or $CD8^+$ T cells. Finally, the state of immune infiltration observed

could be a reflection of the immune landscape within the organ prior to tumorigenesis. For example, for an organ site such as the oral cavity, tumors originating at this site may be biased towards $CD4^+$ T cell enrichment because it is already enriched for $CD4^+$ T cells at steady state. It is important to note that our characterization of the immune landscape revealed that 4-NQO-induced lesions were biased for $CD4^+$ T cells, and the prevalence of $CD4^+$ T cells compared to $CD8^+$ T cells was observed even in control treated, non-tumor-bearing mice, suggestive of enrichment of $CD4^+$ T cells prior to tumorigenesis.

Finally, our analysis revealed that the relative densities of $CD4^+$ Tconv and $FOXP3^+$ Treg cells correlate, providing intriguing evidence that both $CD4^+$ T cell populations may respond to similar or interwoven factors to infiltrate tumors. In the spleen and lymph nodes, T cell-derived IL-2 is a critical factor for maintaining the Treg cell population, particularly central Treg cells (cTregs) that exhibit a naïve phenotype in the periphery[158]. Furthermore, self-reactive CD4 single positive thymocytes have been proposed to be the key IL-2-producing cell population to promote Treg cell differentiation in the thymus[159]. Together, these studies lay out the possibility that self-reactive $CD4^+$ Tconv cells in the tumor provide a key IL-2 niche for intratumoral Treg cell recruitment, retention, and survival. As discussed in the previous section, assessing the repertoire and specificity of tumor-associated $CD4^+$ Tconv cells will provide critical insight to inform this proposed model. Future studies examining the role of T cell-derived factors, whether IL-2 or a tumor-expressed factor, will be key to understanding the concurring presence of $CD4^+$ Tconv and $FOXP3^+$ Treg cells in a subset of human tumors. Given the prevalence of $CD4^+$ T cells detected in oral lesions, the 4-NQO mouse model of carcinogen-induced OSCC provides a unique platform to study the factors dictating $CD4^+$ T cell versus $CD8^+$ T cell tumor infiltration. A better understanding of a more nuanced definition of T cell infiltration, and the diversity of immune

landscapes of tumors, can help to uncover unique strategies to perturb distinct subsets of T cells within the tumor environment.

Conclusion

Prior to this work, current paradigms predicted that Treg cell depletion would lead to tumor regression. However, our studies in an autochthonous mouse model of carcinogen-induced OSCC revealed the opposite finding. Instead, late-stage Treg cell depletion led to an increase in OSCC incidence and burden.

Our work contributes to the growing body of literature that either Treg cell depletion or effector T cell responses can be tumor promoting in distinct contexts, both in mice[43,44,150,151] and humans[49–53], highlighting the dual role of the immune system in both inhibiting tumor growth as well as promoting tumor development and progression[71]. Our findings have important implications for current FDA-approved immune-based therapies, as well as the set of emerging therapies that target cell surface molecules that are either exclusively expressed by or over-expressed by intratumoral Treg cells and have the potential to either deplete or de-stabilize intratumoral Treg cells. These targets include but are not limited to PD-1, CTLA-4, OX40, 4-1BB, GITR, Lag3, TIGIT, and CCR8. Indeed, anti-CTLA-4 treatment has been demonstrated to promote intratumoral Treg cell depletion in mice, depending on the antibody clone and Fc region[64,65]. Similarly, preclinical experiments in mouse models demonstrated that anti-GITR, anti-OX40, and anti-CCR8 treatments can promote intratumoral Treg cell depletion[66–68,79]. Future studies will require a deeper investigation of the direct impact of immunotherapy on intratumoral Treg cells in patients, and

determine the beneficial or harmful effects of targeting intratumoral Treg cells for depletion or de-stabilization.

Mechanistically, we observed that the increase in OSCC incidence and burden following late-stage Treg cell ablation was dependent on effector T cells, suggesting that effector T cell-derived factor(s) drive the rapid emergence of OSCC. Currently, it is not known if the rapid emergence of OSCC following late-stage Treg cell depletion is due to direct T cell-tumor cell interactions, involves other cells within the environment, or is due to paracrine-mediated modulation of the tumor milieu. At this point, it is also unclear if the enhanced emergence of OSCC is due to progression of dysplasia to OSCC, or rapid expansion and proliferation of pre-existing carcinoma cells. Together, our studies highlight the need to understand the molecular and cellular mechanisms driving emergence of OSCC upon late-stage Treg cell ablation, and delineating predictive biomarkers to identify patients who are at risk of adverse events.

Future Issues

1. What is the impact of the microbiome on carcinogen-induced OSCC? Is the development and progression of carcinogenesis affected by antibiotic treatment or in germ-free mice? Does the local microbiome community resident within the oral cavity impart a unique influence during tumorigenesis of oral lesions, compared to distal microbial communities in the gut or skin?
2. Establish cell lines derived from 4-NQO-induced lesions. Use of tumor cell lines derived from distinct lesions would allow one to test the immunogenicity of tumors derived from immune-sufficient versus immune-deficient hosts, assess the reactivity of tumor-infiltrating T cells to matched and unmatched lesions *in vitro*, and allow for the manipulation of tumor cells via CRISPR-Cas9 approaches to determine the role of a gene of interest expressed by tumor cells.
3. Determine the molecular characteristics that dictate progression from pre-neoplasia to invasive OSCC by analyzing the genome and transcriptome of micro-dissected pre-neoplastic dysplasias and invasive OSCCs.
4. What is the mechanism of the emergence of OSCC following late-stage Treg cell ablation? What are the effector T cell-derived factor(s) mediating this outcome? Is the enhanced emergence of OSCC following late-stage Treg cell ablation due to progression of dysplasia to OSCC, or rapid expansion and proliferation of pre-existing OSCCs?
5. What is the impact of expanding the tumor-associated Treg cell population? Will increasing the relative ratio of Treg cells to effector T cells in the tumor environment promote tumor regression, the opposite effect of late-stage Treg cell ablation?

6. Are there predictive biomarkers to stratify patients who may maintain a durable response to immunotherapy from patients who may experience adverse consequences and detrimental effects with immunotherapy treatment, such as hyper-progression? Identification of predictive biomarkers requires properly controlled phase 3 clinical trials that includes a control group of patients who do not receive immunotherapy, and the ability to assess tumor growth rates before and after start of treatment.
7. Do T cells impose unique selective pressures on developing tumors? What are the genomic features of 4-NQO-induced lesions in the presence or absence of T cells?
8. What are the peptides recognized by the tumor-associated Treg clones identified? Are the peptides derived from a self-protein, a microbe present in the oral cavity, or a tumor-specific protein?
9. What are the developmental origins of the tumor-associated Treg cells found in 4-NQO-treated mice? Do tumor-associated Treg cells express Foxp3 prior to tumorigenesis? Are tumor-associated Treg cells thymic-derived tTregs or peripherally-induced pTregs?
10. What is the TCR repertoire of tumor-associated $CD4^+$ Tconv cells? Does the TCR repertoire overlap with the TCR repertoire of tumor-associated Treg cells? Do tumor-associated $CD4^+$ Tconv and Treg cells share reactivity to similar antigens?
11. What are the factors that dictate T cell infiltration into and survival within the tumor environment? Are these factors distinct or overlapping for $CD4^+$ T cells and $CD8^+$ T cells? Is the observation that a subset of tumors are enriched for either $CD4^+$ T cells or $CD8^+$ T cells due a tumor cell-intrinsic or tumor cell-extrinsic effect?

REFERENCES

1. Chao JL, Savage PA. Unlocking the Complexities of Tumor-Associated Regulatory T Cells. J Immunol Baltim Md 1950. 2018 15;200(2):415–21.

2. Matzinger P. The danger model: a renewed sense of self. Science. 2002 Apr 12;296(5566):301–5.

3. Janeway CA, Medzhitov R. Innate immune recognition. Annu Rev Immunol. 2002;20:197–216.

4. Jung D, Alt FW. Unraveling V(D)J recombination; insights into gene regulation. Cell. 2004 Jan 23;116(2):299–311.

5. Starr TK, Jameson SC, Hogquist KA. Positive and negative selection of T cells. Annu Rev Immunol. 2003;21:139–76.

6. Xing Y, Hogquist KA. T-cell tolerance: central and peripheral. Cold Spring Harb Perspect Biol. 2012 Jun 1;4(6).

7. Stritesky GL, Jameson SC, Hogquist KA. Selection of self-reactive T cells in the thymus. Annu Rev Immunol. 2012;30:95–114.

8. Savage PA, Klawon DEJ, Miller CH. Regulatory T Cell Development. Annu Rev Immunol. 2020 Apr 26;38:421–53.

9. Lathrop SK, Bloom SM, Rao SM, Nutsch K, Lio C-W, Santacruz N, et al. Peripheral education of the immune system by colonic commensal microbiota. Nature. 2011 Sep 21;478(7368):250–4.

10. Kretschmer K, Apostolou I, Hawiger D, Khazaie K, Nussenzweig MC, von Boehmer H. Inducing and expanding regulatory T cell populations by foreign antigen. Nat Immunol. 2005 Dec;6(12):1219–27.

11. Nutsch K, Chai JN, Ai TL, Russler-Germain E, Feehley T, Nagler CR, et al. Rapid and Efficient Generation of Regulatory T Cells to Commensal Antigens in the Periphery. Cell Rep. 2016 Sep 27;17(1):206–20.

12. Starnes CO. Coley's toxins in perspective. Nature. 1992 May 7;357(6373):11–2.

13. Burnet FM. Immunological surveillance in neoplasia. Transplant Rev. 1971;7:3–25.

14. Schreiber RD, Old LJ, Smyth MJ. Cancer immunoediting: integrating immunity's roles in cancer suppression and promotion. Science. 2011 Mar 25;331(6024):1565–70.

15. Shankaran V, Ikeda H, Bruce AT, White JM, Swanson PE, Old LJ, et al. IFNgamma and lymphocytes prevent primary tumour development and shape tumour immunogenicity. Nature. 2001 Apr 26;410(6832):1107–11.

16. Rooney MS, Shukla SA, Wu CJ, Getz G, Hacohen N. Molecular and genetic properties of tumors associated with local immune cytolytic activity. Cell. 2015 Jan 15;160(1–2):48–61.

17. McGranahan N, Rosenthal R, Hiley CT, Rowan AJ, Watkins TBK, Wilson GA, et al. Allele-Specific HLA Loss and Immune Escape in Lung Cancer Evolution. Cell. 2017 Nov 30;171(6):1259-1271.e11.

18. McGranahan N, Furness AJS, Rosenthal R, Ramskov S, Lyngaa R, Saini SK, et al. Clonal neoantigens elicit T cell immunoreactivity and sensitivity to immune checkpoint blockade. Science. 2016 Mar 25;351(6280):1463–9.

19. Chen DS, Mellman I. Oncology meets immunology: the cancer-immunity cycle. Immunity. 2013 Jul 25;39(1):1–10.

20. Ribas A, Wolchok JD. Cancer immunotherapy using checkpoint blockade. Science. 2018 Mar 23;359(6382):1350–5.

21. Feldman SA, Assadipour Y, Kriley I, Goff SL, Rosenberg SA. Adoptive Cell Therapy--Tumor-Infiltrating Lymphocytes, T-Cell Receptors, and Chimeric Antigen Receptors. Semin Oncol. 2015 Aug;42(4):626–39.

22. Singh AK, McGuirk JP. CAR T cells: continuation in a revolution of immunotherapy. Lancet Oncol. 2020 Mar;21(3):e168–78.

23. Peng M, Mo Y, Wang Y, Wu P, Zhang Y, Xiong F, et al. Neoantigen vaccine: an emerging tumor immunotherapy. Mol Cancer. 2019 Aug 23;18(1):128.

24. Sahin U, Türeci Ö. Personalized vaccines for cancer immunotherapy. Science. 2018 Mar 23;359(6382):1355–60.

25. Nishimura H, Nose M, Hiai H, Minato N, Honjo T. Development of lupus-like autoimmune diseases by disruption of the PD-1 gene encoding an ITIM motif-carrying immunoreceptor. Immunity. 1999 Aug;11(2):141–51.

26. Nishimura H, Okazaki T, Tanaka Y, Nakatani K, Hara M, Matsumori A, et al. Autoimmune dilated cardiomyopathy in PD-1 receptor-deficient mice. Science. 2001 Jan 12;291(5502):319–22.

27. Walunas TL, Lenschow DJ, Bakker CY, Linsley PS, Freeman GJ, Green JM, et al. CTLA-4 can function as a negative regulator of T cell activation. Immunity. 1994 Aug;1(5):405–13.

28. Iwai Y, Ishida M, Tanaka Y, Okazaki T, Honjo T, Minato N. Involvement of PD-L1 on tumor cells in the escape from host immune system and tumor immunotherapy by PD-L1 blockade. Proc Natl Acad Sci U S A. 2002 Sep 17;99(19):12293–7.

29. Leach DR, Krummel MF, Allison JP. Enhancement of antitumor immunity by CTLA-4 blockade. Science. 1996 Mar 22;271(5256):1734–6.

30. Brahmer JR, Drake CG, Wollner I, Powderly JD, Picus J, Sharfman WH, et al. Phase I study of single-agent anti-programmed death-1 (MDX-1106) in refractory solid tumors: safety, clinical activity, pharmacodynamics, and immunologic correlates. J Clin Oncol Off J Am Soc Clin Oncol. 2010 Jul 1;28(19):3167–75.

31. Hodi FS, O'Day SJ, McDermott DF, Weber RW, Sosman JA, Haanen JB, et al. Improved survival with ipilimumab in patients with metastatic melanoma. N Engl J Med. 2010 Aug 19;363(8):711–23.

32. Chen DS, Mellman I. Elements of cancer immunity and the cancer-immune set point. Nature. 2017 18;541(7637):321–30.

33. Fridman WH, Zitvogel L, Sautès-Fridman C, Kroemer G. The immune contexture in cancer prognosis and treatment. Nat Rev Clin Oncol. 2017 Dec;14(12):717–34.

34. Gajewski TF, Corrales L, Williams J, Horton B, Sivan A, Spranger S. Cancer Immunotherapy Targets Based on Understanding the T Cell-Inflamed Versus Non-T Cell-Inflamed Tumor Microenvironment. Adv Exp Med Biol. 2017;1036:19–31.

35. Trujillo JA, Sweis RF, Bao R, Luke JJ. T Cell-Inflamed versus Non-T Cell-Inflamed Tumors: A Conceptual Framework for Cancer Immunotherapy Drug Development and Combination Therapy Selection. Cancer Immunol Res. 2018;6(9):990–1000.

36. Duan Q, Zhang H, Zheng J, Zhang L. Turning Cold into Hot: Firing up the Tumor Microenvironment. Trends Cancer. 2020 Jul;6(7):605–18.

37. Grasso CS, Tsoi J, Onyshchenko M, Abril-Rodriguez G, Ross-Macdonald P, Wind-Rotolo M, et al. Conserved Interferon-γ Signaling Drives Clinical Response to Immune Checkpoint Blockade Therapy in Melanoma. Cancer Cell. 2020 Sep 8;

38. Kaplan DH, Shankaran V, Dighe AS, Stockert E, Aguet M, Old LJ, et al. Demonstration of an interferon gamma-dependent tumor surveillance system in immunocompetent mice. Proc Natl Acad Sci U S A. 1998 Jun 23;95(13):7556–61.

39. He Y-F, Wang X-H, Zhang G-M, Chen H-T, Zhang H, Feng Z-H. Sustained low-level expression of interferon-gamma promotes tumor development: potential insights in tumor prevention and tumor immunotherapy. Cancer Immunol Immunother CII. 2005 Sep;54(9):891–7.

40. Pai C-CS, Huang JT, Lu X, Simons DM, Park C, Chang A, et al. Clonal Deletion of Tumor-Specific T Cells by Interferon-γ Confers Therapeutic Resistance to Combination Immune Checkpoint Blockade. Immunity. 2019 Feb 19;50(2):477-492.e8.

41. Song M, Ping Y, Zhang K, Yang L, Li F, Zhang C, et al. Low-Dose IFNγ Induces Tumor Cell Stemness in Tumor Microenvironment of Non-Small Cell Lung Cancer. Cancer Res. 2019 Jul 15;79(14):3737–48.

42. Xiao M, Wang C, Zhang J, Li Z, Zhao X, Qin Z. IFNgamma promotes papilloma development by up-regulating Th17-associated inflammation. Cancer Res. 2009 Mar 1;69(5):2010–7.

43. DeNardo DG, Barreto JB, Andreu P, Vasquez L, Tawfik D, Kolhatkar N, et al. CD4(+) T cells regulate pulmonary metastasis of mammary carcinomas by enhancing protumor properties of macrophages. Cancer Cell. 2009 Aug 4;16(2):91–102.

44. Tan W, Zhang W, Strasner A, Grivennikov S, Cheng JQ, Hoffman RM, et al. Tumour-infiltrating regulatory T cells stimulate mammary cancer metastasis through RANKL-RANK signalling. Nature. 2011 Feb 24;470(7335):548–53.

45. Beaugerie L, Itzkowitz SH. Cancers complicating inflammatory bowel disease. N Engl J Med. 2015 Apr 9;372(15):1441–52.

46. Nadeem MS, Kumar V, Al-Abbasi FA, Kamal MA, Anwar F. Risk of colorectal cancer in inflammatory bowel diseases. Semin Cancer Biol. 2020 Aug;64:51–60.

47. Blatner NR, Mulcahy MF, Dennis KL, Scholtens D, Bentrem DJ, Phillips JD, et al. Expression of RORγt marks a pathogenic regulatory T cell subset in human colon cancer. Sci Transl Med. 2012 Dec 12;4(164):164ra159.

48. Gounaris E, Blatner NR, Dennis K, Magnusson F, Gurish MF, Strom TB, et al. T-regulatory cells shift from a protective anti-inflammatory to a cancer-promoting proinflammatory phenotype in polyposis. Cancer Res. 2009 Jul 1;69(13):5490–7.

49. Champiat S, Dercle L, Ammari S, Massard C, Hollebecque A, Postel-Vinay S, et al. Hyperprogressive Disease Is a New Pattern of Progression in Cancer Patients Treated by Anti-PD-1/PD-L1. Clin Cancer Res Off J Am Assoc Cancer Res. 2017 15;23(8):1920–8.

50. Ferrara R, Mezquita L, Texier M, Lahmar J, Audigier-Valette C, Tessonnier L, et al. Hyperprogressive Disease in Patients With Advanced Non-Small Cell Lung Cancer Treated With PD-1/PD-L1 Inhibitors or With Single-Agent Chemotherapy. JAMA Oncol. 2018 01;4(11):1543–52.

51. Kato S, Goodman A, Walavalkar V, Barkauskas DA, Sharabi A, Kurzrock R. Hyperprogressors after Immunotherapy: Analysis of Genomic Alterations Associated with Accelerated Growth Rate. Clin Cancer Res Off J Am Assoc Cancer Res. 2017 Aug 1;23(15):4242–50.

52. Kim JY, Lee KH, Kang J, Borcoman E, Saada-Bouzid E, Kronbichler A, et al. Hyperprogressive Disease during Anti-PD-1 (PDCD1) / PD-L1 (CD274) Therapy: A Systematic Review and Meta-Analysis. Cancers. 2019 Nov 1;11(11).

53. Saâda-Bouzid E, Defaucheux C, Karabajakian A, Coloma VP, Servois V, Paoletti X, et al. Hyperprogression during anti-PD-1/PD-L1 therapy in patients with recurrent and/or metastatic head and neck squamous cell carcinoma. Ann Oncol Off J Eur Soc Med Oncol. 2017 Jul 1;28(7):1605–11.

54. deLeeuw RJ, Kost SE, Kakal JA, Nelson BH. The prognostic value of FoxP3+ tumor-infiltrating lymphocytes in cancer: a critical review of the literature. Clin Cancer Res Off J Am Assoc Cancer Res. 2012 Jun 1;18(11):3022–9.

55. Ladoire S, Martin F, Ghiringhelli F. Prognostic role of FOXP3+ regulatory T cells infiltrating human carcinomas: the paradox of colorectal cancer. Cancer Immunol Immunother CII. 2011 Jul;60(7):909–18.

56. Qi Z, Liu Y, Mints M, Mullins R, Sample R, Law T, et al. Single-Cell Deconvolution of Head and Neck Squamous Cell Carcinoma. Cancers. 2021 Mar 11;13(6).

57. Shang B, Liu Y, Jiang S, Liu Y. Prognostic value of tumor-infiltrating FoxP3+ regulatory T cells in cancers: a systematic review and meta-analysis. Sci Rep. 2015 Oct 14;5:15179.

58. Burzyn D, Benoist C, Mathis D. Regulatory T cells in nonlymphoid tissues. Nat Immunol. 2013 Oct;14(10):1007–13.

59. Campbell DJ, Koch MA. Phenotypical and functional specialization of FOXP3+ regulatory T cells. Nat Rev Immunol. 2011 Feb;11(2):119–30.

60. Josefowicz SZ, Lu L-F, Rudensky AY. Regulatory T cells: mechanisms of differentiation and function. Annu Rev Immunol. 2012;30:531–64.

61. Bos PD, Plitas G, Rudra D, Lee SY, Rudensky AY. Transient regulatory T cell ablation deters oncogene-driven breast cancer and enhances radiotherapy. J Exp Med. 2013 Oct 21;210(11):2435–66.

62. Jang J-E, Hajdu CH, Liot C, Miller G, Dustin ML, Bar-Sagi D. Crosstalk between Regulatory T Cells and Tumor-Associated Dendritic Cells Negates Anti-tumor Immunity in Pancreatic Cancer. Cell Rep. 2017 Jul 18;20(3):558–71.

63. Kim JM, Rasmussen JP, Rudensky AY. Regulatory T cells prevent catastrophic autoimmunity throughout the lifespan of mice. Nat Immunol. 2007 Feb;8(2):191–7.

64. Simpson TR, Li F, Montalvo-Ortiz W, Sepulveda MA, Bergerhoff K, Arce F, et al. Fc-dependent depletion of tumor-infiltrating regulatory T cells co-defines the efficacy of anti-CTLA-4 therapy against melanoma. J Exp Med. 2013 Aug 26;210(9):1695–710.

65. Selby MJ, Engelhardt JJ, Quigley M, Henning KA, Chen T, Srinivasan M, et al. Anti-CTLA-4 antibodies of IgG2a isotype enhance antitumor activity through reduction of intratumoral regulatory T cells. Cancer Immunol Res. 2013 Jul;1(1):32–42.

66. Bulliard Y, Jolicoeur R, Windman M, Rue SM, Ettenberg S, Knee DA, et al. Activating Fc γ receptors contribute to the antitumor activities of immunoregulatory receptor-targeting antibodies. J Exp Med. 2013 Aug 26;210(9):1685–93.

67. Coe D, Begom S, Addey C, White M, Dyson J, Chai J-G. Depletion of regulatory T cells by anti-GITR mAb as a novel mechanism for cancer immunotherapy. Cancer Immunol Immunother CII. 2010 Sep;59(9):1367–77.

68. Bulliard Y, Jolicoeur R, Zhang J, Dranoff G, Wilson NS, Brogdon JL. OX40 engagement depletes intratumoral Tregs via activating FcγRs, leading to antitumor efficacy. Immunol Cell Biol. 2014 Jul;92(6):475–80.

69. Furness AJS, Vargas FA, Peggs KS, Quezada SA. Impact of tumour microenvironment and Fc receptors on the activity of immunomodulatory antibodies. Trends Immunol. 2014 Jul;35(7):290–8.

70. Zappasodi R, Serganova I, Cohen IJ, Maeda M, Shindo M, Senbabaoglu Y, et al. CTLA-4 blockade drives loss of Treg stability in glycolysis-low tumours. Nature. 2021 Mar;591(7851):652–8.

71. Hanahan D, Weinberg RA. Hallmarks of cancer: the next generation. Cell. 2011 Mar 4;144(5):646–74.

72. Bruder D, Probst-Kepper M, Westendorf AM, Geffers R, Beissert S, Loser K, et al. Neuropilin-1: a surface marker of regulatory T cells. Eur J Immunol. 2004 Mar;34(3):623–30.

73. Sarris M, Andersen KG, Randow F, Mayr L, Betz AG. Neuropilin-1 expression on regulatory T cells enhances their interactions with dendritic cells during antigen recognition. Immunity. 2008 Mar;28(3):402–13.

74. Hansen W, Hutzler M, Abel S, Alter C, Stockmann C, Kliche S, et al. Neuropilin 1 deficiency on CD4+Foxp3+ regulatory T cells impairs mouse melanoma growth. J Exp Med. 2012 Oct 22;209(11):2001–16.

75. Delgoffe GM, Woo S-R, Turnis ME, Gravano DM, Guy C, Overacre AE, et al. Stability and function of regulatory T cells is maintained by a neuropilin-1-semaphorin-4a axis. Nature. 2013 Sep 12;501(7466):252–6.

76. Overacre-Delgoffe AE, Chikina M, Dadey RE, Yano H, Brunazzi EA, Shayan G, et al. Interferon-γ Drives Treg Fragility to Promote Anti-tumor Immunity. Cell. 2017 Jun 1;169(6):1130-1141.e11.

77. Luo CT, Liao W, Dadi S, Toure A, Li MO. Graded Foxo1 activity in Treg cells differentiates tumour immunity from spontaneous autoimmunity. Nature. 2016 Jan 28;529(7587):532–6.

78. Plitas G, Konopacki C, Wu K, Bos PD, Morrow M, Putintseva EV, et al. Regulatory T Cells Exhibit Distinct Features in Human Breast Cancer. Immunity. 2016 Nov 15;45(5):1122–34.

79. Campbell JR, McDonald BR, Mesko PB, Siemers NO, Singh PB, Selby M, et al. Fc-optimized Anti-CCR8 Antibody Depletes Regulatory T Cells in Human Tumor Models. Cancer Res. 2021 Mar 23;

80. De Simone M, Arrigoni A, Rossetti G, Gruarin P, Ranzani V, Politano C, et al. Transcriptional Landscape of Human Tissue Lymphocytes Unveils Uniqueness of Tumor-Infiltrating T Regulatory Cells. Immunity. 2016 Nov 15;45(5):1135–47.

81. Zheng C, Zheng L, Yoo J-K, Guo H, Zhang Y, Guo X, et al. Landscape of Infiltrating T Cells in Liver Cancer Revealed by Single-Cell Sequencing. Cell. 2017 Jun 15;169(7):1342-1356.e16.

82. Tirosh I, Izar B, Prakadan SM, Wadsworth MH, Treacy D, Trombetta JJ, et al. Dissecting the multicellular ecosystem of metastatic melanoma by single-cell RNA-seq. Science. 2016 Apr 8;352(6282):189–96.

83. Malchow S, Leventhal DS, Nishi S, Fischer BI, Shen L, Paner GP, et al. Aire-dependent thymic development of tumor-associated regulatory T cells. Science. 2013 Mar 8;339(6124):1219–24.

84. Cipolletta D, Feuerer M, Li A, Kamei N, Lee J, Shoelson SE, et al. PPAR-γ is a major driver of the accumulation and phenotype of adipose tissue Treg cells. Nature. 2012 Jun 28;486(7404):549–53.

85. Feuerer M, Herrero L, Cipolletta D, Naaz A, Wong J, Nayer A, et al. Lean, but not obese, fat is enriched for a unique population of regulatory T cells that affect metabolic parameters. Nat Med. 2009 Aug;15(8):930–9.

86. Kolodin D, van Panhuys N, Li C, Magnuson AM, Cipolletta D, Miller CM, et al. Antigen- and cytokine-driven accumulation of regulatory T cells in visceral adipose tissue of lean mice. Cell Metab. 2015 Apr 7;21(4):543–57.

87. Rider P, Voronov E, Dinarello CA, Apte RN, Cohen I. Alarmins: Feel the Stress. J Immunol Baltim Md 1950. 2017 Feb 15;198(4):1395–402.

88. Arpaia N, Green JA, Moltedo B, Arvey A, Hemmers S, Yuan S, et al. A Distinct Function of Regulatory T Cells in Tissue Protection. Cell. 2015 Aug 27;162(5):1078–89.

89. Burzyn D, Kuswanto W, Kolodin D, Shadrach JL, Cerletti M, Jang Y, et al. A special population of regulatory T cells potentiates muscle repair. Cell. 2013 Dec 5;155(6):1282–95.

90. Green JA, Arpaia N, Schizas M, Dobrin A, Rudensky AY. A nonimmune function of T cells in promoting lung tumor progression. J Exp Med. 2017 Dec 4;214(12):3565–75.

91. Ali N, Zirak B, Rodriguez RS, Pauli ML, Truong H-A, Lai K, et al. Regulatory T Cells in Skin Facilitate Epithelial Stem Cell Differentiation. Cell. 2017 Jun 1;169(6):1119-1129.e11.

92. Liu Z, Fan F, Wang A, Zheng S, Lu Y. Dll4-Notch signaling in regulation of tumor angiogenesis. J Cancer Res Clin Oncol. 2014 Apr;140(4):525–36.

93. Lobry C, Oh P, Aifantis I. Oncogenic and tumor suppressor functions of Notch in cancer: it's NOTCH what you think. J Exp Med. 2011 Sep 26;208(10):1931–5.

94. Nowell CS, Radtke F. Notch as a tumour suppressor. Nat Rev Cancer. 2017 Mar;17(3):145–59.

95. Chow LQM. Head and Neck Cancer. N Engl J Med. 2020 Jan 2;382(1):60–72.

96. Cancer Genome Atlas Network. Comprehensive genomic characterization of head and neck squamous cell carcinomas. Nature. 2015 Jan 29;517(7536):576–82.

97. Keck MK, Zuo Z, Khattri A, Stricker TP, Brown CD, Imanguli M, et al. Integrative analysis of head and neck cancer identifies two biologically distinct HPV and three non-HPV subtypes. Clin Cancer Res Off J Am Assoc Cancer Res. 2015 Feb 15;21(4):870–81.

98. Seiwert TY, Zuo Z, Keck MK, Khattri A, Pedamallu CS, Stricker T, et al. Integrative and comparative genomic analysis of HPV-positive and HPV-negative head and neck squamous cell carcinomas. Clin Cancer Res Off J Am Assoc Cancer Res. 2015 Feb 1;21(3):632–41.

99. Alexandrov LB, Nik-Zainal S, Wedge DC, Aparicio SAJR, Behjati S, Biankin AV, et al. Signatures of mutational processes in human cancer. Nature. 2013 Aug 22;500(7463):415–21.

100. Alexandrov LB, Kim J, Haradhvala NJ, Huang MN, Tian Ng AW, Wu Y, et al. The repertoire of mutational signatures in human cancer. Nature. 2020 Feb;578(7793):94–101.

101. Mandal R, Şenbabaoğlu Y, Desrichard A, Havel JJ, Dalin MG, Riaz N, et al. The head and neck cancer immune landscape and its immunotherapeutic implications. JCI Insight. 2016 Oct 20;1(17):e89829.

102. Cillo AR, Kürten CHL, Tabib T, Qi Z, Onkar S, Wang T, et al. Immune Landscape of Viral- and Carcinogen-Driven Head and Neck Cancer. Immunity. 2020 14;52(1):183-199.e9.

103. Cohen EEW, Soulières D, Le Tourneau C, Dinis J, Licitra L, Ahn M-J, et al. Pembrolizumab versus methotrexate, docetaxel, or cetuximab for recurrent or metastatic head-and-neck squamous cell carcinoma (KEYNOTE-040): a randomised, open-label, phase 3 study. Lancet Lond Engl. 2019 12;393(10167):156–67.

104. Seiwert TY, Burtness B, Mehra R, Weiss J, Berger R, Eder JP, et al. Safety and clinical activity of pembrolizumab for treatment of recurrent or metastatic squamous cell carcinoma of the head and neck (KEYNOTE-012): an open-label, multicentre, phase 1b trial. Lancet Oncol. 2016 Jul;17(7):956–65.

105. Echarti A, Hecht M, Büttner-Herold M, Haderlein M, Hartmann A, Fietkau R, et al. CD8+ and Regulatory T cells Differentiate Tumor Immune Phenotypes and Predict Survival in Locally Advanced Head and Neck Cancer. Cancers. 2019 Sep 19;11(9).

106. Seminerio I, Descamps G, Dupont S, de Marrez L, Laigle J-A, Lechien JR, et al. Infiltration of FoxP3+ Regulatory T Cells is a Strong and Independent Prognostic Factor in Head and Neck Squamous Cell Carcinoma. Cancers. 2019 Feb 15;11(2).

107. Zitvogel L, Pitt JM, Daillère R, Smyth MJ, Kroemer G. Mouse models in oncoimmunology. Nat Rev Cancer. 2016 Dec;16(12):759–73.

108. Hasina R, Martin LE, Kasza K, Jones CL, Jalil A, Lingen MW. ABT-510 is an effective chemopreventive agent in the mouse 4-nitroquinoline 1-oxide model of oral carcinogenesis. Cancer Prev Res Phila Pa. 2009 Apr;2(4):385–93.

109. Ishida K, Tomita H, Nakashima T, Hirata A, Tanaka T, Shibata T, et al. Current mouse models of oral squamous cell carcinoma: Genetic and chemically induced models. Oral Oncol. 2017 Oct;73:16–20.

110. Kanojia D, Vaidya MM. 4-nitroquinoline-1-oxide induced experimental oral carcinogenesis. Oral Oncol. 2006 Aug;42(7):655–67.

111. Tang X-H, Knudsen B, Bemis D, Tickoo S, Gudas LJ. Oral cavity and esophageal carcinogenesis modeled in carcinogen-treated mice. Clin Cancer Res Off J Am Assoc Cancer Res. 2004 Jan 1;10(1 Pt 1):301–13.

112. Vitale-Cross L, Czerninski R, Amornphimoltham P, Patel V, Molinolo AA, Gutkind JS. Chemical carcinogenesis models for evaluating molecular-targeted prevention and treatment of oral cancer. Cancer Prev Res Phila Pa. 2009 May;2(5):419–22.

113. Czerninski R, Amornphimoltham P, Patel V, Molinolo AA, Gutkind JS. Targeting mammalian target of rapamycin by rapamycin prevents tumor progression in an oral-specific chemical carcinogenesis model. Cancer Prev Res Phila Pa. 2009 Jan;2(1):27–36.

114. Sequeira I, Rashid M, Tomás IM, Williams MJ, Graham TA, Adams DJ, et al. Genomic landscape and clonal architecture of mouse oral squamous cell carcinomas dictate tumour ecology. Nat Commun. 2020 Nov 9;11(1):5671.

115. Wang Z, Wu VH, Allevato MM, Gilardi M, He Y, Luis Callejas-Valera J, et al. Syngeneic animal models of tobacco-associated oral cancer reveal the activity of in situ anti-CTLA-4. Nat Commun. 2019 Dec 5;10(1):5546.

116. Ozerov IV, Lezhnina KV, Izumchenko E, Artemov AV, Medintsev S, Vanhaelen Q, et al. In silico Pathway Activation Network Decomposition Analysis (iPANDA) as a method for biomarker development. Nat Commun. 2016 16;7:13427.

117. Saloura V, Izumchenko E, Zuo Z, Bao R, Korzinkin M, Ozerov I, et al. Immune profiles in primary squamous cell carcinoma of the head and neck. Oral Oncol. 2019;96:77–88.

118. Puram SV, Tirosh I, Parikh AS, Patel AP, Yizhak K, Gillespie S, et al. Single-Cell Transcriptomic Analysis of Primary and Metastatic Tumor Ecosystems in Head and Neck Cancer. Cell. 2017 Dec 14;171(7):1611-1624.e24.

119. Schelker M, Feau S, Du J, Ranu N, Klipp E, MacBeath G, et al. Estimation of immune cell content in tumour tissue using single-cell RNA-seq data. Nat Commun. 2017 Dec 11;8(1):2032.

120. Aran D, Hu Z, Butte AJ. xCell: digitally portraying the tissue cellular heterogeneity landscape. Genome Biol. 2017 Nov 15;18(1):220.

121. Schindelin J, Arganda-Carreras I, Frise E, Kaynig V, Longair M, Pietzsch T, et al. Fiji: an open-source platform for biological-image analysis. Nat Methods. 2012 Jun 28;9(7):676–82.

122. Leonard JD, Gilmore DC, Dileepan T, Nawrocka WI, Chao JL, Schoenbach MH, et al. Identification of Natural Regulatory T Cell Epitopes Reveals Convergence on a Dominant Autoantigen. Immunity. 2017 18;47(1):107-117.e8.

123. Dash P, McClaren JL, Oguin TH, Rothwell W, Todd B, Morris MY, et al. Paired analysis of TCRα and TCRβ chains at the single-cell level in mice. J Clin Invest. 2011 Jan;121(1):288–95.

124. Miller CH, Klawon DEJ, Zeng S, Lee V, Socci ND, Savage PA. Eomes identifies thymic precursors of self-specific memory-phenotype CD8+ T cells. Nat Immunol. 2020 May;21(5):567–77.

125. Moon JJ, Chu HH, Pepper M, McSorley SJ, Jameson SC, Kedl RM, et al. Naive CD4(+) T cell frequency varies for different epitopes and predicts repertoire diversity and response magnitude. Immunity. 2007 Aug;27(2):203–13.

126. R Core Team. R: The R Project for Statistical Computing [Internet]. [cited 2021 Feb 5]. Available from: https://www.r-project.org/

127. Malchow S, Leventhal DS, Lee V, Nishi S, Socci ND, Savage PA. Aire Enforces Immune Tolerance by Directing Autoreactive T Cells into the Regulatory T Cell Lineage. Immunity. 2016 May 17;44(5):1102–13.

128. McDonald BD, Bunker JJ, Erickson SA, Oh-Hora M, Bendelac A. Crossreactive αβ T Cell Receptors Are the Predominant Targets of Thymocyte Negative Selection. Immunity. 2015 Nov 17;43(5):859–69.

129. Thorsson V, Gibbs DL, Brown SD, Wolf D, Bortone DS, Ou Yang T-H, et al. The Immune Landscape of Cancer. Immunity. 2018 17;48(4):812-830.e14.

130. Nishikawa H, Sakaguchi S. Regulatory T cells in cancer immunotherapy. Curr Opin Immunol. 2014 Apr;27:1–7.

131. Tanaka A, Sakaguchi S. Regulatory T cells in cancer immunotherapy. Cell Res. 2017 Jan;27(1):109–18.

132. Togashi Y, Shitara K, Nishikawa H. Regulatory T cells in cancer immunosuppression - implications for anticancer therapy. Nat Rev Clin Oncol. 2019;16(6):356–71.

133. Roychoudhuri R, Eil RL, Restifo NP. The interplay of effector and regulatory T cells in cancer. Curr Opin Immunol. 2015 Apr;33:101–11.

134. Makarev E, Schubert AD, Kanherkar RR, London N, Teka M, Ozerov I, et al. In silico analysis of pathways activation landscape in oral squamous cell carcinoma and oral leukoplakia. Cell Death Discov. 2017;3:17022.

135. Boxberg M, Leising L, Steiger K, Jesinghaus M, Alkhamas A, Mielke M, et al. Composition and Clinical Impact of the Immunologic Tumor Microenvironment in Oral Squamous Cell Carcinoma. J Immunol Baltim Md 1950. 2019 01;202(1):278–91.

136. Chatzopoulos K, Sotiriou S, Collins AR, Kartsidis P, Schmitt AC, Chen X, et al. Transcriptomic and Immunophenotypic Characterization of Tumor Immune Microenvironment in Squamous Cell Carcinoma of the Oral Tongue. Head Neck Pathol. 2020 Oct 3;

137. Liu X, Chen J, Lu W, Zeng Z, Li J, Jiang X, et al. Systematic Profiling of Immune Risk Model to Predict Survival and Immunotherapy Response in Head and Neck Squamous Cell Carcinoma. Front Genet. 2020;11:576566.

138. Koike K, Dehari H, Ogi K, Shimizu S, Nishiyama K, Sonoda T, et al. Prognostic value of FoxP3 and CTLA-4 expression in patients with oral squamous cell carcinoma. PloS One. 2020;15(8):e0237465.

139. Salama P, Phillips M, Grieu F, Morris M, Zeps N, Joseph D, et al. Tumor-infiltrating FOXP3+ T regulatory cells show strong prognostic significance in colorectal cancer. J Clin Oncol Off J Am Soc Clin Oncol. 2009 Jan 10;27(2):186–92.

140. Yao Y, Yan Z, Lian S, Wei L, Zhou C, Feng D, et al. Prognostic value of novel immune-related genomic biomarkers identified in head and neck squamous cell carcinoma. J Immunother Cancer. 2020 Jul;8(2).

141. Park J-Y, Chung H, DiPalma DT, Tai X, Park J-H. Immune quiescence in the oral mucosa is maintained by a uniquely large population of highly activated Foxp3+ regulatory T cells. Mucosal Immunol. 2018 Jul;11(4):1092–102.

142. Wu R, Zhang D, Zanvit P, Jin W, Wang H, Chen W. Identification and Regulation of TCRαβ+CD8αα+ Intraepithelial Lymphocytes in Murine Oral Mucosa. Front Immunol. 2020;11:1702.

143. Kachler K, Holzinger C, Trufa DI, Sirbu H, Finotto S. The role of Foxp3 and Tbet co-expressing Treg cells in lung carcinoma. Oncoimmunology. 2018;7(8):e1456612.

144. Meinicke H, Bremser A, Brack M, Akeus P, Pearson C, Bullers S, et al. Tumour-associated changes in intestinal epithelial cells cause local accumulation of KLRG1+ GATA3+ regulatory T cells in mice. Immunology. 2017 Sep;152(1):74–88.

145. Leemans CR, Snijders PJF, Brakenhoff RH. The molecular landscape of head and neck cancer. Nat Rev Cancer. 2018 May;18(5):269–82.

146. Schumacher TN, Schreiber RD. Neoantigens in cancer immunotherapy. Science. 2015 Apr 3;348(6230):69–74.

147. Ayers M, Lunceford J, Nebozhyn M, Murphy E, Loboda A, Kaufman DR, et al. IFN-γ-related mRNA profile predicts clinical response to PD-1 blockade. J Clin Invest. 2017 Aug 1;127(8):2930–40.

148. Pastille E, Bardini K, Fleissner D, Adamczyk A, Frede A, Wadwa M, et al. Transient ablation of regulatory T cells improves antitumor immunity in colitis-associated colon cancer. Cancer Res. 2014 Aug 15;74(16):4258–69.

149. Teng MWL, Ngiow SF, von Scheidt B, McLaughlin N, Sparwasser T, Smyth MJ. Conditional regulatory T-cell depletion releases adaptive immunity preventing carcinogenesis and suppressing established tumor growth. Cancer Res. 2010 Oct 15;70(20):7800–9.

150. Zhang Y, Lazarus J, Steele NG, Yan W, Lee H-J, Nwosu ZC, et al. Regulatory T-cell Depletion Alters the Tumor Microenvironment and Accelerates Pancreatic Carcinogenesis. Cancer Discov. 2020;10(3):422–39.

151. Martinez LM, Robila V, Clark NM, Du W, Idowu MO, Rutkowski MR, et al. Regulatory T Cells Control the Switch From in situ to Invasive Breast Cancer. Front Immunol. 2019;10:1942.

152. Zappasodi R, Budhu S, Hellmann MD, Postow MA, Senbabaoglu Y, Manne S, et al. Non-conventional Inhibitory CD4+Foxp3-PD-1hi T Cells as a Biomarker of Immune Checkpoint Blockade Activity. Cancer Cell. 2018 Jun 11;33(6):1017-1032.e7.

153. Spranger S, Spaapen RM, Zha Y, Williams J, Meng Y, Ha TT, et al. Up-regulation of PD-L1, IDO, and T(regs) in the melanoma tumor microenvironment is driven by CD8(+) T cells. Sci Transl Med. 2013 Aug 28;5(200):200ra116.

154. Ahmadzadeh M, Pasetto A, Jia L, Deniger DC, Stevanović S, Robbins PF, et al. Tumor-infiltrating human CD4+ regulatory T cells display a distinct TCR repertoire and exhibit tumor and neoantigen reactivity. Sci Immunol. 2019 Jan 11;4(31).

155. Petzold C, Steinbronn N, Gereke M, Strasser RH, Sparwasser T, Bruder D, et al. Fluorochrome-based definition of naturally occurring Foxp3(+) regulatory T cells of intra- and extrathymic origin. Eur J Immunol. 2014 Dec;44(12):3632–45.

156. Xydia M, Rahbari R, Ruggiero E, Macaulay I, Tarabichi M, Lohmayer R, et al. Common clonal origin of conventional T cells and induced regulatory T cells in breast cancer patients. Nat Commun. 2021 Feb 18;12(1):1119.

157. Spranger S, Bao R, Gajewski TF. Melanoma-intrinsic β-catenin signalling prevents anti-tumour immunity. Nature. 2015 Jul 9;523(7559):231–5.

158. Owen DL, Mahmud SA, Vang KB, Kelly RM, Blazar BR, Smith KA, et al. Identification of Cellular Sources of IL-2 Needed for Regulatory T Cell Development and Homeostasis. J Immunol Baltim Md 1950. 2018 Jun 15;200(12):3926–33.

159. Hemmers S, Schizas M, Azizi E, Dikiy S, Zhong Y, Feng Y, et al. IL-2 production by self-reactive CD4 thymocytes scales regulatory T cell generation in the thymus. J Exp Med. 2019 Nov 4;216(11):2466–78.